UNIVERSITAT DE BARCELONA

Carotid Artery Ultrasound Image-Based Cardiovascular Risk Prediction using Deep Learning

Maria del Mar Vila Muñoz

Carotid Artery Ultrasound Image-Based Cardiovascular Risk Prediction using Deep Learning

Maria del Mar Vila Muñoz

Universitat de Barcelona

A dissertation submitted to Universitat de Barcelona in accordance with the requirements of the degree of Doctor of Philosophy in Computer Science in the *Facultat de Matemàtiques i Informàtica, Universitat de Barcelona*

Director: Dr. Laura Igual Muñoz.
Facultat de Matemàtiques i Informàtica, Universitat de Barcelona
Co-Director: Dr. María Grau Magaña.
Facultat de Medicina i Ciències de la Salut, Universitat de Barcelona
Tutor: Dr. Petia Ivanova Radeva.

January 2024

Dedicated to:
All the children born during the elaboration of this thesis: Àgata, Telma, Ester, Arnau, Luca, and Alba. And to all the researching mothers.

Dedicat a:
Totes les filles i fills nascuts durant l'elaboració d'aquesta tesis: l'Àgata, la Telma, l'Ester, l'Arnau, el Luca i l'Alba. I a totes les mares investigadores.

Abstract

Cardiovascular Diseases (CVDs), the leading cause of death in developed countries, often involve atherosclerosis, which is a chronic inflammatory thickening of the inner artery layer. Monitoring atherosclerotic plaque detection and its characteristics is crucial for assessing future cardiovascular events. Carotid Artery (CA) Ultrasound (US) images are utilized for subclinical atherosclerosis detection by measuring carotid Intima Media Thickness (IMT) and identifying atherosclerotic plaques. This thesis introduces Deep Learning (DL) methods to segment CA US images and characterize atherosclerotic plaque, aiming to improve cardiovascular risk prediction.

First, we address the segmentation of the Carotid Intima-Media (CIM) region, where the IMT is estimated. In this work, we introduce a fully automated method based on Convolutional Neural Networks that accurately localizes the carotid IMT region in longitudinal B-mode CA US images. In particular, we present a novel single-step approach using DenseNets for semantic segmentation, resulting in enhanced subclinical atherosclerosis detection through efficient carotid IMT estimation and atherosclerotic plaque detection.

This thesis introduces two clinical applications of carotid IMT estimation and atherosclerotic plaque detection. The first study evaluates cardiovascular event risk in autoimmune disease patients, focusing on chronic inflammation's impact on subclinical atherosclerosis. In the second study, we examine the coexistence of subclinical atherosclerosis in the lower limb (Ankle-Brachial Index) and carotid arteries. The findings of both studies highlights the systemic nature of atherosclerosis, suggesting a correlation between biomarkers in different areas and the likelihood of subclinical disease.

Finally, we explore new ways of improving cardiovascular risk prediction using DL techniques to extract information from CA US. In cardiovascular epidemiology, risk prediction functions assess the likelihood of a cardiovascular event based on individual clinical variables, using survival models. Despite their accurate stratification into

low, moderate, and high-risk groups, a significant number of cardiovascular events still occur in the medium-risk category. This study introduces a novel approach for CA characterization, integrating individual artery condition data into traditional survival models. The work presents an innovative survival model that incorporates CA US image features derived from Deep Neural Networks, enabling effective cardiovascular risk prediction and the reclassification of individuals from the moderate to the high-risk category within the survival model.

Acknowledgements

This work has been partially funded by: the Ministry of Economy and Competitiveness of Spain through the *Instituto de Salud Carlos III-FEDER* (CIBERCV and FIS CPII17/00012); and the *Agència de Gesció d'Ajuts Universitaris de Recerca de Cataluña* (2017-SGR-222 and 2017-SGR-1742). I appreciate the access to the database of the del *Sistema d'Informació per al Desenvolupament de la Investigació en Atenció Primària* (SIDIAP) and the expert review on autoimmune diseases conducted by Dr. Albert Escola Campabadal. I would like to express my gratitude for the English language revision of certain parts of the text conducted by Elaine Lilly, PhD. I also want to extend special thanks to Neus Goday, Martina Sidera, Virtu, and the UDETMA team for their collaboration in helping me understand, interpret, and capture ultrasound images of the carotid artery. I gratefully acknowledge the support of NVIDIA Corporation with the donation of the GPUs used during this research.

I also want to deeply thank my colleagues, family, and friends for their support throughout this entire journey. Special thanks to:
Laura, for her teachings, guidance, and advice, crucial for the development and success of this thesis. Thank you for making me a better researcher.
María, for sharing her deep knowledge in this field, teaching me values beyond scientific methodology, and always providing the necessary support to carry out this thesis. Thank you for always helping me, thinking about what is best for me and for the project.
Bea, for her constant contributions, always making everything better. Thank you for always being by our side.
Roberto and Jaume. Thank you for giving me the opportunity to be part of the REGICOR team.
The REGICOR team, especially the Volleyball team and my office mates Leny and Silvia. Thank you for your conversations, laughter, and all the shared moments.
Alessa and Abril for their fabulous yoga classes.
Aura Yoga, and specifically my teacher Márcia. Thank you for imparting the knowledge

of yoga, which has given me the tools necessary to approach this thesis with efficiency and wholeness.
My parents, for being the seed of everything. Thank you for being there.
Ágata and Ester for being the driving force of my life. Thank you for your patience, your drawings, and your hugs.
And to Ferran, my life partner, to whom I owe a large part of this work. Thank you for your unconditional support and for always being by my side.

To all of you, thank you.

Aquest treball ha estat finançat parcialment per: el Ministeri d'Economia i Competitivitat d'Espanya a través de l'Institut de Salut Carlos III-FEDER (CIBERCV i FIS CPII17/00012); i la Agència de Gesció d'Ajuts Universitaris de Recerca de Cataluña (2017-SGR-222 i 2017-SGR-1742). Agraeixo l'accés a la base de dades del Sistema d'Informació per al Desenvolupament de la Investigació en Atenció Primària (SIDIAP) i la revisió experta sobre malalties autoimmunes realitzada pel Dr. Albert Escola Campabadal. Vull agrair la revisió de l'anglès d'algunes parts del text feta per Elaine Lilly, PhD. I també agrair especialment la col·laboració de Neus Goday, Martina Sidera, La Virtu i l'equip UDETMA per ajudar-me a entendre, interpretar i capturar imatges d'ecografia de l'artèria caròtida. Agraeixo el suport de NVIDIA Corporation amb la donació de les GPU utilitzades durant aquesta investigació.

També vull agrair profundament als meus companys, familiars i amics el seu suport durant tot aquest temps. Amb especial agraïment:
A la Laura, per les seves ensenyances, orientació i consells, fonamentals pel desenvolupament i èxit d'aquesta tesis. Gràcies per fer-me millor investigadora.
A la Maria, per compartir el seu profund coneixement en aquest camp, per ensenyar-me valors més enllà de la metodologia científica i per donar-me sempre tot el suport necessari per tirar endavant aquesta tesis. Gràcies per ajudar-me pensant sempre en la millor solució per mi i pel projecte.
A la Bea per les seves constants aportacions, sempre fent-ho tot millor. Gràcies per ser sempre al nostre costat.
Al Roberto i al Jaume. Gràcies per donar-me la oportunitat de formar part de l'equip REGICOR.
A l'equip REGICOR, a l'equip de Volei i en especial a les meves companyes de despatx Leny i Silvia. Gràcies per les vostres converses, riures i tots els moments compartits.
A l'Alessa i a l'Abril per les seves fabuloses classes de ioga.
A Aura ioga, i en concret a la meva professora Màrcia. Gràcies per transmetre'm els

coneixements del ioga que m'han donat les eines necessàries per portar aquesta tesi amb eficàcia i enteresa.
Als meus pares, per ser la llavor de tot plegat. Gràcies per ser-hi.
A l'Àgata i l'Ester per ser el meu motor de la vida. Gràcies per la vostra paciència, els vostres dibuixos i les vostres abraçades.
I al Ferran, el meu company de la vida, a qui li dec gran part d'aquest treball. Gràcies pel teu suport incondicional i per ser sempre al meu costat.

A tots vosaltres, gràcies.

Declaration

I declare that the work contained in this dissertation has been composed solely by myself and has not been accepted in any previous application for a degree. Except when specifically referenced in the text, all the work presented in this document is my own. Any collaborative work or work assisted by others is clearly indicated as such. I confirm that I have acknowledged all sources of information used in this thesis.

(Maria del Mar Vila Muñoz)

Contents

List of Tables

List of Figures

Chapter 1

Introduction

1.1 Clinical introduction

1.1.1 Cardiovascular diseases

Cardiovascular Diseases (CVDs) are a group of disorders that involve the heart and blood vessels[1]. These diseases can affect the heart's function (e.g., heart attacks, heart failure) or the blood vessels (e.g., atherosclerosis, peripheral artery disease). CVDs are a major global health concern and a leading cause of death worldwide (approximately 17.9 million lives annually). In particular, more than four out of five CVD deaths are due to heart attacks and strokes, with a significant proportion occurring prematurely in individuals under the age of 70.

The common basis of CVDs is the occurrence of adverse structural and functional changes within vascular walls –the layers of tissue that form the structure of blood vessels–. These changes specifically include atherosclerosis and arteriosclerosis. Arteriosclerosis is the thickening and hardening of arterial walls, leading to reduced elasticity and potentially affecting blood pressure regulation and overall cardiovascular health. Atherosclerosis, a specific type of arteriosclerosis, involves the accumulation of fatty deposits –plaques– on the inner arterial walls, which can further compromise blood flow and increase the risk of heart-related issues. Both, atherosclerosis and arteriosclerosis, tend to coexist, causing progressive, diffuse, and age-related deterioration in all vascular beds [2]. Atherosclerosis is a chronic inflammatory and degenerative process that mainly occurs in large and medium-sized arteries and is morphologically characterized by asymmetric focal thickenings of the innermost layer of the artery [3]. Atherosclerotic lesions are fatty deposits or plaque buildup within artery walls, consisting of cholesterol, fat, calcium, and other substances. As they progress over time, they narrow

and thicken the arteries, leading to reduced blood flow. Atherosclerosis begins early in life, progresses with age, and typically manifests with subclinical arterial wall alterations—changes that occur without causing apparent symptoms. These alterations precede cardiovascular events, which are incidents resulting from the progression or complications of CVDs. Examples include stroke, myocardial infarction (heart attack), or chest pain.

1.1.2 Detection of subclinical atherosclerosis using carotid artery ultrasound images.

Carotid Arteries (CA) are vital blood vessels located on each side of the neck that supply oxygen-rich blood to the brain (see Figure 1.1). They are part of the cardiovascular system and they are also susceptible to the development of atherosclerosis. The development of plaque buildup in these arteries can lead to reduced blood flow or plaque rupture, increasing the risk of cardiovascular events and suggesting potential problems in other arteries. Moreover, the presence of atherosclerosis in a particular vascular bed is frequently associated with this disease in other vascular territories [4]. Consequently, the presence of atherosclerosis in the CA has a significant impact on cardiovascular health. Thus, preventing and treating CA atherosclerosis becomes crucial to avoid severe cardiovascular consequences.

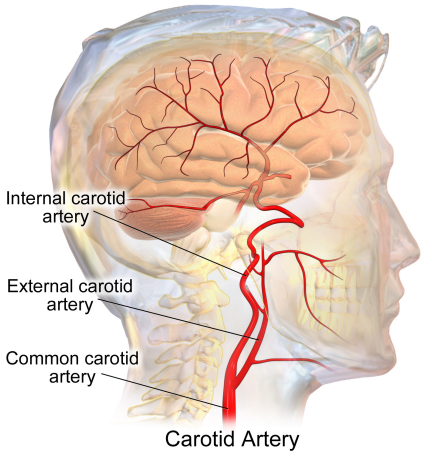

Figure 1.1: Illustration of the CA and its different segments (CCA, ICA, and external CA). The bulb is the junction between these segments [5].

Subclinical atherosclerosis is the early stage of artery narrowing caused by fatty deposits. It occurs without noticeable symptoms and is often detected through the use of medical images. Since a person can have atherosclerotic plaques in the arteries for a long time without presenting any symptoms, it is important to identify them to prevent future cardiovascular problems. CA B-mode Ultrasound (US) image is currently

being used in the clinical practice to detect the burden of subclinical atherosclerosis since it provides a measurement of the Intima Media Thickness (IMT) of the artery. CA B-mode US is a cross-sectional –it does not provide a continuous view along the length of a structure– image constructed from echoes that are generated by reflection of US waves at tissue boundaries. US image is a medical imaging technique that uses high-frequency sound waves (typically in the range of 2 to 18 megahertz) to create a real-time visual representation of internal body structures [6]. The B-mode conveys information about tissue density and reflectivity. Brighter areas typically correspond to dense or highly reflective structures, such as bones or tissues, while darker areas represent less dense or less reflective tissues, such as fluids like blood. As a result, B-mode US allows healthcare professionals to visualize tissues and organ boundaries in a grayscale image. In particular, the IMT measurement in the clinical examination requires the longitudinal view —aligned in a plane parallel to the artery's direction (as shown in both images from Figure 1.2)— rather than a transverse perspective. These images are the data source employed for evaluating CA in this thesis.

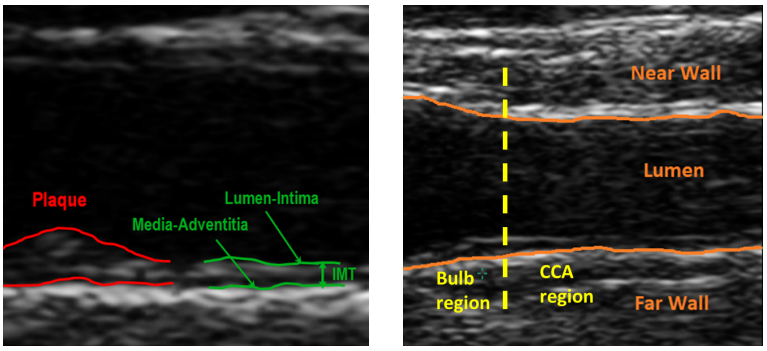

(a) (b)

Figure 1.2: Two examples of longitudinal B-mode CA US images: (a) the red lines show the presence of atherosclerosis plaque and the green lines show the IMT measurement; and (b) the five anatomical regions represented in a CCA B-mode US image.

IMT is defined as the distance between Lumen-Intima (LI) and Media-Adventitia (MA) interfaces, and it is commonly estimated in the far wall of the CA [7]. From now on, we will refer to the region where IMT is estimated as the Carotid Intima-Media (CIM) region. Figure 1.2 shows two B-mode US images of the CA where different anatomical regions are distinguished: the LI and MA tissues between which the IMT is measured, the atherosclerotic plaque, the CCA and bulb territories, the wall of the artery closest to the skin ("Near Wall") and the wall of the artery most distal to the skin ("Far Wall"), and the blood ("Lumen") between these two walls. The measurement of the carotid IMT using B-mode US is a non-invasive, sensitive, and relatively inexpensive image technique. Moreover, the IMT measurement is considered as an indicator of the

presence of plaque, as is stated in the Mannheim consensus [7]. This consensus defines a sufficient criterion for plaque detection: Plaques are focal structures encroaching into the arterial lumen of at least 0.5 mm or 50% of the surrounding IMT value, or demonstrates a thickness $>$ 1.5 mm as measured from the LI interface to the MA interface.

Carotid arterial wall assessment may include different CA territories, the Common CA (CCA), the Internal CA (ICA), or bulb territory of the CA (see Figure 1.1). Atherosclerotic thickening and plaque are commonly found at the bifurcation of the CA and the beginning of the ICA, but only occasionally occur in the CCA. However, it is well known that noise represents the most prominent problem in US imaging and, in particular, noise is more evident in internal areas such as bulb or ICA. Therefore, most B-mode US studies are performed assessing the CCA due to its accessibility, which makes the quality of the CCA images better compared to those of other artery territories.

There is a clinical motivation to automate IMT estimation and plaque detection. Manual detection of the LI and MA walls in US images is a slow and tedious task, and inter-individual and inter-observer variability in the measurements is a common issue in these estimations [7]. This is mainly due to two aspects: one, anatomical variations encompassing vessel morphology and changes related to atherosclerosis; and two, image quality, which, aside from having noise and the presence of speckles, is strongly influenced by the scanner and its configuration. Consequently, automated methods are necessary to analyze large quantities of images in a fast manner, reduce measurement variability and avoid reproducibility issues, a crucial requirement for high-quality studies.

1.1.3 Cardiovascular disease prevention

Survival models for risk classification

In the field of cardiovascular epidemiology, practitioners use risk prediction functions [8, 9, 10, 11, 12] to estimate the risk of suffering a cardiovascular event in a period of time. These function are called *risk functions* in the literature. These functions are based on survival models which are statistical methods used to analyze and predict the time until an event of interest occurs, such as death, failure, or any other defined outcome. In particular, the survival models used in cardiovascular risk functions are mathematical models designed to estimate an individual's likelihood of developing any CVD. It takes into account various risk factors such as age, gender, blood pressure, cholesterol levels, smoking status, and family history of heart disease etc. By analyzing these factors, the prediction function provides a numerical value or percentage that indicates the probability of experiencing a cardiovascular event within a specified time

interval for a particular individual [13]. Cox Proportional Hazards model (CoxPh) is a specific type of survival model that assess the relationship between predictor variables –covariates– and the probability of an event happening at a given time –the outcome– [14]. Most of the risk prediction functions in the field of cardiovascular epidemiology are based on CoxPh [8, 9, 10, 12] where the outcome is the time until an event occurs, and the predictor covariates are the risk factors.

Improvement of risk classification

Classically, the predictive results of risk functions are divided into different risk categories for stratification. Each risk category is defined by an interval probability of suffering a cardiovascular event in the next ten years [8, 9]. These functions accurately stratify individuals into different categories and one example is shown in Table 1.1. Table 1.1 shows data on the ten-year incidence rate of cardiovascular events (specifically stroke, myocardial infarction or chest pain) in a population of 3,724 individuals aged between 35 and 74 years who participated in REGICOR study [8]. The risk category for each subject is based on the percentage probability of suffering a cardiovascular event in the next ten years (first column). The second and third columns indicate the number of subjects in each category and the number of events respectively. The last column shows the percentage of events that occurred in a period of ten years for each risk category. As can be seen, the percentage of events falls inside each interval probability. More specifically, the percentage of subjects in the *low*, *moderate*, and *high* categories is 1.2%, 6.32%, and 12.50%, respectively, which is within the interval probability estimated: [0, 5)%, [5, 15)%, and [15,.)%.

Table 1.1: REGICOR data [8] on the ten-year incidence rate of CVD event.

Risk category and interval probability	Subjects (%)	Subjects with event (%)	event in the risk group (%)
Low < 5	2449 (65.76%)	31 (25.83%)	1.27%
Moderate $\in [5, 15)$	1139 (30.59%)	72 (60.00%)	6.32%
High ≥ 15	136 (3.65%)	17(14.17%)	12.50%
TOTAL	3724 (100%)	120 (100%)	3.22%

Despite these functions accurately stratify individuals into different categories, the majority of cardiovascular events occur in individuals classified as being at medium risk [13]. One example are the values in the third column in Table 1.1 which show that the *moderate* category concentrates the highest percentage of events (60%). Moreover, the cut-off points that define the risk stratification in *low*-risk group, *moderate*-risk group, and *high*-risk group have practical implications for deciding pharmacological intervention measures. According to [15], treating populations is only cost-effective in

the high-risk category. In particular, this study discusses the effectiveness of statins –treatment used to lower cholesterol levels in the blood and reduce the risk of heart disease– in a population with varying heart disease risk classification. The authors suggest that the treatment may benefit intermediate-risk patients, but decisions should consider net benefit, safety, and patient preferences due to a higher number of individuals included in this category. Statin treatment reduces cardiovascular risk and should remain a priority in managing patients at high risk. Nonetheless, the substantial number of individuals falling within the intermediate-risk category requiring treatment raises suitability concerns.

These examples provide evidence of the poor discriminative ability of classical risk factors, which is a recurrent observation in cardiovascular risk classification [13]. In particular, this fact makes the stratification strategy ineffective in treating the population of the *moderate* group. Therefore, new pathological information should be considered to reclassify individuals from this group to the *high*-risk group.

Risk assessment using CA US images

The tissue of CA walls provides information about the patients' arteries and cardiovascular health. For this reason, the study of CA US plaque images has been considered clinically relevant. Moreover, the long induction period of atherosclerosis makes it suitable for the study of subclinical CVD for preventive purposes. Several attempts in the literature tried to assess the cardiovascular risk of subjects using CA image features ([16, 17, 18, 19]). These works use CA image features related to IMT and atherosclerotic plaque (such the size or texture based on gray level). These features are combined with other risk factors to create risk prediction functions. While all risk functions are improved by adding these types of features, there has been no significant improvement in the predictive capacity of classical risk factors [13]. Additionally, these types of features have not been specifically tested to observe improvements in reclassification. The central aim of the clinical research in this thesis is to address these questions, which also serve as motivation for all the technical research carried out.

1.2 Technical introduction

1.2.1 Artificial intelligence and computer vision

Artificial Intelligence (AI) involves the development of algorithms and systems –a collection of hardware, software, and algorithms, that work together– that enable machines to perform tasks that typically require human cognitive functions, such as learning, reasoning, problem-solving, perception, language understanding, and decision-making. AI

has applications in various fields, including robotics, healthcare, finance, entertainment and so on [20].

Computer vision is a subfield of AI that specifically deals with the interpretation and understanding of visual information from the world, just like humans do. AI techniques, such as Machine Learning (ML) and Deep Learning (DL), play a crucial role in advancing computer vision. These techniques enable computers to learn from visual data, allowing them to recognize patterns, objects, and features within images and videos. Some of the current applications of computer vision include optical character recognition, mechanical inspection, warehouse picking, self-driving cars, drone-based photogrammetry and medical imaging [21].

The field of ML can be described as the study and development of computer algorithms that allow the creation of models to automatically learn patterns and make predictions or decisions based on data [22]. In the context of computer vision, traditional ML techniques often involve the manual extraction of relevant image features –numerically representation that summarize the image in question– that allow to better discriminate and classify the different labels –categories, classes, or identifiers assigned to images or elements within them–. These features could include aspects like edges, textures, or color histograms and they are used to train the models[21].

DL is a subset of ML that uses Neural Networks (NN), which are composed of multiple interconnected layers (called hidden layers) of nodes. NN takes input data through an input layer, processes it through hidden layers using learned weights, and produces an output through an output layer. NN are able to extract a high level representation of data that are most relevant for a specific learning task such as pattern recognition –the process of identifying and classifying patterns within visual data–. In computer vision, DL has revolutionized the field by allowing computers to learn directly from raw image data, without the need for manual feature engineering. DL has proven to be highly effective in handling complex visual tasks, leading to many advancements in computer vision[21].

Deep Neural Networks (DNNs) are NN with a significant number of hidden layers allowing to improve learning capacity. Convolutional Neural Networks (CNNs) are the most commonly DNNs used for image-related tasks. Its most basic characteristic is that they are composed of convolutional layers, among others. Convolutional layers apply convolution operations over image pixels, creating multiple level representations of the structures appearing on the images. These structures go from basic edges and colours in the initial layers to more complex object parts or spatial object relationships in the final layers [23].

1.2.2 Artificial intelligence in healthcare

Artificial intelligence has undergone a rapid growth in recent years, covering advances in both theoretical and practical aspects. In the healthcare sector, AI-based methods and tools have played a critical role in solving a variety of medical and healthcare-related issues, saving time, costs, and lives as well as fostering economic resilience particularly under the COVID-19 pandemic environments [24].

In particular, CNNs have gained significant relevance in the clinical field due to their remarkable ability to analyze medical images and contribute to improved diagnostics and patient care. CNNs demonstrate exceptional performance in tasks like detecting abnormalities, tumors, and disease-related features in a wide range of medical imaging modalities, including X-rays, Computerized Tomography (CT), Positron Emission Tomography (PET), and Magnetic Resonance Imaging (MRI), among others. This technology enhances the accuracy and speed of diagnoses, enabling healthcare professionals to identify conditions at earlier stages and make treatment decisions. Moreover, CNNs aid in reducing human error and variability, while also assisting in surgical planning (such as preoperative scans, to identify important structures, anomalies, or potential areas of concern), and monitoring patient progress.

1.3 Regicor project and dataset

The REGICOR project[1] began in 1978 as the Girona Heart Registry at the Josep Trueta Hospital in Girona. Later, it became a population registry that included several hospitals in the territory of the province of Girona. Now the project brings together more than 50 researchers from the Hospital del Mar Medical Research Institute (IMIM), from the Cardiology Services unit at Josep Trueta Hospital and the primary care research unit in Girona. The research focus is the population distribution of CVDs and associated risk factors, and improved prevention tools and strategies. The REGICOR mission is to contribute to the available knowledge about the magnitude and causes of CVDs. The final objective is to contribute to a significant reduction in the burden of these diseases.

The REGICOR project investigates the role in the development of CVDs from molecular bases to population perspective. A branch of this project is a cohort study with a follow-up of more than 30 years which began the first recruitment between 1995 and 2005 [25]. This study randomly selected a group of individuals –7,571 (52.0% women) inhabitants, to be precise– from the province of Girona to represent the general population older than 25 years. These individuals were actively followed [8]. The study

[1] https://regicor.cat/

consists of three recruitment stages: in 1995, 2000 and 2005 (involving 1480, 2540 and 3551 individuals, respectively). In the third recruitment, the subjects were older than 35 years. All these stages involved three face-to-face encounters (the baseline and two follow-ups) with the recruited individuals for data collection. In particular, general data such as sociodemographic information, risk factors, anthropometric measurements, diet, medications, etc., were collected from these individuals in an initial assessment and two subsequent follow-up assessments. Furthermore, non-face-to-face follow-ups were conducted annually from the beginning of the study to gather information on cardiovascular events.

Moreover, in this project branch, during the first face-to-face follow-up, cross-sectional US images of the three segments (CCA, bulb, and ICA) of the CAs (left and right) were collected from approximately 5,000 individuals. The scans were performed between 2005 and 2015 using the Acuson XP128 US system equipped with an L75-10 MHz transducer. Longitudinal US images were obtained in B-mode with a resolution of 0.043 mm/pixel and a size of 470x445 pixels. The original images were saved in DICOM format and then converted to PNG. Additionally, images of approximately 50% of these individuals were sent to the Academic Vascular Image Center in Amsterdam[2] (AVICA) for analysis. All images were analyzed by AVICA experts who, using the validated semi-automatic software e-track [26, 27], extracted the IMT value for each image.

The main dataset for this thesis comprises the REGICOR images, the IMT values obtained using the semi-automatic method, clinical data from both the baseline and the first follow-up, and information about cardiovascular events.

1.4 Goals and objectives of the thesis

The final objective of this thesis is to improve the prediction of cardiovascular risk using CA US images. The necessary path taken to achieve this main objective is composed of five conceptual stages which are described below:

(1) CIM region segmentation: To delineate the CA region where the IMT measurement is supposed to be estimated.

(2) IMT estimation: To compute the IMT from the CIM region segmented before.

(3) Plaque detection: To detect the presence of atherosclerotic plaque (if there is any) and its location within the CIM region.

(4) CIM region and plaque characterization: To characterize the CA wall and

[2]https://www.abc.uva.nl/research/institutes/institute-articles/academic-medical-center-amc.html

the plaque (if there is any) by learning relevant visual features from the CA image.

(5) Cardiovascular risk prediction improvement: To use relevant learned features from the CA image, particularly from the atherosclerotic plaque, that enhance cardiovascular risk prediction, specifically the reclassification.

Figure 1.3 illustrates these stages and the thesis contributions derived from each one of them.

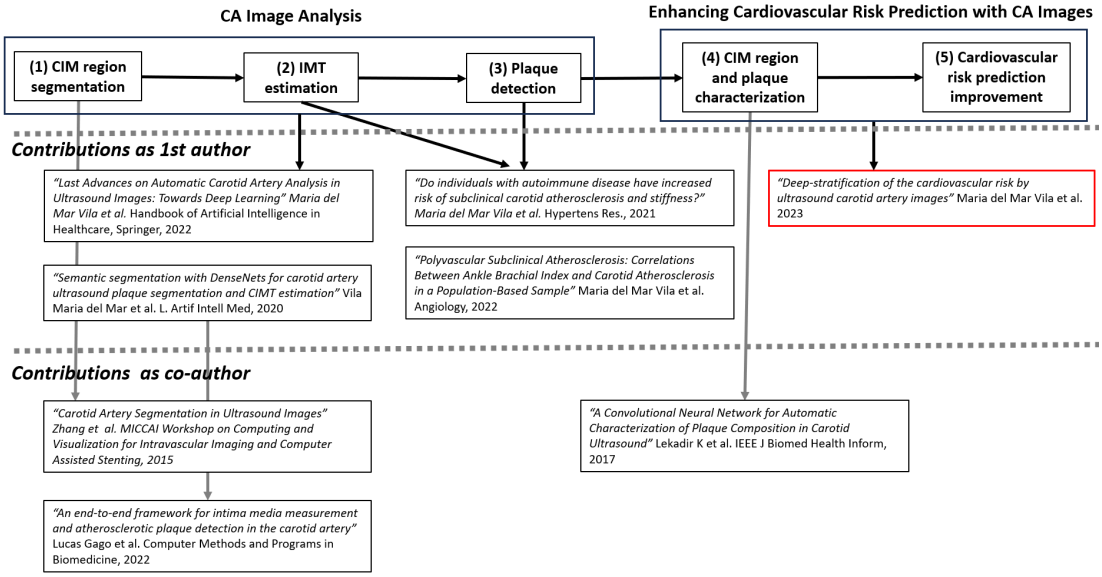

Figure 1.3: This figure shows the conceptual stages addressed in this thesis. Below the dotted line, the research contributions related with each stage are shown.

Next, we detail the goals and clinical applications that we face in this thesis:

i) Given the common use of CA US images for subclinical atherosclerosis detection, which involves measuring arterial IMT and identifying atherosclerotic plaques, it is essential to employ automated segmentation approaches to delineate the CIM region and accurately estimate the IMT value. CNNs have gained prominence in the clinical field due to their exceptional capacity for analyzing medical images. Thus, the first goal of this thesis is to develop a CNN-based method for the precise identification and interpretation of specific anatomical components within the CA, with a particular focus on plaque detection. Importantly, this approach aims to facilitate the rapid and efficient estimation of IMT and plaque detection across extensive image datasets. This proposal encompasses stages 1, 2 and 3 (Figure 1.3) and it is addressed in Chapter 2 of this thesis.

ii) This thesis presents two clinical applications of the IMT value estimation and plaque detection method developed in the stages 2 and 3 (Figure 1.3). The first clinical

application deals with autoimmune diseases. Autoimmune diseases may prematurely lead to arterial degeneration due to chronic inflammation, increasing the risk to develop CVDs. CVDs are caused by changes in the vascular wall and therefore affect all arteries, in particular showing alterations in the IMT and the arterial stiffness of the CA. In our study, we compare the prevalence of subclinical atherosclerosis and arterial stiffness in individuals with longstanding autoimmune disorders to the general population. This study is addressed in Chapter 3 of this thesis.

iii) The second clinical application aims to relate two measures for the detection of subclinical atherosclerosis. The long development period of atherosclerosis allows for preventive study using measures like Ankle Brachial Index (ABI) –a test that compares blood pressure in the ankles to that in the arms– in the lower limb and IMT in the CA to predict cardiovascular events. However, the correlation between lower limb and carotid atherosclerosis, especially in the general population without intermittent claudication history, remain underexplored. The work presented in Chapter 4 of this thesis evaluates this correlation in general population.

iv) The final goal of this research project is to improve the survival model for risk stratification using CA US images. Analyzing these images is useful for cardiovascular risk assessment as they provide information about the vulnerability of atherosclerotic lesions in other arteries. Our research aims to characterize CA wall and plaque, using CA US images and DL techniques, to learn new feature embeddings. These embeddings not only capture underlying data relationships and patterns but also preserve relevant information while filtering out irrelevant details. This enhances risk prediction and stratification for cardiovascular events ranging from moderate to high categories. This approach encompasses stages 4 and 5 (Figure 1.3) and it is addressed in Chapter 5 of this thesis.

1.5 Contributions

This work contributes to research in the field of ML and healthcare imaging through the following publications during the thesis period:

Primary Contributions (publications as first author)

1. Published (citations 32) *"Semantic segmentation with DenseNets for CA ultrasound plaque segmentation and CIMT estimation". Maria del Mar Vila, Beatriz Remeseiro, María Grau, Roberto Elosua, Àngels Betriu, Elvira Fernandez-Giraldez, Laura Igual. Artif Intell Med 2020* [28]. This article focuses on medical image processing, specifically the development of a DL method designed to segment and contextualize the CIM region, estimate IMT, and detect the presence

of atherosclerotic plaque.

2. Published (citations 2) *"Do individuals with autoimmune disease have increased risk of subclinical carotid atherosclerosis and stiffness?". Maria del Mar Vila, Beatriz Remeseiro, Laura Igual, Roberto Elosua, Rafael Ramos, José Manuel Valdivielso, Ruth Martí-Lluch, Jaume Marrugat,María Grau. Hypertens Res. 2021* [29]. This article is a clinical application of IMT measurement estimation and plaque detection that analyzes the relationship between IMT measurements and autoimmune diseases.

3. Published (citations 1) *"Polyvascular Subclinical Atherosclerosis: Correlations Between ABI and Carotid Atherosclerosis in a Population-Based Sample". Maria del Mar Vila, Laura Igual, Beatriz Remeseiro, Roberto Elosua, Rafel Ramos, Jose Manuel Valdivielso, Ruth Martí-Lluch, Jaume Marrugat, Maria Grau. Angiology Vol 74(5) 443-451 2022* [30]. This article is a clinical application of IMT measurement estimation and plaque detection that analyzes the relationship between subclinical measurements of atherosclerosis: IMT and ABI.

4. Published (citations 15) *"Last Advances on Automatic Carotid Artery Analysis in Ultrasound Images: Towards Deep Learning". Maria del Mar Vila, Beatriz Remeseiro, María Grau, Roberto Elosua, and Laura Igual. Handbook of Artificial Intelligence in Healthcare, Springer, 2022* [24]. This book chapter presents a review of automatic techniques for IMT measurement and plaque assessment from CA US images.

5. Sent (Q2 journal) *"Deep-stratification of the cardiovascular risk by ultrasound CA images". Maria del Mar Vila, Lucas Gago, Pablo Pérez Sánchez, Beatriz Remeseiro, Maria Grau, Laura Igual.* This article is about the creation of a cardiovascular risk prediction function that utilizes information from CA US images extracted with NNs.

Secondary contributions (publications as co-author)

6. Published *"Carotid Artery Segmentation in Ultrasound Images". Chen Zhang, Maira del Mar Vila, Petia Radeva, Roberto Elosua, María Grau, Àngels Betriu, Elvira Fernandez-Giraldez, Laura Igual. MICCAI Workshop on Computing and Visualization for Intravascular Imaging and Computer Assisted Stenting 2015* [31]. This work proposes a ML method for CIM region segmentation in CA US images.

7. Published (citations 132) *"A Convolutional Neural Network for Automatic Characterization of Plaque Composition in Carotid Ultrasound". Karim Lekadir, Alfiia Galimzianova, Àngels Betriu, Maria del Mar Vila, Laura Igual, Daniel L. Rubin, Elvira Fernández, Petia Radeva and Sandy Napel. IEEE J Biomed Health Inform 2017; 21(1): 48-55*[32]. This article proposes a DL approach based on CNNs to automatically identify different constituents of atherosclerotic plaque (plaque composition characterization) in CA US images.

8. Published (citations 5) *"An end-to-end framework for intima media measurement and atherosclerotic plaque detection in the carotid artery". Lucas Gago, Maria del Mar Vila, María Grau, Beatriz Remeseiro, Laura Igual. Computer Methods and Programs in Biomedicine 223, 2022* [33]. This article presents an improved DL method for estimating IMT and detecting the presence of atherosclerotic plaque, continuing from previous research [28].

Figure 1.3 illustrates the contributions, both as the first author and a co-author, derived from the stages mentioned in the previous section.

1.6 Thesis organization

This section provides an overview of the organization and structure of this thesis, including the chapters and their respective topics to guide the reader through the work.

Chapter 2 This chapter involves the stages 1, 2 and 3 from Section 1.4 (see Figure 1.3). Thus, it reviews automatic techniques that have been introduced in the literature for CA segmentation, allowing IMT measurement and plaque detection in CA longitudinal B-mode US images. Moreover, this chapter presents a DL approach for IMT estimation and plaque detection, using a fully automatic single-step approach based on CA semantic segmentation.

Chapter 3 & **Chapter 4** These chapters present two clinical applications derived from the stages 2 and 3 from Section 1.4 (see Figure 1.3). **Chapter 3** presents a study about the impact of chronic inflammation in autoimmune diseases on subclinical atherosclerosis and arterial stiffness. **Chapter 4** contains the work that explores the correlation between lower limb atherosclerosis biomarkers and carotid atherosclerosis indicators such as CCA IMT and plaque presence.

Chapter 5 This chapter involves the stages 4 and 5 from Section 1.4 (see Figure 1.3). Thus, it reviews image-based techniques to characterize atherosclerotic plaques and CA walls in B-mode US longitudinal images in order to predict cardiovascular risk and

events. Moreover, this chapter presents a DL approach that uses deep CA US image features to improve risk stratification and reclassification.

Chapter 6 This chapter presents a summary of the key findings and contributions of the thesis and discusses their implications. Moreover it exposes the limitations, offers suggestions for future research and discusses the revolution of DL techniques in medical imaging.

Chapter 2

Deep learning proposal for carotid IMT estimation and plaque detection

2.1 Introduction

This section studies the problems of CIM region segmentation, IMT estimation, and plaque detection in CA longitudinal B-mode US images. In this section, we review the state-of-the-art of automatic methods to solve these image analysis problems (part of this review is included in our chapter "Last Advances on Automatic Carotid Artery Analysis in Ultrasound Images: Towards Deep Learning" published in [24]). Moreover, we introduce our approach presented in [28], which is a fully automatic single-step, based on DL, approach for CA Semantic Segmentation (SS). This SS method involves distinguishing various anatomical components in the CA image and encompasses CIM region segmentation, IMT estimation, and plaque detection in CA longitudinal B-mode US images

2.2 State of the art

B-mode longitudinal US images are commonly used for carotid IMT estimation and to detect sublcinical atherosclerosis. The carotid IMT is conventionally measured manually by a trained operator from the B-mode US scan images. The methodology is highly user-dependent, time-consuming, tedious, and infeasible when using large image databases.

Several computerized techniques have been developed for automatically estimating the carotid IMT measurement. The automated procedure for estimating carotid IMT first requires a CA image interpretation to identify and segment the CIM region, where the IMT is then measured. CA image interpretation consists of localizing the different anatomical components of the CA, such as lumen, far wall, near wall, Bulb, and CCA (see Figure 2.1 (left)). In particular, Mannheim consensus [7] states that the IMT for CCA images is estimated 1cm distal from the Bulb, which reflects this necessity. As it is shown in Figure 2.1 (left), carotid IMT estimation and plaque detection only needs the segmentation of the region between LI and MA interfaces. We call Region of Interest (ROI) the bounding box in the image containing these both interfaces. The LI and MA interfaces delimit the segmentation of CIM region within that ROI. Carotid arterial wall assessment may include the CCA, bulb or ICA segments. Figure 2.1 shows an example of the CIM region in CCA (left) and bulb (right) segments. The ICA has an anatomically similar shape to that of the CCA; however, it has poorer image quality because it is less accessible with the US device.

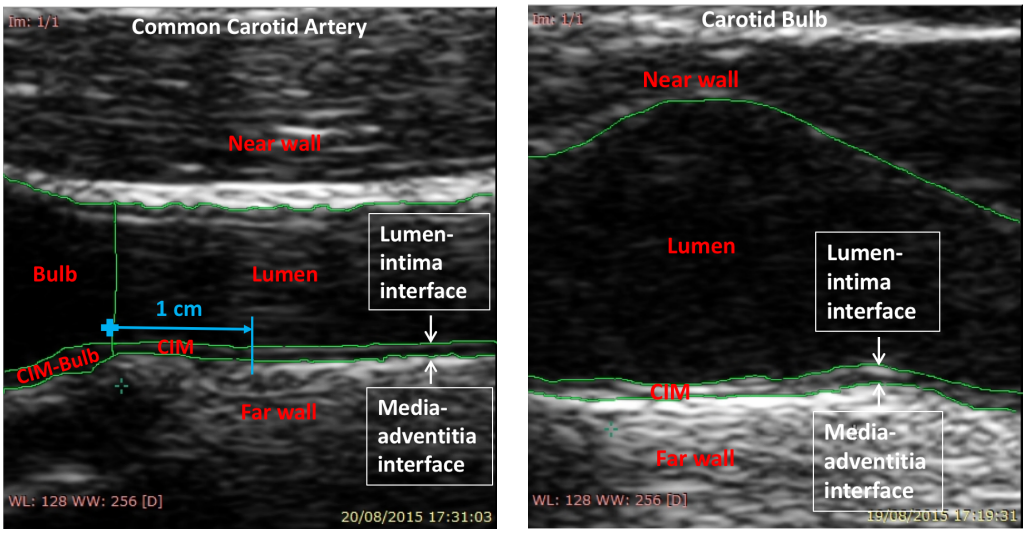

Figure 2.1: CCA (left) and Bulb (right) longitudinal B-mode US images. The different parts of the CA are delimited with green lines. In both cases the IMT is estimated in the CIM region from the far wall. The IMT in the CCA is measured approximately 1 cm distal from the carotid Bulb.

The difficulties in CA segmentation in B-mode US scan images come from the following issues:

1. These images have a low signal-to-noise ratio. It is well known that noise and the presence of speckles represent the most prominent problem in US imaging.

2. The acquisition of the US is user-dependent, and the quality of the image strongly

depends on the scanner used and its settings.

3. The high variability in vessel morphology in general together with the variability due to atherosclerosis disease make the task difficult.

Basic image processing techniques for CIM region delineation and atherosclerotic plaque segmentation presented in the literature include, among others, Hough transform [34], edge detection [35, 36] and snakes [37, 38, 39, 40]. Moreover, AI solutions, such as ML and DL approaches, serve the same purpose. On one hand, ML techniques are based on handcrafted features to segment the CIM region. In this case, the feature extraction is independent of the actual model of classification [31, 41, 42]. On the other hand, the feature extraction and model characterization are indifferent of each other in DL methods; i.e., the system has the ability to automatically learn the features of the model which better discriminate for the CIM region segmentation [28, 33, 38, 43, 44, 45, 46, 47].

Review articles [48, 49] present more references of studies that use image processing, basic ML techniques and also statistical methods. More recent reviews [50, 51] show the evolution and impact of the fast-changing AI technology on CIM region and atherosclerotic plaque segmentation. The first review [50], show the influence of automatic AI techniques in a clinical practice guidelines for CVD risk to improve patient outcomes. In particular, it includes a quantitative search of the latest ML and DL techniques for automated carotid IMT measurement techniques and how they have evolved in the last 15 years. The second review [51] presents a categorization consisting of three generations for CIM region and atherosclerotic plaque segmentation systems: (1) conventional methods (image processing methods based on the primary threshold to get the edges of the CIM region), (2) contour-based methods and (3) intelligence-based methods using the ML and DL methods. In particular this review focus on how ML and DL techniques can be used for this purpose and it presents the details about studies using CCA images.

2.2.1 Fully automated methods for CIM region segmentation

According to Loizou [49], the methods can be broadly classified into two categories. The first category includes techniques that require user interaction, i.e., semi-automatic; whereas the second one includes fully automatic methods. Semi-automatic approaches [36, 40] require user interaction for manual initialization to select the ROI and/or to correct wrong results during examination. In general, the manual ROI selection together with this type of interactions result in better performance. The best semi-automatic methods found in the literature for clinical practice are the ones that offer visual feedback during image acquisition instead of analyzing stored images [36].

In contrast, fully automatic methods [28, 31, 33, 37, 41, 42, 43, 45, 47] run without any initial setting or user interaction. The main advantage of these techniques is that they are able to process large amounts of data. Furthermore, they allow the reproducibility of results, and save time and resources. Preliminary efforts using ML [31, 41, 42] and DL [38, 43, 44, 45, 46, 52, 53, 54] in fully automatic carotid IMT evaluation are presented in the literature. Among all these, the $AtheroEdge^{TM}$ [41] system is remarkable; it is a patented software frequently used in the literature. Its proposal is a method based on splines and elastic contours that achieves clear edge tracing but fails in noisy corners. Lara et al. proposed several carotid IMT estimation methods using windowing processes on a ROI and a feed-forward network for pixel classification [52, 53, 54]. Standard multi-layer perceptron was introduced in [54], but the best results from the same author are obtained in [43] where an auto-encoder was also proposed for CA image interpretation. However, despite all these sophisticated techniques, these approaches do not outperform the snake-based method presented in [37]. For their part, Zhang et al. [31] proposed a two-step segmentation method of the CIM region based on patch-based classification and stacked sequential learning. Later, patch-based CNNs were used in different steps for carotid IMT estimation [45]. More specifically, this work uses US videos instead of a unique frame and adds an extra first step for selecting a specific cardiac cycle period. Despite the DL advantages, ML techniques applied to CIM region segmentation are still present in the literature. For instance, Qian and Yang [42] presented an approach to automatically segment plaque that uses several ML methods and combines them in an iterative algorithm. Rajasekaran et al. [38] used a CNN for the detection of a ROI, although snake algorithm was further used to extract the boundaries of LI and MA layers. Biswas et al. [46, 44] proposed two interesting approaches based on a combination of two DL models. Firstly, they used a method that consists of a convolutional encoder/decoder to first extract features and then created the segmented images from them [46]. In particular, the training system uses two kinds of GT, one for LI and other for MA, which lead to the design of two DL systems. However, the final stage of this approach still needs a ML-based "refinement" in order to increase the accuracy of the system. More recently, they proposed an interesting two-stage method based on two independent DL models [44]. In this case, one model uses a CNN with patch images as input to form the ROI, and the other model uses a FCN to segment the CIM region within that ROI. In particular, this DL approach uses patches instead of the whole image at once, allowing a better control of the small regions of the image. Despite the novelty of these proposals, they require a complex system because they are composed of two sophisticated DL models.

Single-step approaches

To the best of our knowledge, all the aforementioned DL segmentation techniques are two-step approaches that define separate methods to first locate the ROI (performed manually in the case of semi-automatic methods); and second, delineate the CIM region within the ROI. On the contrary, our proposal Vila et al. [28], presented a single-step DL approach for automatic CA image interpretation. This approach is based on SS using Densely Connected Convolutional Networks (DenseNets) [55], which were designed to facilitate the training of very deep networks due to a reduction in the number of parameters and the reuse of feature maps. This proposal represents the first attempt in the literature to accurately segment and interpret the different anatomical components of the CA (lumen, far wall, near wall, Bulb, CIM region and CIM-Bulb region, see Figure 2.1), which has demonstrated to be helpful in the proper estimation of the IMT. Using the segmented regions, a straightforward approach for carotid IMT estimation and plaque detection is defined. Later, this work was enhanced by the study proposed in [33], which is a SS model based on U-Net with EfficientNet as the backbone for CCA and bulb territories. Moreover, this study proposes another model consisting of a regression and classification model, using the original image and the segmented image as the input. This novel method is based on a CNN designed using Bayesian optimization and is capable of making real-time predictions of the maximum and average carotid IMT and the presence of atherosclerotic plaque, also in CCA and bulb territories. Another single-step DL approach is presented in [47], which performs a comparison of several methods based on the U-Net architecture to assess the atherosclerotic plaque segmentation in CCA and ICA territories.

2.2.2 Comparison of relevant works for CIM region segmentation and IMT estimation

Table 2.1 summarizes the most relevant proposals for CIM region segmentation and IMT estimation presented in the literature and it compares several characteristics of every method. The different characteristics reported are the following:

- Column "Segmentation Method". A little more than a half of the recent methods are based on DL techniques. In particular, different architectures of NNs are adopted in 9 out of the 16 works reported.
- Column "Method SA/FA". It is worth mentioning that the Semi-Automatic methods do not achieve better results than the Fully-Automatic methods in all cases.
- Column "Proc. Time per Frame". The information of the processing time per frame is not provided in all the papers. It is important to note that even if the

Author	Year	Segmentation Method	Method SA/FA	Proc. Time per Frame	Image Modality	Territory	Presence of Plaque	N	Different Devices	Mean IMT Error (mm)
Faita et al. [36]	2008	Edge Detection	SA(2)	*NS*	V	CCA	No	150	No	0.001
Molinari et al. [35]	2012	Edge Detection	FA(2)	<15s	UF	CCA	*NS*	365	Yes	0.078
Loizou et al. [39]	2013	Snakes	SA(2)	28s	UF	CCA	Yes	20	No	0.065
Molinari et al. [41] $AtheroEdge^{TM}$	2014	Snakes & Basic ML techniques	FA(2)	2s	UF	CCA	*NS*	885	No	0.022
Menchón-Lara et al. [43]	2015	NN & Auto-Encoders	FA(2)	1.4s	UF	CCA	*NS*	55	No	0.018
Bastida-Jumilla et al.[37]	2015	Frequency-Domain & Snakes	FA(2)	12.2s	UF	CCA	*NS*	46	No	0.014
Zhang et al. [31]	2015	Patch-based & Basic ML techniques	FA(2)	*NS*	UF	CCA	Yes	100	Yes	1.37% (point-to-point relative error)
Shin et al. [45]	2016	CNN & Patch-based	FA(2)	*NS*	V	CCA	*NS*	92	No	0.023 per interface (LI and MA)
Zhao et al. [40]	2017	Snakes	SA(2)	0.24s	V	*NS*	Yes	*NS*	Yes	0.053
Qian et al. [42]	2018	Patch-based & Basic ML techniques	FA(2)	6min	UF	CCA	Yes	29	No	0.34 (average point-to-point distance)
Biswas et al. [46]	2018	CNN	FA(2)	*NS*	UF	CCA	Yes	407	No	0.124
Rajasekaran et al. [38]	2019	CNN for ROI & Active contour	FA(2)	*NS*	UF	*NS*	*NS*	500	No	0.066
Biswas et al. [44]	2020	CNN	FA(2)	*NS*	UF	CCA	Yes	250	No	0.0935
Vila et al. [28]	2020	FCN	FA(1)	0.79s	UF	CCA & Bulb	Yes	4,751 (CCA) 3,733 (Bulb)	Generalization Test	0.022 (CCA) 0.06 (Bulb)
Gago et al.[33]	2022	FCN for semgentation CNN for regression	FA(1)	0.04	UF	CCA & Bulb	Yes	4,727 (CCA) 3721 (Bulb)	No No	0.0082 (CCA) 0.0321 (Bulb)
Pankaj et al.[47]	2022	FCN	FA(1)	*NS*	UF	CCA & ICA	Yes	379 (CCA) 970 (ICA)	Yes	-

UF: Unique Frame, V: Video, SA: Semi-Automatic, FA: Fully-Automatic, *NS*: Not Specified in the referenced paper

Table 2.1: Most recent/relevant techniques for CA segmentation and IMT estimation together with their main characteristics: author(s) and reference, year of publication, the segmentation method used, if the method is semi-automatic or fully-automatic ("(1)": one-step, and "(2)": two-step), the processing time per frame, the type of data as a unique frame or video, the artery territory, the presence of plaque in the images of the dataset, the number of images of the dataset (N), if the images were acquired from different devices, and the mean IMT error in mm.

DL methods can take quite a long time to be trained (depending on the power of the hardware, Graphics Processing Unit (GPU), and other properties), the important factor to consider is the time spent on testing, which is generally fast.

- Column "Image Modality". Regarding the image modality, there are several works which consider video instead of an unique frame. These videos are sequences of images that capture two phases of the cardiac cycle: diastole (when the heart relaxes) and systole (when it contracts). These phases, and consequently the videos themselves, exhibit distinct characteristics based on the health of the artery. This variation enables videos to estimate carotid IMT during both periods, yielding additional information about arterial atherosclerosis. Considering videos allows for the analysis of a specific cardiac cycle period, such as end-diastolic US frames [45], or both periods [36, 40]. Using both periods enhances the method's assessment robustness.

- Column "Territory". Most of the presented works and reference values from the guidelines focus only on CCA images. The image quality of other territories, such as Bulb or ICA, is worse than CCA (poorer contrast and more affected by noise, see Section 1.1.2). Moreover, successful imaging depends on the anatomy of subjects. These facts make the segmentation of the CIM region in these other territories difficult. According to Table 2.1, only [28, 33] deals with Bulb images and [47] with ICA images. However, automatic segmentation of different territories would be very useful and should be addressed if there is a will to have an impact on clinical practice.

- Column "Presence of Plaque". The shape variability of the CIM region makes difficult the design of a robust segmentation method. In the non-plaque images (i.e., images in which the plaque does not appear), the CIM region is observed as a straight thin shape, whereas the presence of plaque leads to a focal thickening of the CIM region, resulting in an irregular shape (see Figure 1.2(a)). As a consequence, most of the previous works found in the literature only face the problem of measuring the carotid IMT within plaque-free regions and discard images with the presence of plaque. Some methods reported in Table 2.1 [28, 33, 39, 40, 46, 47] broaden the target and build a general method capable of accurately estimating carotid IMT values even in the presence of plaque. This property makes the methods useful for datasets of population studies (such as the datasets considered in [28, 33]). Moreover, the presence of plaque in the dataset allows to evaluate the plaque detection ability of the proposals.

- Column "N". In terms of the number of images processed, the size of the considered datasets in the carotid IMT estimation studies is quite small. Although these sample sizes guarantee an adequate level of study power, a large-scale study (as in [28, 33]) is required to carefully assess the effect of variability on segmentation performance, and also to evaluate the systems before their application in the real praxis.

- Column "Different Devices". The different devices and settings used for image acquisition provide datasets with different image characteristics. Dealing with these differences implies a difficult challenge for the robust segmentation of CA components and IMT estimation. For this reason, most of the methods in the literature use datasets provided by a single device. Conversely, the datasets used in [28, 35, 40, 47] contain images from different clinical centers. In particular, in our work, Vila et al. [28], we validate the robustness and generalization power of our method by applying it to a second dataset, which contains images provided by a different equipment.

- Column "Mean IMT Error (mm)". A proper validation procedure should evaluate several proposals comparing the obtained carotid IMT estimation with other state-of-the-art approaches to demonstrate the superior performance of the proposed method, as done in [28]. The direct comparison of the error values presented in Table 2.1 is not fair since these values are completely influenced by the considered datasets. Even so, we can highlight the results reported in [28], since only two FA methods [43, 37] reach minor errors, although these values could be influenced by the small size of their datasets.

Author	Method	Territory	IoU	DC	Prec.	Sens.
Vila et al. [28]	DenseNets	CCA	71.21	82.99	82.17	85.30
Gago et al. [33]	U-Net with EfficientNet [56]	CCA	87.12	99.59	99.76	99.42
Pankaj et al. [47]	U-Net	CCA	-	88.37	93.28	84.57
Vila et al. [28]	DenseNets	Bulb	57.11	69.45	69.30	73.13
Gago et al. [33]	U-Net with EfficientNet [56]	Bulb	92.73	96.94	97.41	97.21
Pankaj et al. [47]	U-Net	ICA	-	89.32	93.7	85.72

IoU intersection over union, Dice Coefficient, Prec Precision, Sens Sensitivity

Table 2.2: Most relevant single-step DL approaches for CA image interpretation and their respective results in segmentation evaluation.

Table 2.2 shows a comparison of segmentation performance evaluation in DL single-step approaches for CA image interpretation. This table presents several metric evaluations for CIM region segmentation [28, 33] and the best method of atherosclerotic plaque segmentation presented in [47] in different CA territories. The first three rows of the

table show the segmentation results in CCA images, while the rest of the rows show the evaluation of segmentation in images where the image quality is worse: Bulb and ICA images. The table shows better results for segmentation using U-Net architectures, especially if the down-sampling component is replaced with a pre-trained EfficientNet B0 [33]. Note that the direct comparison of these evaluation metrics is not fair, as these values are completely influenced by the considered dataset.

2.3 Contributions of our study

As it has been shown in the previous section most of DL techniques for the CIM region segmentation are two-step approaches that define separate methods to, first, localize the ROI (made manually in case of semi-automatic methods); and second, delineate the CIM region within the ROI. In contrast, our method proposed in [28], which is presented in this chapter, employs a segmentation technique that works in an end-to-end framework. An "end-to-end framework" refers to an integrated system that addresses the entirety of CA segmentation without the need for intermediate steps that would require separate handling. This work enables the segmentation of the CIM region and other anatomical components in the CA image. Moreover, it efficiently estimates the carotid IMT and detects the presence of plaques in extensive datasets of CA longitudinal B-mode US images.

In particular, this work proposes a novel single-step (see column named "Method SA/FA" Table 2.1) DL approach for automatic CA image interpretation. This approach is based on SS using Densely Connected Convolutional Networks (DenseNets) [55], which were designed to facilitate the training of very deep networks due to a reduction in the number of parameters used and the reuse of feature maps. Our proposal represents the first attempt in the literature to accurately localize and interpret the different anatomical components of the CA (lumen, far wall, near wall, bulb, CIM region and CIM-bulb region, see Figure 2.1), which can be helpful in the proper estimation of the IMT. Using the segmented region, we define a straightforward approach for carotid IMT estimation and plaque detection.

Moreover, the majority of the proposed techniques in the literature restrict their application to five particular conditions of the CA images and datasets, which are summarized in the columns 7-11 in Table 2.1 and are explained below.

1) Most of the presented works and reference values from the guidelines focus only on CCA images. The image quality of other territories, such as Bulb, is worse than CCA (poorer contrast and more affected by noise). Also, successful imaging depends on the subjects anatomy. These facts make the segmentation of the CIM region in

Bulb difficult. None of the revised methods deal with Bulb images (see column named "Artery Territory" in Table 2.1). However, we demonstrate that the method proposed in our work is easily extensible to this different CA territory, after being successfully trained for both CCA and Bulb.

2) In the non-plaque images (i.e. images in which the plaque does not appear), the CIM region is observed as a straight thin shape, whereas the presence of plaque leads to a focal thickening of the CIM region, resulting in an irregular shape (see Figure 2.2). The shape variability of the CIM region makes the definition of a robust segmentation method more difficult. As a consequence, most of the previous works only measure the IMT within plaque free regions and discard images with the presence of plaque (see column named "Presence of Plaque" in Table 2.1). Unlike most previous works, we broaden the target and build a more general method able to accurately estimate the IMT, even in the presence of plaque. This feature makes our method useful for datasets of population studies, such as the one considered in this work. Moreover, the presence of plaque in the dataset allows us to evaluate the plaque detection of our method.

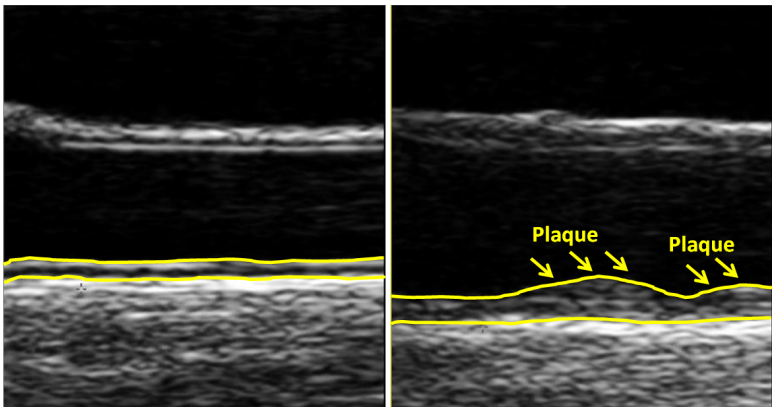

Figure 2.2: US images from CCA without plaque (left) and with atherosclerotic plaque (right).

3) In terms of the number of images processed, the size of the considered datasets in the previous carotid IMT estimation studies is quite small (see column named "N" in Table 2.1). Although these sample sizes guarantee an adequate level of study power, a large-scale study —such as the one presented in this work— is required to carefully assess the effect of variability on segmentation performance, and also to evaluate the systems before their application in the real praxis. In particular, we show an extensive evaluation of the carotid IMT measurement and plaque detection in a large dataset (REGICOR), which contains 8,484 images.

4) The different devices and settings used for image acquisition provide datasets with

different image characteristics. These differences imply difficulties for the robust segmentation of CA components and IMT estimation. For this reason, most of the methods in the literature use datasets provided by a single device (see column named "Different Acquisition Devices" in Table 2.1). In contrast, we validate the robustness and generalization power of our method by applying it to the NEFRONA dataset, which contains images provided by different equipment (see Section 2.5).

5) Regarding the validation procedure, we extensively evaluate our proposals. We compare the obtained carotid IMT estimation with other state-of-the-art approaches to demonstrate the outperformance of the proposed method (see column "Mean IMT Error (mm)" in Table 2.1). Moreover, we compare the CIM region segmentation results with other approaches and we measure the Inter-Observer Variability (IOV) of the manual segmentation showing the degree of difficulty of the problem at hand, especially in the case of Bulb images (see Section 2.5). Lastly we evaluate plaque detection in the large dataset, REGICOR, for which we obtain very promising.

2.4 Methodology

We propose a method for automatic CA image interpretation that integrates SS with other image analysis techniques for carotid IMT estimation. Figure 2.3 depicts the workflow of our approach, subsequently explained in depth.

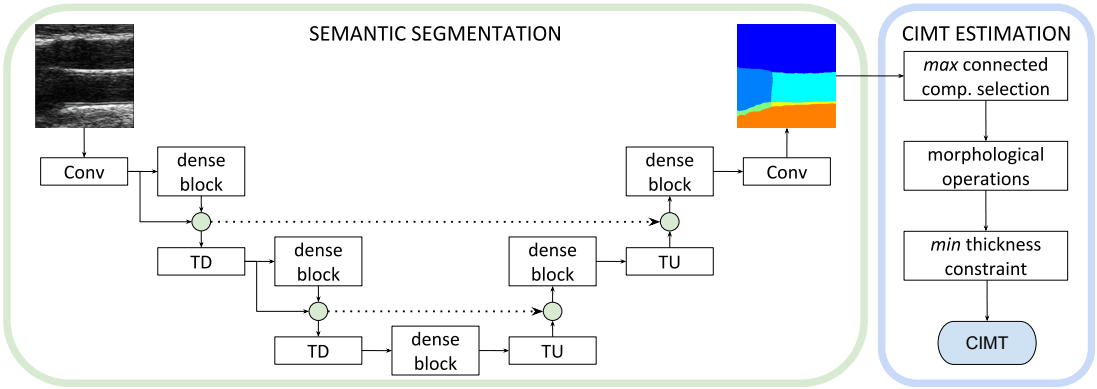

Figure 2.3: Workflow of the proposed method for semantic CA segmentation and carotid IMT estimation. The SS model is composed of a down-sampling path with Transition Down (TD) blocks, and an up-sampling path with Transition Up (TU) blocks, both including dense blocks that create the feature maps. A Convolution (Conv) is applied at the input of the network as well as at the end, to generate the final segmentation. The small circles represent concatenations, and the dotted arrows are the skip connections.

2.4.1 Semantic segmentation

In our research, CA segmentation is about solving the problem of separating the different anatomical components of the CA (i.e. lumen, far wall, near wall, bulb, CIM region, and CIM-bulb region, see Section 2.2), thus obtaining a mask with six or four different labels, depending on whether CCA or Bulb images are being analyzed, respectively. For this purpose, we propose the use of SS algorithms that work in a supervised learning framework, instead of using image features such as shapes or pixel-based features.

Fully Convolutional Networks (FCN) [57], commonly used in SS problems, are a particular case of CNNs that do not use fully-connected layers. They take an image of any size as input data and transform it to obtain a segmented image, with the same spatial resolution, by means of an inference, learning process. Figure 2.4 shows an example of two CA images (inputs to the SS model) and their corresponding segmented images (expected outputs of the SS model).

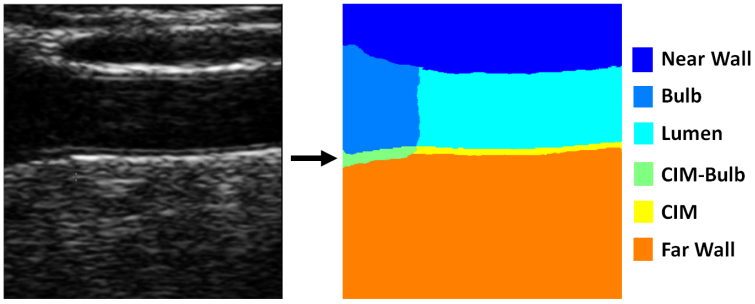

(a) CCA

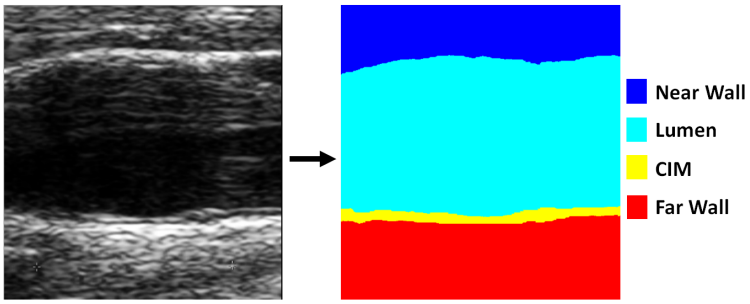

(b) Bulb

Figure 2.4: Example of the input (left) and expected output (right) of the SS model for images of both territories: (a) CCA and (b) Bulb. The legend at right details the segmentation labels.

Any CNN model can be extended to be used as FCNs and so applied to a SS problem. From the state-of-the-art architectures, we have selected Densely Connected Convolutional Networks (DenseNets) [55], an extension of the well-known Residual Networks (ResNets) [58]. DenseNets has been designed to ease the training of very deep networks,

and present some characteristics that make them very appropriate for SS: parameter efficiency, implicit deep supervision, and feature reuse.

As a result of all of these reasons, we have considered the so-called Tiramisu [59], an extension of DenseNets such as FCNs, to solve the CA segmentation problem. The Tiramisu architecture (see Figure 2.3, left) is composed of a down-sampling path with transition down (TD) blocks to extract coarse semantic features, and an up-sampling path with transition up (TU) blocks to recover the input image resolution at the output level. Both paths are connected by means of skip connections that allow the recovery of fine-grained information, and they are defined by a sequence of dense blocks that contain a set of concatenated layers, as proposed in DenseNets. The three types of blocks used in the Tiramisu model are defined as follows:

- Dense blocks are composed of concatenated layers that include Batch Normalization [60], Rectified Linear Unit [61], 3×3 convolution, and Dropout [62] (probability 0.2).
- TD blocks are composed of Batch Normalization, Rectified Linear Unit, 1×1 convolution, Dropout (probability 0.2) and 2×2 max-pooling (stride 2).
- TU blocks are composed of 3×3 transposed convolution (stride 2).

Our implementation of the SS model is in Keras[1], with Theano as backend, and is publicly available for download[2].

2.4.2 IMT estimation and plaque detection

The output of the SS process is a mask divided in different regions (see Figure 2.4: six for CCA images, and four for Bulb images). The information provided by the different regions identified in the mask are used to estimate the IMT, following the next procedure (partially illustrated in Figure 2.5):

1. The biggest connected component, corresponding to the CIM label, is identified (Figure 2.5(a)). In the case that the two biggest connected components have a similar size, we select the largest one that is more similar to the rectangular shape of the CIM region.
2. The borders of the CIM region are smoothed with basic morphological operations. In particular, these operations are *opening*, to remove small objects; and *closing*, to avoid small holes. Rectangles are used as structuring elements for these operations, with dimensions 4×8 for closing and 2×25 for opening.

[1] https://keras.io/
[2] https://github.com/beareme/keras_semantic_segmentation

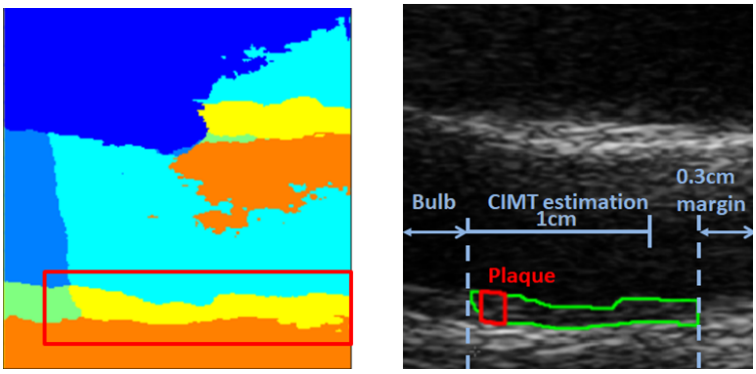

(a) Mask from a CCA image

(b) IMT estimation in CCA

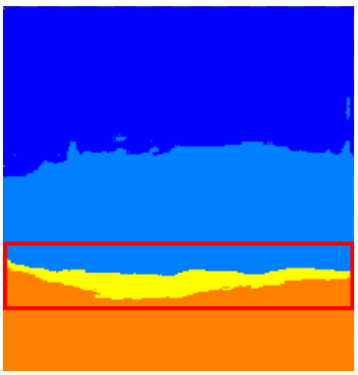

(c) Mask from a Bulb image

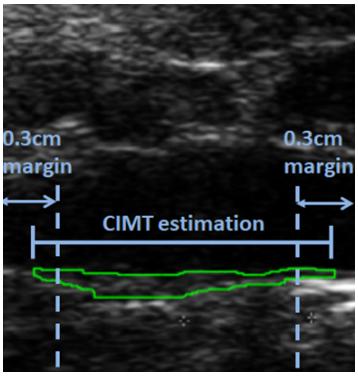

(d) IMT estimation in Bulb

Figure 2.5: Representative example of the IMT estimation procedure for CCA (top) and Bulb images (bottom). At left, masks obtained from the SS model (yellow pixels correspond to CIM region label); and the biggest, largest connected component selected as CIM region (red rectangle). At right, the CIM region obtained from the SS result (in green). (b) Left margin used to discard pixels with IMT value greater than 1.5 mm, carotid IMT estimation area (1 cm after the bulb), and plaque region (in red). (d) Right and left margins are used to discard pixels with the IMT value lower than 0.4 mm, and the carotid IMT estimation area.

3. According to the experience of technicians, image quality is not good at the ends of the image (approximately 0.3 cm in each side). For this reason, we define a margin of 0.3 cm in the right part of the CCA images (see Figure 2.5(b)), and two margins of 0.3 cm in the right and left parts of the Bulb images (see Figure 2.5(d)). Moreover, the mean values from IMT in CCA are, in general, between 0.4 mm and 1.5 mm [63]. Based on this, we discard the pixels of the CIM region that are within the lateral margins, and have an IMT value outside the range [0.4, 1.5] mm.

4. Once the CIM region is obtained, we divide the CIM region in vertical lines (each line corresponds to one pixel). For each vertical line, the absolute distance between the two borders is considered. Finally, we compute the IMT measurement as the mean from all these values.

   For CCA images the IMT is estimated 1 cm distal from the Bulb, justified from a clinical standpoint [7] (see Figure 2.5(b)).

5. Afterwards, each image is classified as containing plaque or non-plaque, using the IMT measurement and following the Mannheim Consensus (see Section 2.2).

2.5 Experiments

2.5.1 Dataset

In this work, we consider two different datasets: REGICOR and NEFRONA. REGICOR consists of a subsample of 2,379 subjects. The set of images collected for each patient were obtained from left and right CA in two different territories (CCA and Bulb), resulting in a total of 8,484 images (4,751 CCA images, and 3,733 Bulb images). The IMT reference values, given by AVICA, were used as the Ground-Truth (GT) for the carotid IMT estimation. Measurements were made in a 1-cm segment in the distal CCA (1 cm proximal to the dilation of the carotid bulb) of both the right and left arteries. Measurements were made every 1 mm in the 1 cm segment, from which the mean values were calculated. Repeatability analysis was performed in 42 participants who were examined by 3 sonographers at 2 different visits. The intraclass correlation coefficients between sonographers and within each sonographer's results for the mean of IMT in CCA were 0.83 and 0.85, respectively. The coefficient of variation was 7.3%, and the average maximum within-subject (absolute) difference was 0.098 mm. Regarding the GT for plaque detection, it was obtained using the provided carotid IMT reference values and applying the Mannheim consensus. Furthermore, the images containing plaque were finally supervised by an expert. Besides the GT for carotid IMT estimation and plaque detection, a segmentation GT was defined for a subset of

the REGICOR images. In order to obtain it, an expert (Expert1) manually delineated and labeled the different regions of the original images, using six labels for CCA and four for Bulb (written in red in Figure 2.1). Since this manual task is difficult and very time-consuming, only a representative subset of REGICOR images was labeled, including 159 CCA images (51 with plaque and 108 without plaque), and 172 Bulb images (68 with plaque and 104 without). The training set contains 141 images for the CCA and 155 images for the Bulb, whilst the rest of them were used for testing. The test images were used for the comparison of the segmentation approaches presented in Section 2.4. Additionally, the test images were manually segmented by a second expert (Expert2) to measure the IOV.

The second dataset, NEFRONA[3], from Atherotrombotic Diseases Unit Detection Hospital Arnau de Vilanova, consists of a collection of B-Mode US of the CA obtained by a Vivid BT09 device (from General Electric), with a 6-13 MHz band. For each subject of the study CCA images were captured. This dataset is formed by 27 images with the corresponding CIM regions and their IMT values (NEFRONA GT), provided by the General Electric device.

2.5.2 Validation setup

This section includes the different experiments carried out to validate our approach results, which are summarized in Table 2.3 and following described in depth.

Experiment 1: Segmentation
Purpose: comparison of different segmentation approaches
dataset: subset of REGICOR. GT: manually segmented images
images: 159 (CCA), 172 (Bulb). Train/test split: $\approx 90\% - 10\%$
Performance measures: accuracy, specificity, sensitivity, precision, Dice coefficient
Experiment 2: carotid IMT estimation
Purpose: comparison of different methods for CIMT estimation
dataset: REGICOR. GT: carotid IMT values
images: 8,484 (all of them used for validation)
Error measurement: correlation coefficient and Bland-Altman analysis
Experiment 3: Plaque detection
Purpose: comparison of different methods for plaque detection
dataset: REGICOR. GT: plaque detection (yes/no)
images: 8,484 (all of them used for validation)
Performance measures: accuracy, specificity, sensitivity
Experiment 4: Generalization power
Purpose: assessment of the generalization power of the proposed method
dataset: NEFRONA. GT: carotid IMT values
images: 27 (all of them used for validation)
Error measurement: correlation coefficient and Bland-Altman analysis

Table 2.3: Summary of the different experiments carried out for validation purposes.

[3] http://www.nefrona.es/

Experiment 1: Segmentation In order to validate the proposed segmentation method, we compared six different approaches applied to a subset of the REGICOR dataset: four DenseNets models based on Tiramisu, the U-Net method [64], and a two-step approach based on the shallow method Random Forest (RF). Regarding the Tiramisu model, we have considered two different configurations varying the depth of the network: Tiramisu56 (a total of 56 layers, 4 per dense block) and Tiramisu103 (a total of 103 layers, from 4 to 12 per block). In order to show if the SS of several anatomical components helps in the CIM region segmentation, we also compared the results provided by the two Tiramisu models (Tiramisu56 and Tiramisu103), but using only two labels (CIM region and *background*). We called this second approach Binary Segmentation (BS), whilst the one with all the labels is referred as SS. Notice that both approaches, BS and SS, were compared by considering two labels in the evaluation measure. In order to demonstrate the adequacy of using DenseNets, the U-Net was also considered in the experimentation. In this sense, it is worthy to point out that the main difference between U-Net and Tiramisu is that U-Net uses standard convolutions instead of the dense blocks proposed in the DenseNet architecture. Finally, in order to compare the NNs with classical methods, we have also considered a two-step approach based on RF. Particularly, we refer as RF2 to the two-step approach in which a ROI is first automatically extracted (pre-processing) and then a patch-based RF (multi-class) is used for pixel-wise classification. In this case, a post-processing specifically designed for this method [31] can be applied, which is referred as RF2-PP.

All the NN models were trained using a GeForce Titan X (Pascal) 12GB GPU from NVIDIA. The models' weights were initialized using the HeUniform initialization [65], and the RMSprop algorithm [66] was used as optimizer. The training process was carried out in two steps, as in [59]: 1) pre-training with random cropping for data augmentation (crop dimension: 224×224 px), learning rate $1e-3$, and batch size 3; 2) fine-tuning with full size images (image dimension: 470×445 px), learning rate $1e-4$ and batch size 1. The outputs were monitored using the pixel-wise accuracy and the dice coefficient, with a patience of 100 during pre-training and 50 during fine-tuning.

A complete set of measures was used to evaluate the performance of the different segmentation models. All of them are defined as follows, considering CIM region (positive) and Background (negative), and using the terms true positive (TP), true negative (TN) false positive (FP), and false negative (FN).

- The pixel-wise accuracy, i.e. the percentage of pixels correctly classified.

$$Acc = \frac{TP + TN}{TP + TN + FP + FN}$$

- Specificity, i.e. the proportion of negatives correctly classified.

$$Spec = \frac{TN}{TN + FP}$$

- Sensitivity, i.e. the proportion of positives correctly classified.

$$Sens = \frac{TP}{TP + FN}$$

- Precision, i.e. the proportion of true positives against all the positives.

$$Prec = \frac{TP}{TP + FP}$$

- Dice coefficient, i.e. the similarity over classes.

$$DC = \frac{2TP}{2TP + FP + FN}$$

Experiment 2: carotid IMT estimation With the aim of evaluating our method in terms of carotid IMT estimation over the REGICOR dataset, we have considered the correlation coefficient (cc) between the GT and the predicted IMT values as well as the Bland-Altman analysis. For a deep comparison, we have considered not only the methods used in the *Experiment 1* (Tiramisu56, Tiramisu103 and RF2-PP), but also other approaches found in the literature (see Section 2.2).

Experiment 3: Plaque detection The target is to evaluate our method in terms of plaque detection over the REGICOR dataset, including a comparison with the two-step approaches (RF2 and RF2-PP). For this purpose, we have used the following metrics, previously defined, considering the presence of plaque as positive and the absence of plaque as negative: Accuracy (Acc), Specificity (Spec), and sensitivity (Sens).

Experiment 4: Generalization power To validate the generalization power of our method, we trained it with the subset of REGICOR used in the *Experiment 1* and evaluate its performance in terms of IMT estimation over the NEFRONA dataset. Images from the two datasets were acquired by different devices, thus, they have different resolutions and image intensity distributions. Hence, we process the data to equate the intensity distribution of all the images and adapt the resolution. In first place, we modify the image gray levels to saturate the bottom 1% and the top 1% of all the image pixels in the two datasets. Next, we transform NEFRONA images so that they have the same resolution than REGICOR images; more precisely, from a resolution of

10.4 pixels/mm (NEFRONA) to 23.5 pixels/mm (REGICOR). In order to do that, we apply a bilinear interpolation, in which the output pixel value is a weighted average of pixels in the nearest 2-by-2 neighborhood. The CIM region of NEFRONA GT was delineated only in a small part of the image and following a different criterion than in REGICOR. For this reason, the validation of the segmentation can only be qualitative. Regarding the validation of the carotid IMT estimation, we consider the cc between IMT value from NEFRONA dataset GT and the estimated IMT, and also show the Bland-Altman analysis.

2.6 Results

In this section we report the results obtained in the four experiments previously described, summarized in Table 2.3.

Experiment 1: Segmentation Figure 2.6 depicts the comparison between the different segmentation approaches in CCA (left) and Bulb (right) test images. It can be seen that the different Tiramisu architectures clearly improve the RF2 results (mainly note improvement in DC). Moreover, making the Tiramisu model deeper by increasing the number of parameters (from 56 to 103) does not improve the results, probably due to the size of the training set. Although the BS is equivalent to SS in CCA images, the semantic information is crucial for the IMT estimation step in these images (see Section 2.4). Note that the improvement using SS is more evident in Bulb images. Regarding U-Net, its results are slightly worse than Tiramisu103 BS and are not included in the graphic. Finally, the IOV results (considering Expert1 as GT, versus Expert2) are low compared with the automatic methods results, specially in Sensitivity and DC, in both CCA and Bulb images. These results and the high standard deviations show the difficulty of reproducing the CA results in clinical trials. It is worth noting that all the measures have been computed using the Expert1's labels as GT, but the values are equivalent for the labels of Expert2.

Figure 2.7 shows qualitative examples of the CIM region segmentation results regarding three methods: a shallow method (RF) and two methods based on CNN (U-Net method and Tiramisu56 method). As can be seen, U-Net does not give an accurate result of the different areas of the image and RF oversegments the CIM region.

Experiment 2: carotid IMT estimation Figure 2.8(a) shows the correlation between the IMT values (GT and predicted) in CCA images for the best method, i.e. "Tiramisu56 SS+IMT estimation", which reaches a high cc of 0.81 (cc=0.77 when applying only Tiramisu56 SS). The result is very similar to Tiramisu103 (cc=0.80),

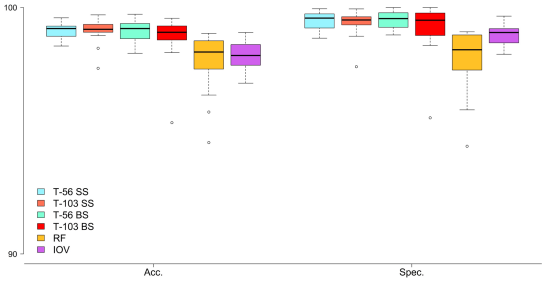

(a) Accuracy and Specificity measurements for CCA images

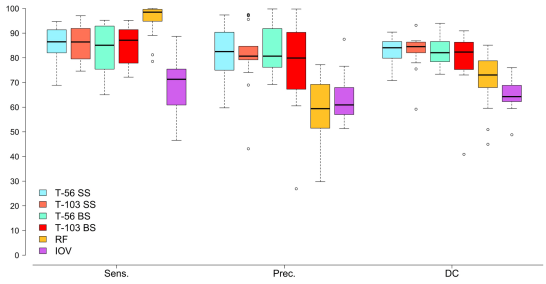

(b) Sensitivity, Precision and Dice Coefficient measurements for CCA images

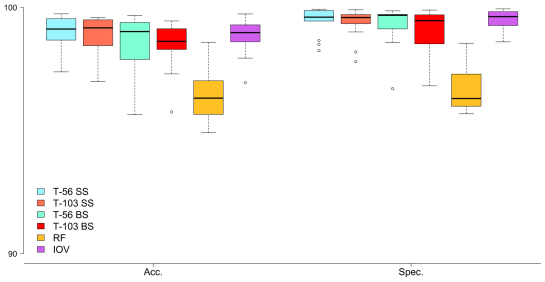

(c) Accuracy and Specificity measurements for Bulb images

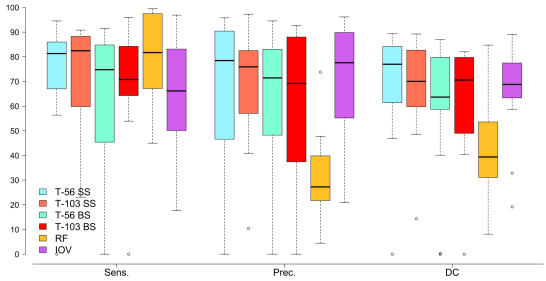

(d) Sensitivity, Precision and Dice Coefficient measurements for Bulb images

Figure 2.6: Box-plot of metrics results for the different segmentation methods and IOV. Note that the overlap measurements are split up for visualization purposes, using different scales in the abscissa axis.

in contrast to RF2-PP (cc=0.72). Regarding Bulb images (see Figure 2.8(c)), "Tiramisu56 SS+IMT estimation" achieves a lower cc of 0.43 (cc=0.34 when applying only Tiramisu56 SS), probably due to the worse quality of the images in Bulb, which makes the task more difficult in this territory. However, our proposal still outperforms RF2-PP, which only reaches a cc of 0.41.

In Figure 2.8(b), the Bland-Altman plot depicts the difference, in CCA images, between the IMT of the corresponding two values (estimated and GT) against the average of both values. This plot shows a high degree of agreement between the two measures, especially in the cases where the IMT is small (<0.5mm), which correspond to healthy population (i.e. without plaque) [63]. Furthermore, this plot shows that the predicted IMT is, on average, slightly underestimated (mean -0.02). The confidence intervals for the "mean of the differences line" (shown in red in Figure 2.8) shows that this bias is statistically significant. Therefore, in order to achieve the interchangeability of the techniques this bias cannot be avoided.

The results are similar for Bland-Altman analysis in Bulb images (see Figure 2.8(d)) and, in this case, the average slightly overestimates the IMT measure (the mean of

(a) Tiramisu56 (b) U-Net (c) RF

Figure 2.7: Qualitative results of the SS procedure using three different methods.

the differences is 0.06 and this bias is also statistically significant). Column named "Mean IMT Error (mm)" in Table 2.1 compares the mean IMT error for our method and several methods in the literature. It should be highlighted that our IMT error is low compared with other fully automatic methods reviewed in the Table. In particular, only the two-step methods [37, 43] reach a IMT error lower than our method, but in a much smaller dataset and only in one territory (CCA). In fact, the size of our dataset is much larger than the ones considered in all the rest of papers (our dataset: 2,379 subj. vs revised datasets: [36-365] subj.). Note that, as can be seen in this column of the Table, the IMT error is not always presented as the mean of the IMT error, in some cases it is presented with point-to-point relative error, average point-to-point distance, or evaluating the mean error for each interface separately.

Figure 2.9 shows qualitative examples of the CIM region segmentation results and plaque detection for four CCA and four Bulb images. The first and third columns show examples of CIM region segmentation, outlined in green, in non-plaque images; whereas the second and the fourth columns show examples of images with plaque, outlined in red.

Finally, it is important to note that the processing time to estimate the carotid IMT and detect a plaque is only 0.79 seconds, as can be also seen in Table 2.1 (column "Proc. Time per Frame").

Experiment 3: Plaque detection Table 2.4 includes the plaque detection results in CCA and Bulb images, showing a promising performance, mostly in CCA. The smaller number of plaques in the dataset gives lower sensitivity values than specificity values. Regarding Bulb images, there is still large room for improvement, probably due to the poorer quality of these images, as commented before. Note that the RF2 method needs

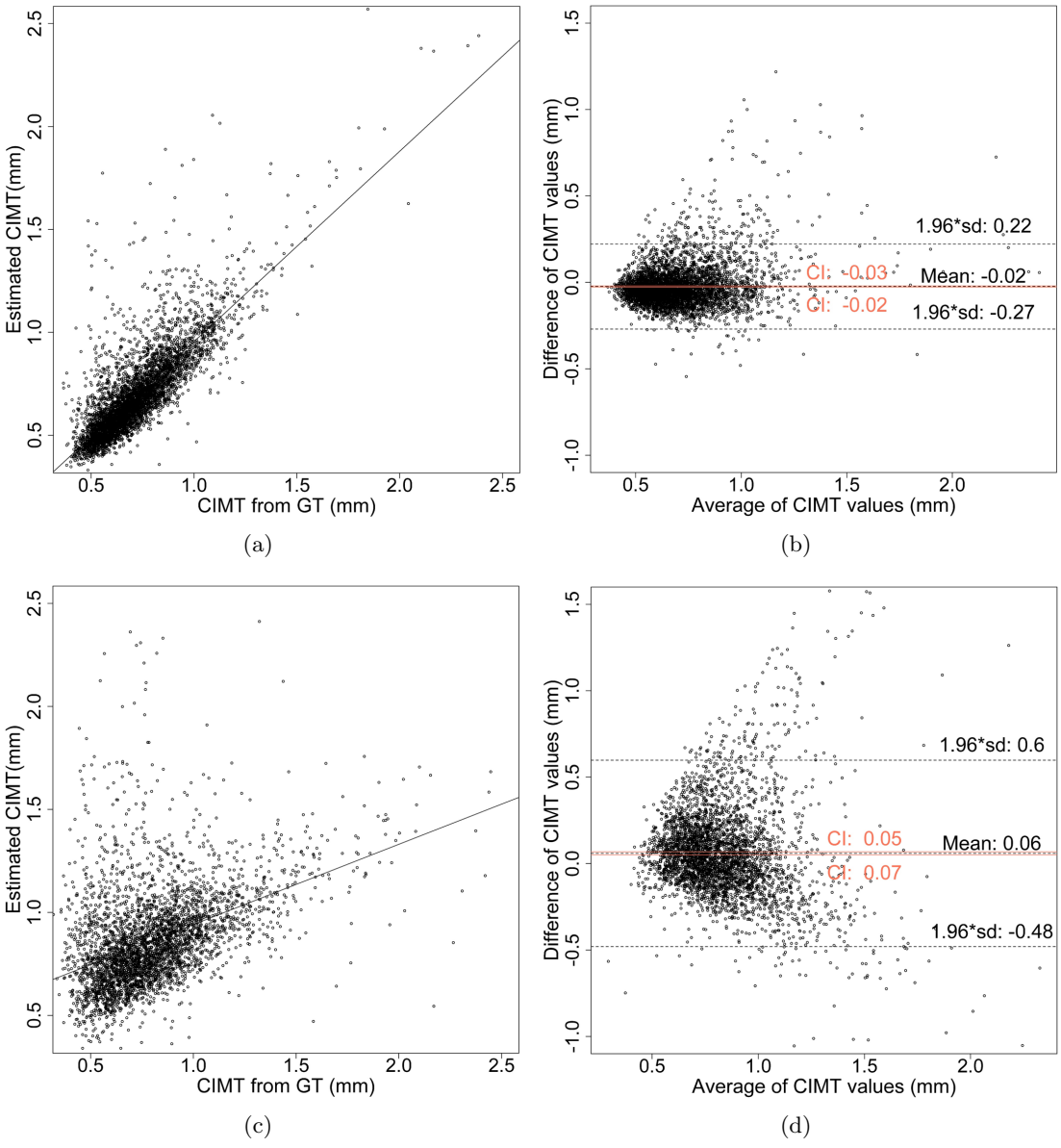

Figure 2.8: Correlation between IMT values (left), and Bland-Altman analysis (right). Both plots show the relation between GT and the estimated values in CCA images, (a) and (b); and in Bulb images, (c) and (d). Red solid lines show the confidence intervals (CI) for the "mean of the differences" line.

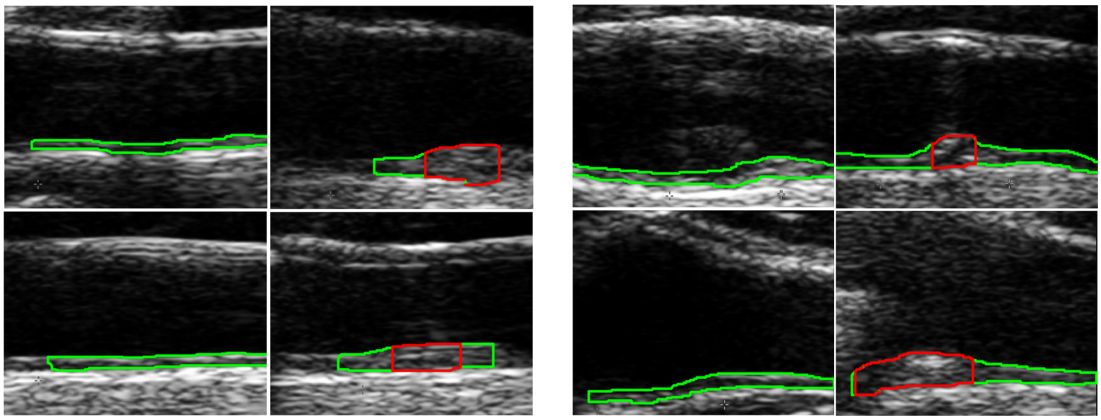

(a) CCA images (b) Bulb images

Figure 2.9: Qualitative results of the CIM region segmentation for eight different images. Green lines are the CIM boundaries and red lines the detected plaque boundaries. Images are cropped for visualization purpose.

a sophisticated post-processing to achieve similar results to our NN method.

Figure 2.9 shows qualitative examples of the plaque detection results.

Territory Images	Method	# Plaques/ Total images	Acc	Sens	Spec
CCA	RF2	50/4,722	50.05%	100.00%	49.00%
	RF2-PP	50/4,722	94.08%	86.00%	94.16%
	Our proposal	50/4,751	96.45%	80.00%	96.63%
Bulb	RF2	240/3,539	35.09%	98.33%	30.49%
	RF2-PP	240/3,539	78.50%	69.58%	79.15%
	Our proposal	264/3,733	78.09%	78.32%	75.00%

Table 2.4: Results of plaque detection in REGICOR images for different methods, the number of plaques in each territory and the following validation measures: Accuracy (Acc), Sensitivity (Sens), and Specificity (Spec).

Experiment 4: Generalization power Figure 2.10 illustrates qualitative results of the segmentation method in some NEFRONA images. It shows the CIM region segmentation result (in green) together with the CIM region from NEFRONA GT (in yellow). We can observe that, generally, the CIM region is slightly over-segmented. According to this, Figure 2.11 (right) shows an overestimation of the IMT in the Bland-Altman plot (mean 0.29, note that the bias is statistically significant). Despite this error, Figure 2.11 (left) shows that the obtained values have a good correspondence with the IMT values of the NEFRONA database, with a cc of 0.58.

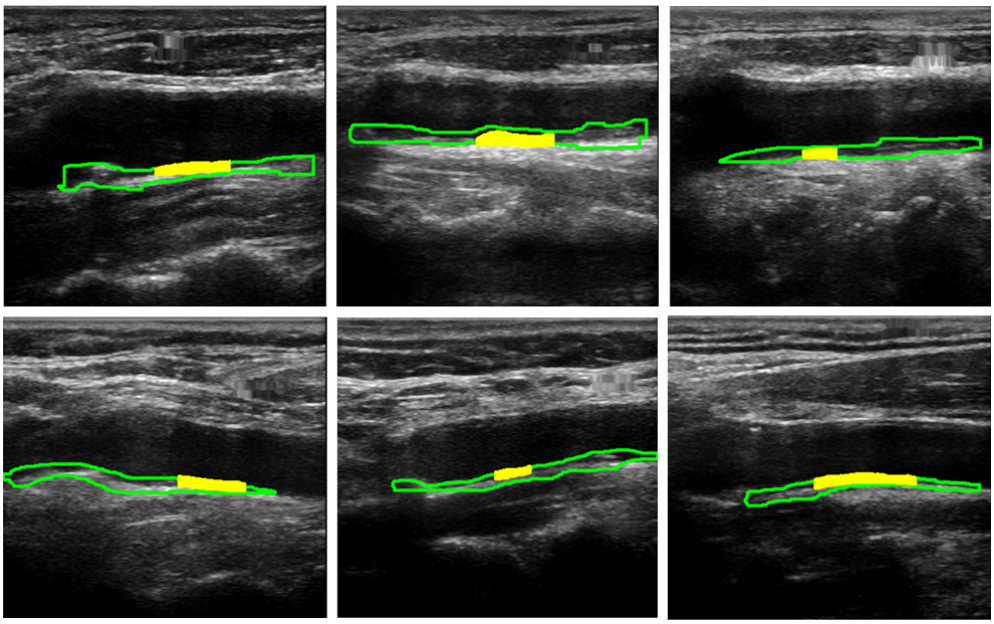

Figure 2.10: Qualitative segmentation results for NEFRONA CCA images. In green, delimitation of CIM region segmentation. In yellow, the CIM region from NEFRONA GT.

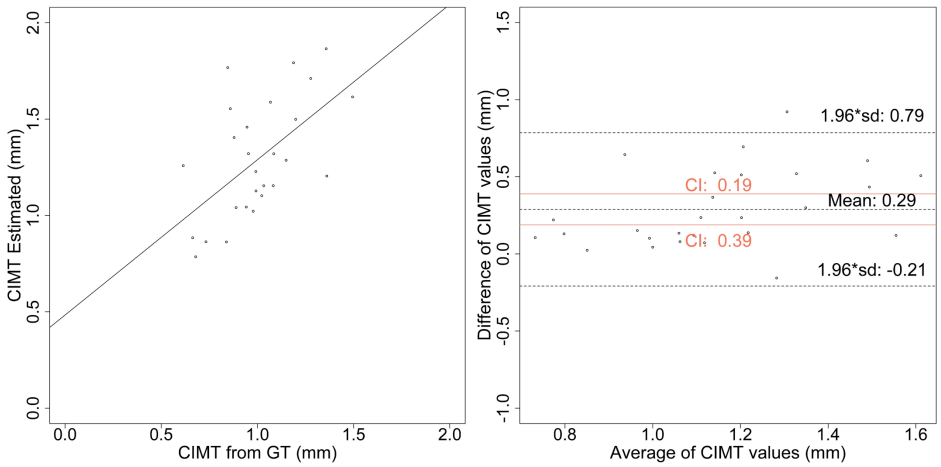

Figure 2.11: Correlation between IMT values (left), and Bland-Altman analysis (right). Both plots show the relation between GT and the estimated values in CCA images from NEFRONA dataset. Red solid line shows the confidence intervals for the "mean of the differences" line.

2.7 Conclusions

In this work, we have presented, for the first time in the literature, a single-step approach, based on DenseNets, for semantic CA segmentation. The proposed method accurately localizes the CIM region in CCA. Given the segmentation, we have validated the carotid IMT estimation and the detection of atherosclerotic plaque with a large dataset of more than 8,000 images. We have compared the results obtained by the proposed method with those of other DL models and shallow approaches, demonstrating more accurate results of the segmentation, more general IMT measurement and good plaque detection results. This superior performance is attributed to the effective use of SS together with the carotid IMT estimation approach. Moreover, we have proven the generalization capability of the method applying the model previously trained with one dataset (REGICOR) in a new test dataset (NEFRONA).

The proposed study has some limitations that are summarized below, and that will be considered in our future work. These limitations mostly arise from the number of images used in some of the experiments, thus the increase in the size of some datasets constitutes the first point of improvement in our study. On the one hand, the segmentation GT only includes a representative subset of the REGICOR images (159 CCA, 172 Bulb). On the other hand, the generalization power test was carried out using a small dataset composed of only 27 images (NEFRONA). Additionally, the proposed method is not applied on image sequences, which could improve reliability by measuring hundreds of images for each subject. Regarding carotid IMT estimation, we propose a pre-processing step that uses a smoothing algorithm based on mathematical morphology. Taking into account the unpredictable effect of this type of algorithms on segmentation results, a more detailed study is required to evaluate the impact of our proposed algorithm and to compare it with other pre-processing techniques. In this part of the methodology, it is also worth noting that the criteria of considering IMT values higher than 0.4 mm (see Section 2.4.2) could exclude real cases with a low IMT. Finally, the division of the CIM region in vertical columns could overestimate the IMT values in case of oblique forms of the CA; thus, this methodological issue could be carefully addressed as suggested by Bianchini et al. [67].

Additionally, we want to further improve the segmentation results in terms of an adequate generalization to other datasets, by exploring new domain transfer techniques. We also plan to add information indicating the presence of plaque into the NN in a way that it can learn the differences in shape between images of healthy subjects (thin CIM region shape) and images of subjects with atherosclerosis (irregular CIM region shape).

Chapter 3

Do individuals with autoimmune disease have increased risk of subclinical carotid atherosclerosis and stiffness?

3.1 Introduction

CVDs, which are the primary cause of death in Western countries [1], result from detrimental alterations in vascular walls, such as atherosclerosis and arteriosclerosis. These conditions coexist, leading to progressive and age-related vascular deterioration [2]. Atherosclerosis, an inflammatory process, mainly affects large arteries, with focal thickenings in the intima [3]. Arteriosclerosis, on the other hand, causes reduced artery flexibility in response to pressure changes.

The premature arterial degeneration observed in individuals with autoimmune disease may be a consequence of the chronic inflammation inherent to these disorders [68, 69, 70, 71]. Additionally, the cardiovascular risk profile, which is significantly worse in individuals with autoimmune diseases than in the general population [72], is directly associated with both carotid IMT and arterial stiffness values [63, 73]. Karakasis et al. [74] have recently presented a review that includes more references about the studies of the pathogenesis of accelerated atherosclerosis in autoimmune rheumatic diseases and the diagnostic techniques currently used, such as IMT in carotid and femoral arteries, among other imaging modalities. Most studies that have addressed subclinical

atherosclerosis included participants with autoimmune disease, who were usually recruited in hospitals; therefore, they were more likely to have advanced disease stages, which somewhat limited the generalizability of the study results.

In this section we present our the study [29], the objective of which is to assess the prevalence of subclinical atherosclerosis (CCA IMT) and arterial stiffness (distensibility and compliance) in individuals with a longstanding ($\geq$ 6 years) diagnosis of autoimmune disorders (inflammatory polyarthropathies, systemic connective tissue disorders, inflammatory bowel diseases, and spondylopathies) compared to the general population.

3.2 Methods

3.2.1 Dataset

A cross-sectional analysis was carried out of a population based sample recruited in Girona Province (northeastern Spain) in 2005 in the context of the REGICOR study. Participants were contacted by a letter informing them of the aims of the study and the tests to be performed. If they were willing to participate, they were asked to fast for at least 10 h before their appointment at the health examination site. The participation rate was 73.8%. Participants were reexamined in 2010, and carotid IMT measurements were performed [63]. All participants were duly informed about the study and provided their written consent to participate, and the results of the examination were sent to each of them. The study protocol was approved by the local ethics committee (CEIm-PSMAR 2008/3046/I; 2016/7075/I). From these data, we selected a sample of exposed individuals diagnosed with autoimmune disease (i.e., inflammatory polyarthropathies, systemic connective tissue disorders, inflammatory bowel diseases, spondylopathies) and nonexposed individuals (no autoimmune diseases). The samples were matched 1:5 by age, sex and education level.

3.2.2 Autoimmune diseases

The diagnosis of autoimmune diseases was obtained from the System for the Development of Research in Primary Care (SIDIAP) database, which includes the anonymized electronic medical records of 80% of the Catalan population [75]. These diagnoses were coded according to the International Classification of Diseases 10th edition (ICD-10) and divided into four groups: (1) inflammatory bowel diseases, (2) inflammatory polyarthropathies, (3) systemic connective tissue disorders, and (4) spondylopathies (Table 3.1).

ICD-10 code	Title
K50eK52	**Inflammatory bowel diseases**
K50	Crohn disease (regional enteritis)
K51	Ulcerative colitis
K52	Other noninfective gastroenteritis and colitis
M05eM14, L40.5	**Inflammatory polyarthropathies**
M05	Seropositive rheumatoid arthritis
M06	Other rheumatoid arthritis
M07	Psoriatic and enteropathic arthropathies
M08	Juvenile arthritis
M09	Juvenile arthritis in diseases classified elsewhere
M10	Gout
M11	Other crystal arthropathies
M12	Other specific arthropathies
M13	Other arthritis
L40.5	Arthropathic psoriasis
M30eM35, G635	**Systemic connective tissue disorders**
M30	Polyarteritis nodosa and related conditions
M31	Other necrotizing vasculopathies
M32	Systemic lupus erythematosus
M33	Dermatopolymyositis
M34	Systemic sclerosis
M35	Other systemic involvement of connective tissue
G63.5	Polyneuropathy in systemic connective tissue disorders
M45eM46	**Spondylopathies**
M45	Ankylosing spondylitis
M46	Other inflammatory spondylopathies

Table 3.1: Autoimmune disorders diagnoses included in each group.

3.2.3 Measurements

Examinations were performed by a team of trained nurses and interviewers. A precision scale that was easy to calibrate was used to measure weight and height with the participants in their underwear and barefoot. Body mass index was determined as the weight divided by the squared height (kg/m2). Blood pressure was measured with a periodically calibrated sphygmomanometer (OMRON 711). A cuff appropriate for the upper arm circumference (young, adult, obese) was selected for each participant. Measurements were performed in a seated position after 5min of rest. Two measurements were taken, and the lower value was recorded for the study. Standardized questionnaires were used to collect sociodemographic and lifestyle variables, along with previous history of and treatments for diabetes, hypertension and hypercholesterolemia. Current smoking was defined as active smoking within the preceding year. Blood was drawn after 10–14 h of fasting. Total and High-Density Lipoprotein (HDL) cholesterol concentrations were directly measured (Roche Diagnostics, Basel, Switzerland). Low-Density Lipoprotein (LDL) cholesterol was calculated by the Friedewald equation whenever triglycerides were <3.4mmol/l (300 mg/dl). The coronary risk in participants aged 35–74 years was calculated by the REGICOR function adapted from the original Framingham function and validated in the Spanish population [76].

3.2.4 Carotid IMT

Two trained sonographers performed carotid US examinations at the follow-up reexamination. An Acuson XP128 US machine equipped with an L75–10 MHz transducer and extended frequency software was used (Acuson-Siemens, Mountainview, California, United States). The image analyses were performed by expert trained readers with validated software (eTRACK) used in previous studies [27].

B-mode US images of the CCA segment were obtained in DICOM format with a resolution of 0.043 mm/p. Image files were recorded and sent to the AVICA for analysis (*gold standard*). To be consistent with clinical literature, in this section, we will use the term *gold standard* to refer to the Ground Truth (GT) set. Measurements were made in a 1-cm segment in the distal CCA (1 cm proximal to the dilation of the carotid bulb) of both the right and left arteries. Measurements were made every 1 mm in the 1-cm segment, from which the mean values were calculated.

A fully automatic DL method able to properly locate the carotid IMT region and then estimate the IMT was used (Table 3.2). This machine-learning procedure is based on CNNs and was validated using the IMT estimates performed in AVICA as the gold standard [28]. Left and right CCA IMT values were obtained for each participant, and the mean was considered in the analysis. As a proxy of the presence of atherosclerotic

	CCA IMT (cm)					
	n	Minimum	Maximum	Mean (SD)	Median [IQR]	ICC
Total images analyzed	1092	0.35	1.64	0.7 (0.17)	0.68 [0.58;0.79]	-
Images analyzed twice (included in the validation dataset)						
Gold Standard	638	0.38	2.04	0.76 (0.19)	0.73 [0.62; 0.87]	Ref.
AI method	638	0.41	1.64	0.69 (0.17)	0.66 [0.57; 0.76]	0.75
Images analyzed once (not included in the validation dataset)						
AI method	454	0.35	1.48	0.72 (0.17)	0.69 [0.60; 0.81]	-

ICC: Intraclass correlation coefficient, IQR: Interquartile Range,SD: Standard deviation
Please note that the images are the unit of analysis (two per participant)

Table 3.2: Comparative values for the IMT estimation in the different datasets.

plaques, men and women with CCA IMT values $\geq$ the 75th percentile of the population reference values were identified [63, 7].

3.2.5 Arterial stiffness

We obtained the arterial distensibility coefficient and compliance coefficient, defined as the relative and absolute change, respectively, in the cross-sectional area per unit of pressure. During the carotid US scan, the anterior and posterior walls of the distal right and left CCAs were visualized in B-mode. To obtain the M-mode anterior wall intima-lumen and posterior wall lumen-intima tracings, the sonographer switched from full B-mode to a 1/3 B-mode 2/3 M-mode image of the distal CCA. The 1/3 B-mode image guides the Mmode. The movement of the arterial walls on the 2/3 Mmode image shows waveforms with double-line patterns of the arterial walls over time. eTRACK software traces the waveforms of the leading edges of the anterior wall LI and posterior wall LI interfaces. If the contours of both walls are identified for at least 2 heartbeats, the software can calculate lumen diameter parameters and heart rates. Based on this information, other outcome parameters (e.g., distensibility and compliance coefficient) were derived using the equations from the Task Force III Summary of Clinical Applications of Arterial Stiffness [77].

3.2.6 Statistical analysis

Continuous variables were summarized as the means (standard deviation) or medians [interquartile range] when they were nonnormally distributed, and categorical variables were summarized as proportions. Effect modification of the relationship of diagnosed

autoimmune diseases with subclinical atherosclerosis and arterial stiffness was anticipated a priori [78, 79] and tested with the -2 loglikelihood test of nested models with and without interaction terms. The sample was stratified by sex.

Chi-square, Student's t, and Mann–Whitney U tests were used as appropriate to compare the prevalence of cardiovascular risk factors at baseline in individuals with and without autoimmune diseases and to ascertain arterial distensibility and compliance and the distribution of cardiovascular risk factors by terciles of common carotid IMT values. We fitted linear regression models for men and women, adjusted for the cardiovascular risk factors that significantly modified arterial distensibility and compliance and CCA IMT. Additionally, a logistic regression was fitted in the case of individuals with a CCA IMT value $\geq$ the 75th percentile. To assess the effects of vasodilation factors and antiinflammatory drugs, we performed a sensitivity analysis excluding current smokers and a multivariable analysis further adjusted for the use of calcium-channel blockers and anti-inflammatory drugs.

The statistical analysis was conducted using R software, version 4.0.3 [80].

3.3 Results

We included 91 individuals with autoimmune disease and 455 without this diagnosis (n = 546). The most common group of autoimmune diseases was inflammatory polyarthropathies in both men (74.0%) and women (51.2%). Systemic connective tissue disorders in women (22.0%) and inflammatory bowel diseases in men (14.0%) were the second most prevalent group of diseases. Men with autoimmune diseases had higher prevalences of hypertension and diabetes, higher LDL cholesterol levels and higher 10-year cardiovascular risk values than those without such diseases. In women, the cardiovascular risk profile did not differ according to the presence of these diseases (Table 3.3).

Biomarkers of subclinical atherosclerosis and arterial stiffness were similar in individuals with and without autoimmune diseases, except for the proportion with IMT $\geq$ percentile 75, which was significantly lower in the group of women with an autoimmune diagnosis (Table 3.4).

The 10-year cardiovascular risk was associated, in all instances, with the tercile of CCA IMT and the distensibility and compliance coefficients (Tables 3.5, 3.6, 3.7). The risk score used to adjust the multivariate models integrated 8 variables (sex, age, systolic and diastolic blood pressure, total and HDL cholesterol, diabetes, and smoking habit), most of which were significantly correlated with the terciles of subclinical atherosclerosis and arterial stiffness.

	Autoimmune diseases					
	Men			Women		
	No N = 256	**Yes N = 50**	***p* value**	**No N = 199**	**Yes N = 41**	***p* value**
Age(years),mean(SD)	67(12)	68(12)	0.813	64(12)	64(12)	0.955
Education level, n(%)			0.986			0.949
No studies or primary school	171(66.8)	34(68.0)		112(56.3)	22(53.7)	
Secondary school	48(18.8)	9(18.0)		56(28.1)	12(29.3)	
University	37(14.5)	7(14.0)		31(15.6)	7(17.1)	
Autoimmune diseases, n(%)			–			–
Inflammatory polyarthropathies	–	37(74.0)		–	21(51.2)	
Systemic connective tissue disorders	–	3(6.0)		–	10(24.4)	
Inflammatory bowel diseases	–	7(14.0)		–	9(22.0)	
Spondylopathies	–	3(6.0)		–	1(2.4)	
Smoker, n(%)			0.393			0.776
Never	59(23.0)	17(34.0)		146(73.4)	31(75.6)	
Former	55(21.5)	8(16.0)		20(10.1)	5(12.2)	
Current	138(53.9)	25(50.0)		29(14.6)	4(9.8)	
Body mass index, mean(SD)	27.4(3.5)	28.4(3.8)	0.104	26.7(4.3)	27.1(5.4)	0.693
Systolic blood pressure(mmHg), mean(SD)	138(20)	142(21)	0.188	128(20)	130(20)	0.675
Diastolic blood pressure(mmHg), mean(SD)	77(10)	78(11)	0.546	73(9)	75(9)	0.229
Hypertension, n(%)	138(55.0)	37(74.0)	0.020	89(45.9)	19(46.3)	0.999
Anti-inflammatory treatment, n(%)	12(4.7)	3(6.0)	0.719	27(13.6)	10(24.4)	0.131
Calcium-channel blockers treatment, n(%)	24(9.4)	9(18.0)	0.121	4(2.0)	1(2.4)	0.999
Total cholesterol(mg/dl), mean(SD)	194(36)	184(35)	0.064	212(37)	210(33)	0.788
HDL cholesterol(mg/dl), mean(SD)	48(11)	46(11)	0.135	57(11)	58(10)	0.540
LDL cholesterol(mg/dl),mean(SD)	124(32)	115(32)	0.056	136(32)	133(27)	0.636
Triglycerides(mg/dl), median [IQR]	97[69;127]	106[68;154]	0.417	89[66;114]	86[68;115]	0.890
Glycemia(mg/dl),median[IQR]	96[90;106]	98[90;117]	0.270	92[85;100]	87[83;96]	0.057
Diabetes, n(%)	65(26.5)	21(42.9)	0.034	32(16.8)	6(14.6)	0.920
10-year cardiovascular risk(%), median [IQR]	4.9[2.9;8.3]	6.6[4.3;10.0]	0.038	2.3[1.5;4.0]	2.3[1.7;3.3]	0.740

IQR: interquartile range, SD: standard deviation

Table 3.3: Characteristics of the whole sample and stratified by sex.

	Autoimmune diseases					
	Men			Women		
	No N = 256	**Yes N = 50**	***p* value**	**No N = 199**	**Yes N = 41**	***p* value**
Atherosclerosis measures						
Common carotid IMT (mm), mean (SD)	0.72(0.14)	0.75(0.16)	0.197	0.68 (0.15)	0.65 (0.10)	0.086
Common carotid IMT–percentile 75, n(%)	41 (16.02)	14 (28.00)	0.069	46 (23.12)	3 (7.32)	0.038
Arterial stiffness measures						
Distensibility ($mmHg^{-}1$), mean(SD)	25.99 (9.75)	25.20 (9.65)	0.604	30.53(11.11)	31.02(12.63)	0.820
Compliance (cm/mmHg), mean(SD)	0.78(0.25)	0.77 (0.26)	0.688	0.72(0.23)	0.75 (0.24)	0.444

SD: standard deviation

Table 3.4: Subclinical atherosclerosis and arterial stiffness biomarkers by diagnosis of autoimmune diseases.

	Men				Women			
	T1 N = 102	T2 N = 102	T3 N = 102	p value	T1 N = 80	T2 N = 80	T3 N = 80	p value
Common carotid IMT (mm), mean (SD)	0.59 (0.05)	0.70 (0.03)	0.88 (0.11)	< 0.001	0.54 (0.04)	0.66(0.03)	0.83(0.12)	< 0.001
Age (years), mean (SD)	60 (13)	68 (11)	74 (9)	<0.001	55 (11)	66 (10)	72 (9)	<0.001
Education level, n (%)				0.031			<0.001	
No studies or primary school	59 (57.8)	66 (64.7)	80 (78.4)		30 (37.5)	48 (60.0)	56 (70.0)	
Secondary school	23 (22.5)	20 (19.6)	14 (13.7)		21 (26.2)	25 (31.2)	22 (27.5)	
University	20 (19.6)	16 (15.7)	8 (7.8)		29 (36.2)	7 (8.8)	2 (2.5)	
Autoimmune diseases	13 (12.7)	21 (20.6)	16 (15.7)	0.310	14 (17.5)	18 (22.5)	9 (11.2)	0.166
Smoker, n (%)	49 (49.0)	57 (57.0)	57 (55.9)	0.469	19 (24.4)	8 (10.1)	6 (7.7)	0.005
Body mass index, mean (SD)	27.7 (3.6)	27.4 (3.9)	27.6 (3.2)	0.788	25.6 (4.7)	27.1 (4.5)	27.7 (4.0)	0.010
Systolic blood pressure (mmHg), mean (SD)	132 (17)	139 (19)	145 (23)	<0.001	117 (16)	130 (19)	138 (19)	<0.001
Diastolic blood pressure (mmHg), mean (SD)	78 (10)	79 (9)	75 (11)	0.009	73 (9)	75 (10)	74 (8)	0.300
Hypertension, n(%)	45 (44.6)	58 (58.0)	72 (72.0)	<0.001	23 (29.9)	34 (43.0)	51 (64.6)	<0.001
Anti-inflammatory treatment, n (%)	5 (4.9)	7 (6.9)	3 (2.9)	0.431	7 (8.8)	15 (18.8)	15 (18.8)	0.129
Calcium-channel blockers treatment, n (%)	8 (7.8)	12 (11.8)	13 (12.7)	0.490	2 (2.5)	2 (2.5)	1 (1.3)	0.999
Total cholesterol (mg/dl), mean (SD)	201 (39)	189 (37)	187 (31)	0.008	202 (39)	214 (31)	219 (37)	0.012
HDL cholesterol (mg/dl), mean (SD)	47 (10)	50 (11)	46 (11)	0.037	57 (10)	58 (12)	56 (10)	0.700
LDL cholesterol (mg/dl), mean (SD)	132 (34)	118 (32)	118 (28)	0.003	128 (33)	136 (27)	141 (31)	0.028
Triglycerides (mg/dl), median [IQR]	104 [74; 139]	85 [63; 129]	95 [73; 127]	0.203	77 [56; 107]	89 [68; 123]	92 [78; 121]	0.012
Glycemia (mg/dl),median [IQR]	96 [89; 106]	96 [91; 108]	97 [91; 109]	0.345	88 [83; 95]	93 [86; 101]	92 [88; 102]	0.005
Diabetes, n (%)	19 (19.2)	26 (27.1)	41 (41.4)	0.002	9 (11.7)	13 (16.7)	16 (20.8)	0.312
10-year cardiovascular risk (%), median [IQR]	4.0 [2.6; 6.6]	5.9 [3.3; 8.7]	8.2 [5.1; 12.6]	<0.001	1.5 [0.9; 2.6]	2.9 [1.7; 5.0]	2.9 [2.3; 4.5]	<0.001

IQR: interquartile range, SD: standard deviation

Table 3.5: Characteristics of the sample by terciles of CCA IMT.

	Men				Women			
	T1 N = 98	T2 N = 98	T3 N = 97	p value	T1 N = 80	T2 N = 80	T3 N = 79	p value
Arterial distensibility ($mmHg^{-}1$), mean (SD)	16.5 (3.6)	24.6 (2.3)	36.7 (7.6)	<0.001	19.1 (4.6)	29.2 (3.0)	43.6 (7.4)	<0.001
Age (years), mean (SD)	73 (10)	68 (11)	59 (13)	<0.001	72 (9)	67 (10)	54 (10)	<0.001
Education level, n (%)				0.069			<0.001	
No studies or primary school	73 (74.5)	59 (60.2)	63 (64.9)		61 (76.2)	47 (58.8)	26 (32.9)	
Secondary school	18 (18.4)	18 (18.4)	20 (20.6)		14 (17.5)	29 (36.2)	24 (30.4)	
University	7 (7.1)	21 (21.4)	14 (14.4)		5 (6.2)	4 (5.0)	29 (36.7)	
Autoimmune diseases	17 (17.3)	14 (14.3)	17 (17.5)	0.789	15 (18.8)	13 (16.2)	13 (16.5)	0.897
Smoker, n (%)	52 (53.6)	54 (55.7)	47 (49.0)	0.633	5 (6.4)	10 (12.7)	18 (23.4)	0.009
Body mass index, mean (SD)	28.2 (4.0)	27.5 (3.4)	26.9 (3.1)	0.044	28.2 (4.1)	27.4 (4.4)	24.9 (4.4)	<0.001
Systolic blood pressure (mmHg), mean (SD)	149 (23)	137 (14)	128 (16)	<0.001	143 (18)	129 (15)	112 (13)	<0.001
Diastolic blood pressure (mmHg), mean (SD)	77 (11)	79 (9)	77 (10)	0.283	76 (10)	75 (8)	70 (8)	<0.001
Hypertension, n (%)	67 (69.8)	56 (57.7)	42 (44.2)	0.002	59 (76.6)	36 (45.6)	12 (15.4)	<0.001
Anti-inflammatory treatment,	4 (4.1)	6 (6.1)	4 (4.1)	0.834	18 (22.5)	13 (16.2)	6 (7.6)	0.033
n (Calcium-channel blockers	19 (19.4)	4 (4.1)	6 (6.2)	0.001	4 (5.0)	1 (1.2)	0 (0.0)	0.131
treatment, n (Total cholesterol (mg/dl), mean (SD)	186 (33)	188 (37)	200 (38)	0.016	211 (32)	218 (37)	205 (40)	0.073
HDL cholesterol (mg/dl), mean (SD)	47 (11)	48 (12)	48 (10)	0.842	55 (12)	57 (11)	58 (10)	0.326
LDL cholesterol (mg/dl), mean (SD)	117 (30)	118 (32)	131 (34)	0.005	133 (26)	142 (31)	130 (34)	0.041
Triglycerides (mg/dl), median [IQR]	104 [73; 135]	98 [68; 132]	94 [64; 124]	0.464	103 [78; 135]	90 [66; 107]	75 [55; 100]	<0.001
Glycemia (mg/dl), median [IQR]	98 [92; 110]	98 [92; 115]	93 [87; 100]	0.001	97 [89; 107]	91 [85; 97]	87 [81; 93]	<0.001
Diabetes, n (%)	35 (36.8)	29 (30.9)	17 (18.5)	0.019	23 (30.7)	10 (12.8)	5 (6.4)	<0.001
10-year cardiovascular risk (%), median [IQR]	7.3 [4.7; 12.5]	6.3 [4.0; 9.3]	3.6 [2.6; 6.2]	<0.001	4.3 [2.6; 6.0]	2.5 [1.8; 4.5]	1.4 [0.9; 2.3]	<0.001

IQR: interquartile range, SD: standard deviation

Table 3.6: Characteristics of the sample by terciles of arterial distensibility.

	Men				Women			
	T1 N = 98	T2 N = 98	T3 N = 97	*p* value	T1 N = 81	T2 N = 81	T3 N = 77	*p* value
Arterial compliance (cm/ mmHg), mean (SD)	0.55 (0.10)	0.79 (0.07)	1.12 (0.21)	<0.001	0.51 (0.10)	0.74 (0.06)	1.06 (0.16)	<0.001
Age (years), mean (SD)	70 (11)	68 (12)	62 (13)	<0.001	69 (11)	65 (11)	58 (12)	<0.001
Education level, n (%)				0.853			<0.001	
No studies or primary school	68 (69.4)	63 (64.3)	64 (66.0)		55 (67.9)	53 (65.4)	26 (33.8)	
Secondary school	16 (16.3)	22 (22.4)	18 (18.6)		23 (28.4)	19 (23.5)	25 (32.5)	
University	14 (14.3)	13 (13.3)	15 (15.5)		3 (3.7)	9 (11.1)	26 (33.8)	
Autoimmune diseases	16 (16.3)	16 (16.3)	16 (16.5)	0.999	15 (18.5)	13 (16.0)	13 (16.9)	0.914
Smoker, n (%)	51 (52.6)	59 (60.8)	43 (44.8)	0.083	7 (8.9)	9 (11.2)	17 (22.7)	0.032
Body mass index, mean (SD)	27.4 (4.0)	28.2 (3.6)	27.0 (3.0)	0.064	27.1 (4.2)	27.1 (4.7)	26.1 (4.4)	0.265
Systolic blood pressure (mmHg), mean (SD)	147 (22)	138 (16)	131 (18)	<0.001	139 (21)	129 (16)	117 (16)	<0.001
Diastolic blood pressure (mmHg), mean (SD)	78 (11)	77 (10)	77 (10)	0.429	76 (9)	74 (8)	72 (9)	0.011
Hypertension, n (%)	64 (67.4)	54 (55.1)	47 (49.5)	0.039	50 (64.1)	35 (43.8)	22 (28.9)	<0.001
Anti-inflammatory treatment, n (%)	5 (5.1)	6 (6.1)	3 (3.1)	0.698	13 (16.0)	17 (21.0)	7 (9.1)	0.116
Calcium-channel blockers treatment, n (%)	12 (12.2)	10 (10.2)	7 (7.2)	0.497	3 (3.7)	1 (1.2)	1 (1.3)	0.624
Total cholesterol (mg/dl,) mean (SD)	193 (38)	189 (36)	193 (36)	0.683	215 (35)	211 (34)	209 (41)	0.580
HDL cholesterol (mg/dl), mean (SD)	49 (12)	48 (11)	47 (10)	0.627	56 (12)	57 (11)	58 (10)	0.612
LDL cholesterol (mg/dl), mean (SD)	123 (34)	119 (31)	125 (33)	0.369	137 (29)	135 (30)	134 (34)	0.841
Triglycerides (mg/dl), median [IQR]	88 [70; 132]	101 [73; 141]	96 [66; 129]	0.353	95 [75; 133]	90 [68; 110]	75 [57; 99]	0.001
Glycemia (mg/dl), median [IQR]	97 [92; 108]	98 [90; 112]	95 [88; 102]	0.219	96 [88; 107]	91 [84; 100]	88 [83; 95]	<0.001
Diabetes, n (%)	30 (32.6)	30 (30.9)	21 (22.8)	0.292	21 (27.3)	12 (15.4)	5 (6.6)	0.002
10-year cardiovascular risk (%), median [IQR]	7.6 [4.3; 11.4]	6.1 [3.4; 9.2]	3.6 [2.7; 6.2]	<0.001	3.3 [2.1; 5.4]	2.5 [1.6; 4.5]	1.7 [0.9; 2.8]	<0.001

IQR: interquartile range, SD: standard deviation.

Table 3.7: Characteristics of the sample by terciles of arterial compliance.

The models adjusted for 10-year cardiovascular risk showed that a diagnosis of autoimmune disease in men was associated with a significantly higher mean CCA IMT values [beta-coefficient (95% confidence interval): 0.058 (0.009; 0.108); p value = 0.022]. This association was not significant in women [-0.023 (-0.071; 0.025); p value = 0.353]. In addition, the prevalence of CCA IMT $\geq$ 75th percentile was higher in men with autoimmune diseases than in those without [1.012 (0.145; 1.880); p value = 0.022]; in contrast, women without autoimmune disease were more likely to have IMT $\geq$ 75th percentile [-2.181 (-4.214; -0.149); p value = 0.035]. No significant differences were found for arterial stiffness biomarkers Table 3.11. Finally, no differences were observed in the sensitivity analysis when current smokers were excluded (Table 3.8) or after further adjustment for the use of calcium-channel blockers or antiinflammatory drugs (Tables 3.9 and 3.10).

3.4 Discussion

The diagnosis of autoimmune diseases was a risk factor for subclinical atherosclerosis in men in our cohorts of individuals with and without autoimmune diseases matched by age, sex, and education level. Sex acted as an effect modifier in this association: the difference was not significant in women. In contrast, arterial stiffness, as measured by the coefficients of distensibility and compliance, was not increased in individuals with

	CCA IMT*		**P75 CCA IMT †**		**Arterial distensibility***		**Arterial compliance***	
	Coeff. (95% CI)	p-value	Coeff. (95% CI)	p-value	Coeff. (95% CI)	p-value	Coeff. (95% CI)	p-value
Men								
Autoimmune disease	0.058 (0.009; 0.108)	0.023	1.028 (0.158; 1.898)	0.021	-0.457 (-3.998; 3.083)	0.800	-0.025 (-0.129; 0.079)	0.638
10-year CV risk	0.008 (0.004; 0.011)	<0.001	0.048 (-0.018; 0.115)	0.156	-0.546 (-0.798; -0.294)	<0.001	-0.011 (-0.018; -0.004)	0.004
Women								
Autoimmune disease	-0.023 (-0.071; 0.025)	0.355	-2.168 (-4.202; -0.135)	0.037	-0.656 (-4.129; 2.818)	0.712	0.010 (-0.072; 0.092)	0.811
10-year CV risk	0.016 (0.007; 0.025)	<0.001	-0.053 (-0.245; 0.139)	0.588	-2.671 (-3.303; -2.039)	<0.001	-0.043 (-0.058; -0.028)	<0.001

CI: Confidence interval, Coeff: Coefficient*Linear regression model, †Logistic regression model. All models are mutually adjusted

Table 3.8: Models excluding current smokers.

	CCA IMT*		**P75 CCA IMT †**		**Arterial distensibility***		**Arterial compliance***	
	Coeff. (95% CI)	p-value	Coeff. (95% CI)	p-value	Coeff. (95% CI)	p-value	Coeff. (95% CI)	p-value
Men								
Autoimmune disease	0.058 (0.009; 0.108)	0.023	1.028 (0.158; 1.898)	0.021	-0.457 (-3.998; 3.083)	0.800	-0.025 (-0.129; 0.079)	0.638
10-year CV risk	0.008 (0.004; 0.011)	<0.001	0.048 (-0.018; 0.115)	0.156	-0.546 (-0.798; -0.294)	<0.001	-0.011 (-0.018; -0.004)	0.004
Treatment with calcium channel blockers	-0.001 (-0.072; 0.070)	0.981	-0.826 (-2.507; 0.856)	0.336	-0.142 (-5.601; 5.317)	0.959	0.028 (-0.132; 0.188)	0.730
Women								
Autoimmune disease	-0.023 (-0.071; 0.025)	0.355	-2.168 (-4.202; -0.135)	0.037	-0.656 (-4.129; 2.818)	0.712	0.010 (-0.072; 0.092)	0.811
10-year CV risk	0.016 (0.007; 0.025)	<0.001	-0.053 (-0.245; 0.139)	0.588	-2.671 (-3.303; -2.039)	<0.001	-0.043 (-0.058; -0.028)	<0.001
Treatment with calcium channel blockers	0.001 (-0.119; 0.121)	0.988	-15.037 (-2273; 2243)	0.990	-10.292 (-18.926; -1.660)	0.021	-0.125 (-0.330; 0.079)	0.232

CI: Confidence interval, Coeff: Coefficient *Linear regression model, †Logistic regression model. All models are mutually adjusted

Table 3.9: Sensitivity analysis. Models further adjusted by calcium channel blockers.

	CCA IMT*		**P75 CCA IMT †**		**Arterial distensibility***		**Arterial compliance***	
	Coeff. (95% CI)	p-value	Coeff. (95% CI)	p-value	Coeff. (95% CI)	p-value	Coeff. (95% CI)	p-value
Men								
Autoimmune disease	0.059) (0.009; 0.108)	0.022	1.046 (0.160; 1.931)	0.021	-0.397 (-4.278; 3.483)	0.841	-0.025 (-0.137; 0.087)	0.662
10-year CV risk	0.008 (0.004; 0.011)	<0.001	0.039 (-0.026; 0.103)	0.244	-0.574 (-0.844; -0.303)	<0.001	-0.011 (-0.019; -0.003)	0.005
Treatment with anti-inflammatory drugs	-0.029 (-0.109; 0.051)	0.981	-16.290 (-2407; 2375)	0.989	-0.197 (-6.230; 6.624)	0.952	0.045 (-0.141; 0.230)	0.640
Women								
Autoimmune disease	-0.028 (-0.077; 0.021)	0.265	-2.252 (-4.300; -0.204)	0.032	-0.359) (-4.226; 3.508)	0.856	0.016 (-0.074; 0.107)	0.724
10-year CV risk	0.015 (0.006; 0.024)	<0.001	-0.069) (-0.263; 0.125)	0.484	-2.814 (-3.512; -2.116)	<0.001	-0.046 (-0.062; -0.029)	<0.001
Treatment with anti-inflammatory drugs	0.030 (-0.023; 0.084)	0.269	0.374 (-0.755; 1.503)	0.516	-2.850 (-7.062; 1.363)	0.187	-0.044 (-0.142; 0.055)	0.385

CI: Confidence interval, Coeff: Coefficient *Linear regression model, †Logistic regression model. All models are mutually adjusted

Table 3.10: Sensitivity analysis. Models further adjusted by anti-inflammatory treatment.

	Autoimmune diseases					
	Men			Women		
	Coefficient	95% CI	p value	Coefficient	95% CI	p value
Atherosclerosis biomarkers						
CCA IMT (mm)[a]	0.058	0.009; 0.108	0.022	-0.023	-0.071; 0.025	0.353
CCCA IMT - percentile 75[b]	1.012	0.145; 1.880	0.022	-2.181	-4.214; -0.149	0.035
Arterial stiffness biomarkers						
Arterial distensibility (mmHg-1)[a]	-0.458	-3.988; 3.073	0.800	-0.803	-4.320; 2.714	0.655
Arterial compliance (cm/mmHg)[a]	-0.025	-0.128; 0.078	0.637	0.008	-0.074; 0.091	0.844

SD: standard deviation, CI: confidence interval, [a]Linear regression model, [b]Logistic regression model
All models have been adjusted for 10-year cardiovascular risk

Table 3.11: Subclinical atherosclerosis biomarkers by diagnosis of autoimmune diseases.

autoimmune diseases.

3.4.1 Autoimmune diseases as a risk factor for subclinical atherosclerosis

Previous studies have shown higher prevalences of subclinical atherosclerosis and clinically overt CVD in individuals diagnosed with autoimmune disorders [68, 69, 81, 82, 83, 84] Thus, immune-mediated inflammation is likely to play a pivotal role in the pathogenesis of atherosclerosis, as it is involved in endothelial dysfunction, plaque rupture and thrombosis [71, 85]. Specifically, for inflammatory joint diseases, the central event in synovitis and autoimmune atherosclerosis is the accumulation of inflammatory cells and mediators in the synovial tissue and vessel wall, respectively [86]. Therefore, the most recent European League Against Rheumatism guidelines promote the proactive management of cardiovascular risk in individuals with inflammatory polyarthritis and spondylopathies. The primary preventive and therapeutic goal is to control the underlying autoimmune inflammatory process [87]. These recommendations have also been proposed for individuals with systemic lupus erythematosus [88] but could likely be extended to individuals with any systemic connective tissue disorder.

3.4.2 Participant sex modified the effect of autoimmune diseases on IMT

Several studies in the general population revealed an association between inflammatory biomarkers and arterial stiffness [70, 89, 90, 91]. However, our cross-sectional study did not show significant differences in these biomarkers between individuals with and without autoimmune diseases. First, the individuals with autoimmune diseases had varying disease severity because they were selected randomly from a population [25]. Second, most previous studies used carotid-femoral pulse wave velocity, the gold standard for assessing regional arterial stiffness, which is a value usually obtained by tonometry or

mechanotransducers [89, 90, 91]. Since we performed an US analysis, which is commonly used to assess local mechanical properties of arterial walls, the measures used to assess arterial stiffness were carotid distensibility and compliance [92]. Nevertheless, the adjusted coefficients indicated higher resistance to vascular deformation in individuals with autoimmune diseases but did not reach statistical significance.

3.4.3 Limitations

Our study has several limitations. First, the added value of CCA IMT for cardiovascular risk prediction beyond the classic risk factors remains controversial [93, 94]. In addition, the reproducibility of IMT measures is a controversial issue [95] that we have optimized by adopting the use of a previously validated machine-learning method [28]. The use of carotid US enabled the detection of arterial stiffness in the carotid wall but did not allow the measurement of carotid-femoral pulse wave velocity, which is the gold standard for assessing this variable. Second, it was beyond the scope of the objectives of our study to measure blood biomarkers (e.g., systemic inflammation, endothelial dysfunction, prothrombotic state) to explore the potential mechanisms that may accelerate atherosclerosis in patients with autoimmune disease [96]. To avoid misclassification bias, we used the medical diagnosis of autoimmune disease as a robust marker of inflammatory status. Although these diagnoses were extracted from routinely collected data that may reflect underreporting, the SIDIAP database has been validated for research in cardiovascular epidemiology [97] and rheumatic diseases [98]. Indeed, the prevalence of autoimmune diseases found in SIDIAP concurred with the results reported in previous studies based on other datasets [99, 100, 101]. Third, a low prevalence of autoimmune diseases was reflected in our population-based study. Nevertheless, we obtained consistent results from our multivariable analysis adjusted for 10-year cardiovascular risk, which was represented by a composite score with variables that showed significant differences in the bivariate analysis. Indeed, the sensitivity analysis yielded similar results when adjusted for the use of drugs with anti-inflammatory or vasodilation effects (e.g., calcium-channel blockers) and after the exclusion of current smokers. In addition, cigarette smoking has been shown to attenuate endothelium-dependent vasodilation [102]. A priori, this effect might be similar in smokers with and without autoimmune diseases because the sample selection was not based on this variable. Finally, to avoid selection bias, our cohorts were matched by age, sex and education level and did not present significant differences in 10-year cardiovascular risk. Although this approach may reduce the representativeness of the population, the associations found between cardiovascular risk factors and CCA IMT concur with those reported in previous studies [63, 83].

3.5 Conclusions

This study aimed to assess the prevalence of subclinical atherosclerosis measured with IMT and arterial stiffness (distensibility and compliance) in individuals with long-standing diagnoses of autoimmune disorders in comparison to the general population. Reproducibility issues of IMT measurements were addressed using a validated machine-learning method. The study revealed a low prevalence of autoimmune diseases in the population but still found consistent results in multivariable analysis adjusted for cardiovascular risk. Sensitivity analysis confirmed the findings, even when accounting for drug use and excluding current smokers. Matched cohorts for age, sex, and education level maintained the associations between cardiovascular risk factors and CCA IMT, in line with previous studies.

In conclusion, subclinical carotid atherosclerosis, but not stiffness, was more common in men with autoimmune diseases than in the general population. No significant differences were found in women with and without autoimmune diseases in these carotid features. Sex was an effect modifier for the association between the diagnosis of autoimmune diseases and the CCA IMT values.

Chapter 4

Polyvascular subclinical atherosclerosis: correlation between ABI and carotid atherosclerosis in a population-Based sample

4.1 Introduction

CVDs are the main cause of death in western countries and the common basis of this group of diseases is atherosclerosis. The presence of atherosclerosis in different vascular beds defines polyvascular subclinical disease, pointing out the systemic nature of the atherosclerotic process [103, 104, 105].

The long induction period of atherosclerosis makes it suitable for the study of subclinical disease for preventive purposes. On the one hand, low Ankle Brachial Index (ABI) values, as a subclinical indicator of lower extremity peripheral artery disease, provide a potent predictor of future cardiovascular events and death [106, 107]. On the other hand, as it is mentioned in Section 1.1.2 carotid US can be used to detect subclinical disease because it measures IMT and the presence of atherosclerotic plaques [7, 108, 109]. Most studies have addressed the coexistence atherosclerosis of the lower limbs and CA in selected samples (eg, patientswith diabetes, history of stroke, or advanced age) [110, 111, 112, 113]. However, these correlations have not been assessed in general population or specifically in individuals with no history of intermittent claudication.

In addition, most of the studies did not use automated methods based on ML procedures that minimize the reproducibility problem linked to IMT and carotid plaque interpretation [28, 95].

This section presents our study [30], the objective of which is to assess the correlation between the biomarkers of lower limb atherosclerosis (ABI) and of carotid atherosclerosis (eg, CCA IMT and presence of atherosclerotic plaque) in a general population and in a subsample with no history of intermittent claudication.

4.2 Methods

4.2.1 Dataset

Cross-sectional study conducted in the context of the REGICOR study.Participants were randomly selected in 2005 and reexamined in 2010, when ABI and carotid US were performed. The participants included were free of terminal disease. Participants were contacted by a letter informing them of the aims of the study and the tests to be performed. If willing to participate, they were asked to fast (water allowed) for at least 10 h before their appointment at the health examination site. The participation rate in the reexamination was 78.1% [63]. All participants were duly informed and provided their written consent to participate in the study and the results of the examination were sent to each of them. The study protocol was approved by the local ethics committee (CEIm-PSMAR 2008/3046/I).

4.2.2 Measurements

Examinations were performed by a team of trained nurses and interviewers using the same methods. A precision scale of easy calibration was used for weight and height measurement with participants in underwear and barefoot. Body mass index was determined as weight divided by squared height (kg/m2). Blood pressure was measured with a periodically calibrated sphygmomanometer (OMRON711, Shimogyō-ku, Japan). Acuff adapted to the upper arm perimeter (young, adult, obese) was selected for each participant. Measurements were performed in a seated position after a 5 min rest. Twomeasurements were taken and the lower valuewas recorded for the study. Standardized questionnaires were used to collect sociodemographic and lifestyle variables, along with previous history and treatments for diabetes, hypertension, and hypercholesterolemia. Current smoking was defined as actively smoking within the preceding year. Claudicationwas assessed using the Edinburgh questionnaire.19 Blood was withdrawn

after 10-14 h of fasting. Total and High-Density Lipoprotein (HDL) cholesterol concentrations were determined by direct methodology (Roche Diagnostics, Basel, Switzerland). Low-Density Lipoprotein (LDL) cholesterol was calculated by the Friedewald equation whenever triglycerides were <3.4 mmol/l (300 mg/dl).

4.2.3 ABI Measure

ABI was measured in accordance with current guidelines [106]. After 5 min rest and with the participant in supine position, systolic blood pressure was measured in the brachial artery in the antecubital fossa in the control arm with a continuous Doppler device, then in the distal calf, using the Doppler probe to determine systolic blood pressure in the supine position at the right and left posterior and anterior tibial arteries. Right and left ABI were calculated as the ratio of the higher of 2 systolic pressures in the lower limbs (posterior and anterior tibial arteries) to the control brachial systolic pressures. The lowest of the values obtained was used for analysis. We discarded the individuals with ABI > 1.4 because of the high probability of medial arterial calcification [106].

4.2.4 Carotid IMT

Two trained sonographers performed the carotid US examinations. An Acuson XP128 US machine equipped with an L75-10 MHz transducer and extended frequency software was used (Acuson-Siemens, Mountainview, California, United States). B-mode US images of the CCA segment were obtained in DICOM format with a resolution of 0.043 mm/p. Image files were recorded and sent to the AVICA. Measurements of IMT were made in a 1 cm segment in the distal CCA (1 cm proximal to the dilation of the carotid bulb) of both right and left arteries. Measurements were made every 1 mm in the 1 cm segment, from which the mean values were calculated. To interpret the full set of images, a fully automatic deep-learning method able to properly localize the intima-media regi on and then estimate the IMT was used (see Table 4.1. This deep-learning procedure is based on CNNs and was validated using the subset of IMT estimates performed in AVICA as the *gold standard* [28]. To be consistent with clinical literature, in this section, we will use the term *gold standard* to refer to the Ground Truth (GT) set. Left and right CCA IMT were obtained for each participant and the mean was considered in the analysis. For those individuals with just one estimate (eg, left or right), this single value was considered. Finally, the presence of carotid plaque was also assessed with a deep-learning model and according to the definition in the Mannheim consensus: focal structure encroaching into the arterial lumen of at least 0.5 mm or 50% of the surrounding IMT value, or a thickness >1.5 mm as measured from the MA interface to the LI interface [7].

	CCA IMT (cm)						
	n	Minimum	Maximum	Mean (SD)	Median [IQR]	ICC	Plaque %
Total images analyzed	3307	0.44	2.12	0.76 (0.16)	0.73 [0.65; 0.84]	-	
Images analyzed twice (included in the validation dataset)							
Gold Standard	809	0.42	1.44	0.73 (0.15)	0.70 [0.62;0.81]	Ref.	
AI method	809	0.47	2.12	0.76 (0.17)	0.73 [0,65;0.84]	0.80	7.4
Images analyzed once (not included in the validation dataset)							
AI method	2498	0.44	2.02	0.76 (0.16)	0.73 [0.65;0.84]	-	6.6

ICC: Intraclass correlation coefficient, IQR: Interquartile range, SD: Standard deviation

Table 4.1: Comparative values for CCA IMT estimations.

4.2.5 Statistical analysis

According to the sample size, a correlation coefficient of 0.05 between ABI and CCA IMT could be found as statistically significant accepting an alpha risk of 0.05 and a beta risk of 0.2.

All analysis was stratified by sex. Continuous variables were summarized as mean (standard deviation), or median [interquartile range] when their distribution departed from normal, and categorical variables as proportions. The correlation between the tertiles of ABI was ascertained using the mean values of carotid IMT, the prevalence of carotid plaque and other cardiovascular risk factors, ANOVA, Wilcoxon, and Chi-square, as appropriate. To compare the prevalence of cardiovascular risk factors and the mean values of ABI by the presence of atherosclerotic plaque, the Chi-Square, Student-t, and Mann-Whitney U tests were used as appropriate Unadjusted generalized additive models were fitted to find associations of ABI and other cardiovascular risk factors (independent variables) with IMT (dependent variable). This more flexible modeling approach allows for non-linearity in the relationship and contributes to a more accurate exploration of continuous variables, providing a pattern which reflects the shape and trend of the association. Breakpoint regression analysis was used to test whether an apparent change in the correlation trend between ABI and IMT was statistically significant [114]. Multivariable models were fitted by potential confounders that showed significant associations with the tertiles of ABI and CCA IMT. Finally, to assess the probability of carotid plaque in individuals with peripheral artery disease (symptomatic or asymptomatic), multivariable logistic regression models were adjusted for age. A subanalysis was performed, excluding participants with history of intermittent claudication reported by the participant or assessed with the Edinburgh questionnaire.

The effect modification of the relationship of ABI with common carotid IMT by age

	Men n =1516	Women n= 1791
Age, years, mean (SD)	61 (12)	60 (11)
Education level (University), n (%)	399 (260.5)	398 (220.4)
ABI, mean (SD)	1.11 (0.12)	1.09 (0.10)
Peripheral arteriopathy, n (%)	114 (70.5)	116 (60.5)
Asymptomatic peripheral arteriopathy, n (%)	63 (40.2)	38 (20.1)
Claudication, n (%)	51 (30.4)	78 (40.4)
Smoker, n (%)	712 (47.3)	301 (16.9)
Body mass index, mean (SD)	27.7 (3.7)	26.7 (4.9)
Systolic blood pressure (mmHg), mean (SD)	134 (18)	126 (20)
Diastolic blood pressure (mmHg), mean (SD)	79 (10)	75 (10)
Hypertension, n (%)	718 (48.1)	681 (38.7)
Total cholesterol (mg/dl), mean (SD)	196 (36)	206 (35)
HDL cholesterol (mg/dl), mean (SD)	47 (10)	56 (11)
LDL cholesterol (mg/dl), mean (SD)	127 (31)	132 (30)
Lipid-lowering treatment, n (%)	338 (22.8)	338 (19.2)
Triglycerides, median [IQR]	92 [68; 126]	79 [59; 111]
Glycemia (mg/dl), median [IQR]	95 [88; 105]	88 [83; 96]
Diabetes, n (%)	300 (20.3)	192 (11.0)
CCA IMT, mean (SD)	0.69 (0.14)	0.66 (0.14)
Atherosclerotic plaque, n (%)	129 (8.5)	97 (5.4)

IQR: Interquartile range, SD: Standard deviation

Table 4.2: Characteristics of the sample at baseline and follow-up, by sex.

[115] was tested with the -2 loglikelihood test of nested models with and without interaction terms. In a secondary analysis, the sample was stratified by age (<60 and ≥60 years).

The statistical analysis was conducted using R software, version 4.0.3 [80].

4.3 Results

We included 3307 individuals (1516 men and 1791 women), mean age 60 years (standard deviation 11). Table 4.2 includes the sociodemographic and clinical characteristics of the sample by sex.

CCA IMT significantly decreased by ABI tertiles, both in men [ABI tertile (T) 1: 0.70 mm (standard deviation 0.14); T2: 0.69 (0.16); T3: 0.67 (0.13); p <0.001] and in women [T1: 0.67 (0.13); T2: 0.66 (0.16); T3: 0.64 (0.14); $p = 0.005$]. No significant differences were found in the prevalence of atherosclerotic plaque by tertiles of ABI (Table 4.3).

In the regression of CCA IMT with ABI, we found similarly significant associations in men [Beta-coefficient (95% confidence interval) = -0.173 (-0.232; -0.114); p <0.001] and in women [-0.134 (0.200; -0.068); $p < 0.001$]. Individuals with no claudication also presented with significant correlations (< 0.001) between IMT and ABI [-0.182 (0.243;

	Men				Women			
	1st Tertile [.52, 1.08) n = 515	2nd Tertile [1.08, 1.17) n = 532	3rd Tertile [1.17, 1.40] n = 469	p	1st Tertile [.50, 1.06) n = 614	2nd Tertile [1.06, 1.14) n = 633	3rd Tertile [1.14, 1.40] n = 544	p
Age, years, mean (SD)	63 (12)	60 (11)	59 (11)	<0.001	62 (12)	59 (11)	59 (11)	<0.001
Education level (University) n (%),	105 (20.6)	160 (30.3)	134 (28.8)	0.001	108 (17.8)	149 (23.6)	141 (26.2)	0.002
Smoker, n (%)	268 (52.2)	248 (46.8)	196 (42.3)	0.008	88 (14.4)	120 (19.0)	93 (17.2)	0.095
Body mass index, mean (SD)	27.4 (3.5)	27.6 (3.7)	28.0 (4.0)	0.026	26.9 (4.9)	26.5 (5.1)	26.8 (4.8)	0.315
SBP (mmHg), mean (SD)	138 (20)	133 (17)	130 (17)	<0.001	132 (22)	124 (19)	121 (17)	<0.001
DBP (mmHg), mean (SD)	79 (11)	79 (10)	78 (9)	0.281	76 (10)	74 (10)	73 (9)	<0.001
Hypertension, n (%)	284 (55.9)	248 (47.4)	186 (40.3)	<0.001	304 (50.6)	214 (34.5)	163 (30.2)	<0.001
Total cholesterol (mg/dl),mean (SD)	196 (39)	197 (34)	193 (35)	0.284	207 (36)	207 (34)	205 (35)	0.640
HDL cholesterol (mg/dl),mean (SD)	47 (11)	48 (11)	47 (10)	0.431	55 (11)	57 (12)	57 (11)	0.040
LDL cholesterol (mg/dl),mean (SD)	127 (33)	127 (29)	127 (31)	0.973	132 (31)	132 (30)	131 (30)	0.708
Triglycerides,median [IQR]	93 [70;132]	95 [68; 130]	86 [66; 116]	0.002	85 [61;118]	78 [58; 107]	76 [58; 103]	0.002
Glycemia (mg/dl),median [IQR]	96 [89;108]	94 [88; 103]	95 [88; 104]	0.080	89 [83; 98]	88 [83; 96]	88 [83; 95]	0.514
Diabetes, n (%)	124 (24.7)	97 (18.8)	79 (17.3)	0.009	89 (14.9)	63 (10.3)	40 (7.5)	<0.001
CCA IMT mean (SD)	0.70 (0.14)	0.69 (0.16)	0.67 (0.13)	<0.001	0.67 (0.13)	0.66 (0.16)	0.64 (0.14)	0.005
Atherosclerotic plaque, n (%)	52 (10.1)	44 (8.3)	33 (7.1)	0.222	41 (6.7)	31 (4.9)	25 (4.6)	0.229

IQR: Interquartile range, PAD: Peripheral artery disease, SD: Standard deviation, SBP: Systolic blood pressure, DBP: Diastolic blood pressure.

Table 4.3: Characteristics of participants by tertiles of ABI.

Men				Women			
	Model[a]				Model[b]		
ABI Range	N	Beta Coefficient (95% CI)[a]	p	ABI Range	n	Beta Coefficient (95% CI)[b]	p
All	1516	-0.068 (-0.123; -0.012)	0.016	All	1791	-0.011 (-0.070;0.048)	0.723
$[0.5; 1, 2)$	1181	-0.071 (-0.147;0.005)	0.066	[0.5; 1.2]	1586	-0.029 (-0.105;0.047)	0.456
[1.2; 1.4]	335	0.121 (-0.149;0.391)	0.382	(1.2; 1.4]	205	0.007 (-0.340; 0.492)	0.721
Men with no claudication				Women with no claudication			
All	1465	-0.073 (-0.130; -0.017)	0.011	All	1713	-0.006 (-0.067;0.055)	0.848
[0.5; 1.0]	169	-0.027 (-0.195;0.141)	0.751	[.4; 1.2)	1419	-0.010 (-0.079;0.060)	0.786
(1.0; 1.4]	1296	-0.048 (-0.133;0.036)	0.261	[1.2; 1.4]	292	0.031 (-0.089;0.008)	0.617

CI: confidence interval, [a]Model adjusted for age and body mass index, [b]Model adjusted for age

Table 4.4: CCA IMT by ABI in the whole sample and stratified by breakpoints in all participants and in those with no claudication.

0.122) and 0.124 (0.192; 0.056) in men and women, respectively] (Figure 4.1).

We adjusted generalized additive multivariable models for the whole sample and for where the slope changed (ie, breakpoint). The results were only significant in men overall and in those with no claudication [-0.068 (0.123; 0.012); $p = 0.016$ and 0.073 (0.130; 0.017); $p = 0.011$, respectively]. No differences were found in women (Table 4.4).

The adjusted risk of atherosclerotic plaque at the CA in individuals with peripheral artery disease significantly increased in all women and in those with no claudication [Odds ratio (95% confidence interval) =2.61, (1.46;4.69); $p = 0.001$ and 2.49 (.99; 6.28); p= 0.053, respectively]. The risk was also significant in men with no claudication [2.08 (1.09; 3.96); p= 0.026] (Figure 2).

The analysis stratified by age found similar results in the correlation between ABI and IMT, with significant associations only in men (see Tables 4.5, 4.6, 4.7, 4.8, 4.9, 4.10 and Figure 4.3). In addition, the probability of carotid plaque in individuals with peripheral artery disease was only significant in older men and women (>60 years) [2.03, (1.13; 3.63); $p = 0.017$ and 2.84 (1.47; 5.49); $p = 0.002$, respectively] (see Figure 4.4).

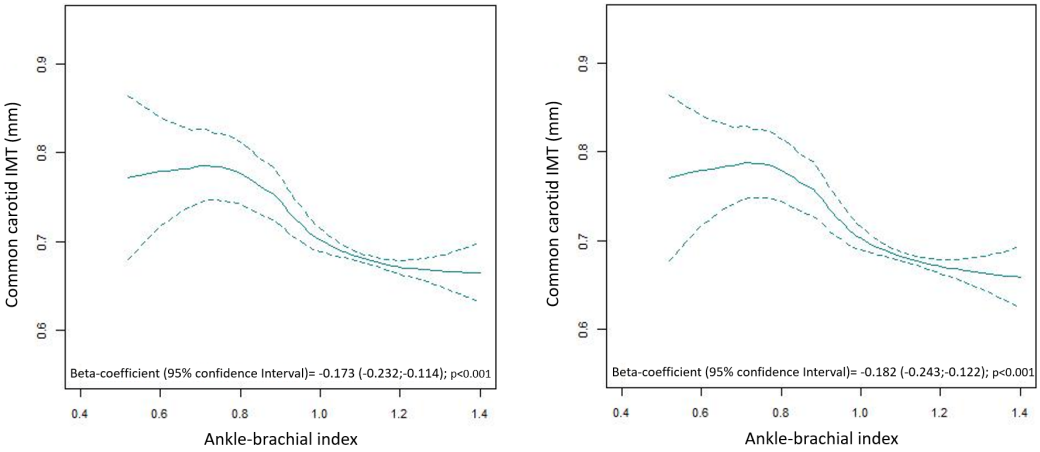

(a) All Men

(b) Men with no Claudication

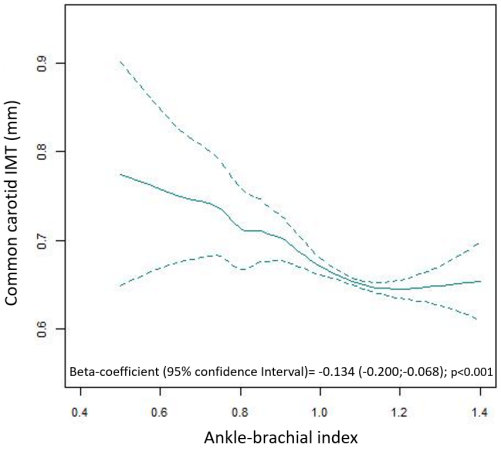

(c) All Women

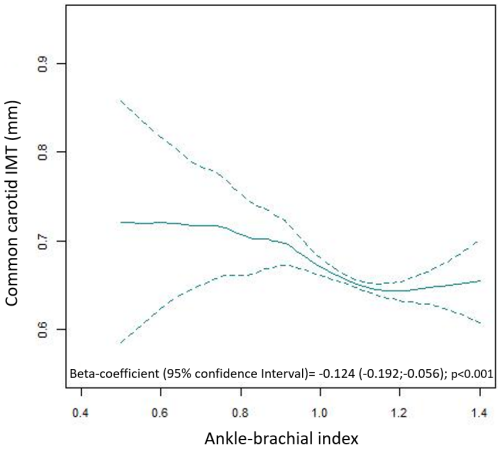

(d) Women with no Claudication

Figure 4.1: Correlations between ABI and CCA IMT by sex in all participants and in those with no claudication.

	Men		Women	
	<60 years old n=738	≥60 years old n=778	<60 years old n=926	≥60 years old n=865
Education level (University), n (%)	241 (32.7)	158 (20.6)	305 (33.2)	93 (10.8)
Ankle-brachial index, mean (SD)	1.13 (0.10)	1.09 (0.14)	1.10 (0.09)	1.08 (0.11)
Peripheral arteriopathy, n (%)	30 (4.1)	84 (10.8)	43 (4.6)	73 (8.4)
Asymptomatic peripheral arteriopathy, n (%)	9 (1.2)	54 (6.9)	8 (0.9)	30 (3.5)
Claudication, n (%)	21 (2.9)	30 (3.9)	35 (3.8)	43 (5.0)
Smoker, n (%)	295 (40.3)	417 (54.0)	229 (24.8)	72 (8.4)
Body mass index, mean (SD)	27.4 (3.8)	27.9 (3.6)	25.6 (4.9)	27.9 (4.7)
Systolic blood pressure (mmHg), mean (SD)	127 (16)	140 (18)	116 (16)	136 (19)
Diastolic blood pressure (mmHg), mean (SD)	80 (10)	78 (10)	74 (10)	75 (9)
Hypertension, n (%)	244 (33.6)	474 (61.8)	184 (20.3)	497 (58.3)
Total cholesterol (mg/dl), mean (SD)	202 (35)	190 (36)	202 (36)	211 (34)
HDL cholesterol (mg/dl), mean (SD)	48 (10)	47 (11)	57 (12)	56 (11)
LDL cholesterol (mg/dl), mean (SD)	133 (30)	122 (31)	128 (31)	135 (29)
Lipid-lowering treatment, n (%)	85 (11.6)	253 (33.7)	81 (8.8)	257 (30.6)
Triglycerides, median [IQR]	89 [67; 127]	93 [70; 125]	69 [53; 95]	92 [68; 121]
Glycemia (mg/dl), median [IQR]	93 [87; 100]	98 [90; 111]	87 [81; 93]	91 [85; 100]
Diabetes, n (%)	75 (10.4)	225 (29.8)	55 (6.1)	137 (16.4)
CCA IMT, mean (SD)	0.64 (0.12)	0.73 (0.15)	0.60 (0.13)	0.72 (0.13)
Carotid atherosclerotic plaque, n (%)	35 (4.8)	94 (12.1)	28 (3.0)	69 (8.0)

IQR: Interquartile range, SD: Standard deviation

Table 4.5: Characteristics of men and women, by age group.

	<60 years old			≥ 60 years old		
	No plaque n=698	Plaque n=35	p	No plaque n=683	Plaque n=94	p
Education level (University), n (%)	223 (32.0)	16 (45.7)	0.131	144 (21.4)	14 (15.1)	0.200
Ankle-brachial index, mean (SD)	1.13 (0.10)	1.11 (0.14)	0.355	1.10 (0.13)	1.07 (0.16)	0.162
Peripheral arteriopathy, n (%)	28 (4.0)	2 (5.7)	0.649	67 (9.8)	17 (18.1)	0.025
Asymptomatic peripheral arteriopathy, n (%)	7 (1.0)	2 (5.7)	0.065	41 (6.0)	3 (13.8)	0.010
Claudication, n (%)	21 (3.0)	0 (0.0)	0.618	26 (3.8)	4 (4.3)	0.776
Smoker, n (%)	276 (39.8)	17 (48.6)	0.394	353 (52.1)	64 (68.1)	0.005
Body mass index, mean (SD)	27.3 (3.8)	28.4 (4.0)	0.115	27.9 (3.6)	28.4 (3.8)	0.238
Systolic blood pressure (mmHg), mean (SD)	127 (15)	134 (19)	0.043	139 (19)	143 (17)	0.060
Diastolic blood pressure (mmHg), mean (SD)	80 (10)	82 (10)	0.156	78 (10)	75 (10)	0.003
Hypertension, n (%)	224 (32.7)	17 (48.6)	0.078	407 (60.3)	66 (72.5)	0.032
Total cholesterol (mg/dl), mean (SD)	203 (35)	199 (30)	0.608	191 (35)	181 (39)	0.022
HDL cholesterol (mg/dl), mean (SD)	48 (10)	46 (10)	0.524	47 (11)	45 (11)	0.131
LDL cholesterol (mg/dl), mean (SD)	133 (30)	133 (26)	0.884	123 (31)	114 (31)	0.014
Lipid-lowering treatment, n (%)	80 (11.5)	4 (11.8)	0.999	211 (31.9)	42 (47.2)	0.006
Triglycerides, median [IQR]	90 [66; 128]	89 [73; 114]	0.704	93 [70; 126]	94 [77; 121]	0.919
Glycemia (mg/dl), median [IQR]	92 [86; 100]	95 [90; 109]	0.066	97 [90; 109]	102 [93; 118]	0.003
Diabetes, n (%)	68 (10.0)	6 (17.1)	0.163	185 (27.8)	40 (44.9)	0.001

IQR: Interquartile range, SD: Standard deviation

Table 4.6: Characteristics of men by the presence of atherosclerotic plaque and age.

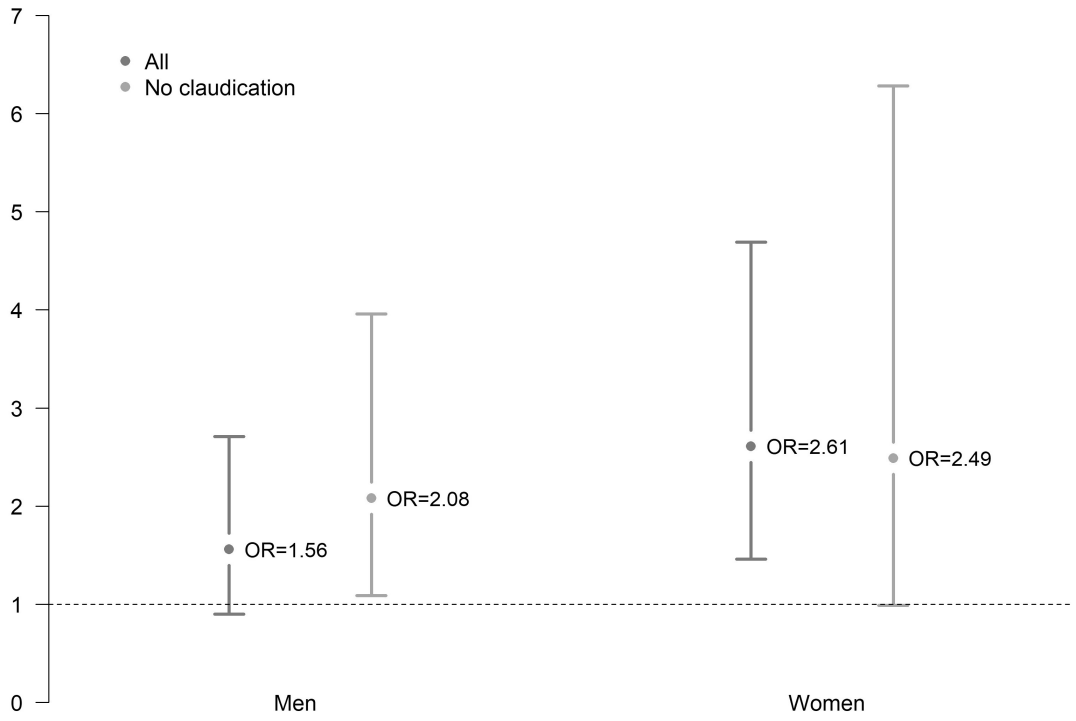

Figure 4.2: Probability of carotid plaque in all individuals and in those with no claudication. Models adjusted for age.

4.4 Discussion

Polyvascular subclinical disease, defined as the coexistence of atherosclerosis in different vascular beds within the same individual, should be considered a systemic process. We measured the coexistence of subclinical atherosclerosis at the lower limb, as measured with ABI, and at the CCA, as measured with IMT or with the presence of atherosclerotic plaque. In men, a linear negative dose-response association between the degree of atherosclerosis at the lower limb and at the CCAs was observed. In women, peripheral artery disease (symptomatic or asymptomatic) significantly increased the risk of atherosclerotic plaque in the CAs

Recognition of the atherosclerosis process as a systemic disease, as reported by numerous authors, is necessary to improve the prevention outcomes [103]. First, core risk factors such as smoking, diabetes, hypertension, hypercholesterolemia, obesity, and family history appear to be shared among all vascular diseases, regardless of the territory affected [116, 117]. Second, subclinical peripheral artery disease in patients with coronary artery disease is associated with a poor prognosis during the first year after an acute coronary syndrome event [118]. Third, CCA IMT or the presence of atherosclerotic plaques at the CAs improve the prediction of incident CVD [95, 119,

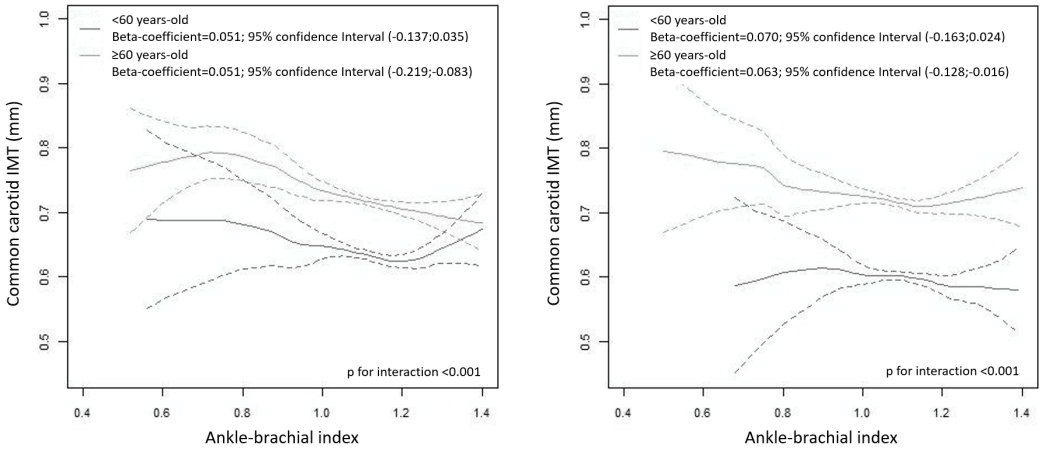

(a) Men (b) Women

Figure 4.3: Correlations between ABI and CCA IMT by sex and age.

	<60 years old			≥ 60 years old		
	No plaque n=894	Plaque n=28	*p*	No plaque n=794	Plaque n=69	*p*
Education level (University), n (%)	294 (33.1)	11 (40.7)	0.534	86 (10.9)	7 (10.3)	0.999
Ankle-brachial index, mean (SD)	1.10 (0.09)	1.09 (0.07)	0.233	1.08 (0.11)	1.06 (0.15)	0.189
Peripheral arteriopathy, n (%)	40 (4.5)	3 (10.7)	0.138	60 (7.6)	13 (18.8)	0.003
Asymptomatic peripheral arteriopathy, n (%)	8 (0.9)	0 (0.0)	0.999	24 (3.0)	6 (8.7)	0.027
Claudication, n (%)	32 (3.6)	3 (10.7)	0.086	36 (4.5)	7 (10.1)	0.074
Smoker, n (%)	223 (25.0)	6 (21.4)	0.835	65 (8.2)	7 (10.6)	0.655
Body mass index, mean (SD)	25.7 (4.9)	26.0 (4.4)	0.668	27.9 (4.7)	27.9 (4.4)	0.918
Systolic blood pressure (mmHg), mean (SD)	116 (16)	122 (21)	0.127	135 (19)	139 (21)	0.223
Diastolic blood pressure (mmHg), mean (SD)	74 (10)	79 (14)	0.080	75 (9)	74 (9)	0.440
Hypertension, n (%)	174 (19.8)	9 (33.3)	0.140	452 (57.9)	44 (63.8)	0.410
Total cholesterol (mg/dl), mean (SD)	201 (35)	209 (38)	0.331	211 (33)	213 (34)	0.634
HDL cholesterol (mg/dl), mean (SD)	57 (12)	55 (10)	0.354	56 (11)	55 (11)	0.372
LDL cholesterol (mg/dl), mean (SD)	128 (31)	134 (33)	0.405	135 (29)	138 (31)	0.389
Lipid-lowering treatment, n (%)	74 (8.3)	7 (25.0)	0.008	233 (30.3)	23 (34.3)	0.579
Triglycerides, median [IQR]	69 [53; 93]	78 [56; 123]	0.103	92 [69; 121]	91 [65; 121]	0.620
Glycemia (mg/dl), median [IQR]	86 [81; 93]	90 [85; 101]	0.011	90 [85; 100]	93 [86; 102]	0.279
Diabetes, n (%)	51 (5.9)	4 (15.4)	0.069	121 (15.8)	16 (23.2)	0.155

IQR: Interquartile range, SD: Standard deviation

Table 4.7: Characteristics of women by the presence of atherosclerotic plaque and age.

	<60 years old				≥60 years old			
	1st tertile [0.56, 1.10) n=280	2nd tertile [1.10, 1.18) n=224	3rd tertile [1.18, 1.40] n=234	p	1st tertile [0.52, 1.07) n=270	2nd tertile [1.07, 1.16) n=265	3rd tertile [1.16, 1.40] n=243	p
Education level (University), n (%)	79 (28.2)	81 (36.2)	81 (34.6)	0.124	39 (14.7)	62 (23.7)	57 (24.0)	0.012
Smoker, n (%)	122 (43.9)	83 (37.2)	90 (38.8)	0.275	156 (57.8)	143 (54.2)	118 (49.4)	0.164
Body mass index, mean (SD)	27.3 (3.6)	27.2 (4.0)	27.6 (3.9)	0.530	27.5 (3.5)	28.1 (3.4)	28.4 (4.0)	0.014
Systolic blood pressure (mmHg), mean (SD)	129 (17)	128 (14)	125 (15)	0.009	144 (20)	140 (17)	135 (17)	<.001
Diastolic blood pressure (mmHg), mean (SD)	81 (10)	80 (9)	79 (9)	0.223	77 (11)	79 (10)	77 (9)	0.163
Hypertension, n (%)	106 (38.6)	76 (34.6)	62 (26.8)	0.020	189 (70.8)	148 (56.5)	137 (57.6)	0.001
Total cholesterol (mg/dl), mean (SD)	208 (35)	199 (34)	198 (35)	0.001	185 (36)	195 (36)	189 (34)	0.009
HDL cholesterol (mg/dl), mean (SD)	47 (10)	48 (12)	47 (9)	0.463	46 (12)	47 (10)	47 (10)	0.558
LDL cholesterol (mg/dl), mean (SD)	137 (29)	130 (29)	132 (31)	0.017	118 (32)	125 (30)	122 (30)	0.022
Triglycerides, median [IQR]	98 [71; 141]	88 [65; 125]	83 [64; 115]	0.001	92 [72; 127]	97 [69; 130]	92 [69; 117]	0.329
Glycemia (mg/dl), median [IQR]	93 [87; 101]	92 [86; 100]	93 [87; 100]	0.434	98 [90; 112]	97 [90; 109]	97 [90; 110]	0.570
Diabetes, n (%)	34 (12.5)	19 (8.7)	22 (9.6)	0.343	94 (35.9)	69 (26.6)	62 (26.4)	0.028
CCA IMT, mean (SD)	0.65 (0.12)	0.62 (0.11)	0.63 (0.12)	0.017	0.75 (0.14)	0.74 (0.17)	0.71 (0.13)	0.004
Atherosclerotic plaque, n (%)	15 (5.8)	10 (4.5)	9 (3.9)	0.592	39 (14.4)	29 (11.9)	26 (10.7)	0.342

IQR: Interquartile range, PAD: Peripheral artery disease, SD: Standard deviation

Table 4.8: Characteristics of the sample by ABI in men by age.

	<60 years old				≥60 years old			
	1st tertile [0.68, 1.07) N=316	2nd tertile [1.07, 1.14) N=315	3rd tertile [1.14, 1.39] N=295	p	1st tertile [0.50, 1.05) N=309	2nd tertile [1.05, 1.13) N=284	3rd tertile [1.13, 1.40] N=272	p
Education level (University), n (%)	95 (30.4)	100 (31.9)	110 (37.7)	0.133	21 (6.9)	39 (13.8)	33 (12.2)	0 0.017
Smoker, n (%)	76 (24.1)	81 (25.8)	72 (24.5)	0.870	21 (6.9)	25 (8.8)	26 (9.6)	0.461
Body mass index, mean (SD)	25.9 (5.3)	25.5 (5.0)	25.6 (4.4)	0.622	27.8 (4.5)	27.5 (4.6)	28.3 (5.1)	0.135
Systolic blood pressure (mmHg), mean (SD)	120 (18)	115 (16)	113 (14)	<.001	142 (20)	134 (18)	130 (17)	<.001
Diastolic blood pressure (mmHg), mean (SD)	76 (10)	73 (10)	73 (9)	<.001	76 (9)	75 (9)	74 (9)	0.091
Hypertension, n (%)	79 (25.7)	59 (19.1)	46 (15.8)	0.008	215 (70.7)	154 (55.4)	128 (47.4)	<.001
Total cholesterol (mg/dl), mean (SD)	200 (39)	205 (34)	200 (33)	0.171	211 (33)	212 (33)	211 (35)	0.866
HDL cholesterol (mg/dl), mean (SD)	56 (12)	58 (12)	57 (11)	0.289	55 (10)	56 (12)	56 (11)	0.068
LDL cholesterol (mg/dl), mean (SD)	127 (34)	131 (30)	127 (29)	0.358	135 (29)	136 (29)	135 (30)	0.883
Triglycerides, median [IQR]	69 [52; 96]	67 [54; 95]	70 [54; 92]	0.953	96 [73; 126]	89 [67; 119]	89 [66; 119]	0.020
Glycemia (mg/dl), median [IQR]	86 [80; 94]	87 [82; 93]	87 [81; 93]	0.348	91 [85; 102]	90 [84; 99]	90 [85; 99]	0.245
Diabetes, n (%)	25 (8.2)	22 (7.2)	8 (2.8)	0.014	63 (21.0)	38 (14.1)	36 (13.4)	0.024
CCA IMT, mean (SD)	0.60 (0.10)	0.60 (0.17)	0.59 (0.10)	0.299	0.73 (0.13)	0.72 (0.12)	0.71 (0.15)	0.226
Atherosclerotic plaque, n (%)	12 (3.8)	9 (2.9)	7 (2.4)	0.589	30 (9.8)	18 (6.3)	21 (7.7)	0.300

IQR: Interquartile range, PAD: Peripheral artery disease, SD: Standard deviation

Table 4.9: Characteristics of the sample by ABI in women by age.

	Men				Women			
	<60 years old		≥ 60 years old		<60 years old		≥ 60 years old	
	Coefficient (95% CI)	p	Coefficient (95% CI)	p	Coefficient (95% CI)	p	Coefficient (95% CI)	p
ABI	-0.051(-0.137; 0.035)	0.247	-0.154(-0.230; -0.077)	0.001	-0.070 (-0.163; 0.024)	0.146	-0.063 (-0.142; 0.016)	0.121
Education level (University)	-0.011(-0.030; 0.007)	0.221	-0.015(-0.041; 0.012)	0.270	-0.025 (-0.042; -0.007)	0.005	-0.026 (-0.054; 0.003)	0.076
Smoker	0.030(0.012; 0.047)	<.001	0.029(0.008; 0.050)	0.008	0.022 (0.003; 0.041)	0.024	0.018 (-0.014; 0.050)	0.262
Body mass index	0.006 (0.004; 0.009)	<.001	-0.001(-0.004; 0.002)	0.388	0.007 (0.006; 0.009)	<.001	0.002 (0.000; 0.004)	0.021
Systolic blood pressure	0.002 (0.001; 0.002)	<.001	0.001(0.000; 0.002)	<.001	0.002 (0.001; 0.002)	<.001	0.001 (0.001; 0.002)	<.001
Diastolic blood pressure	0.002 (0.001; 0.003)	<.001	-0.002 (-0.003; -0.001)	0.003	0.003 (0.002; 0.004)	<.001	-0.001 (-0.002; 0.000)	0.012
Hypertension	0.054(0.036; 0.068)	<.001	0.040(0.018; 0.062)	<.001	0.065 (0.045; 0.085)	<.001	0.042 (0.024; 0.059)	<.001
Total cholesterol	0.000(0.000; 0.000)	0.130	0.000(0.000; 0.000)	0.563	0.000 (0.000; 0.000)	0.195	0.000 (0.000; 0.000)	0.464
HDL cholesterol	0.000 (0.000; 0.001)	0.428	0.000 (-0.001; 0.001)	0.693	-0.001 (-0.002; -0.001)	<.001	-0.001 (-0.002; 0.000)	0.041
LDL cholesterol	0.000 (0.000; 0.000)	0.256	0.000 (0.000; 0.000)	0.416	0.000 (0.000; 0.000)	0.108	0.000 (0.000; 0.000)	0.477
Triglycerides	0.000 (0.000; 0.000)	0.955	0.000 (0.000; 0.000)	0.459	0.000 (0.000; 0.001)	<.001	0.000 (0.000; 0.000)	0.023
Glycemia	0.001(0.001; 0.001)	<.001	0.000(0.000; 0.001)	0.013	0.001 (0.001; 0.002)	<.001	0.000 (0.000; 0.001)	0.819
Diabetes	0.050(0.022; 0.079)	<.001	0.037(0.013; 0.060)	0.002	0.068 (0.034; 0.103)	<.001	0.016 (-0.009; 0.040)	0.205

Table 4.10: Generalized additive multivariable models of CCA IMT and cardiovascular risk factors by sex and age.

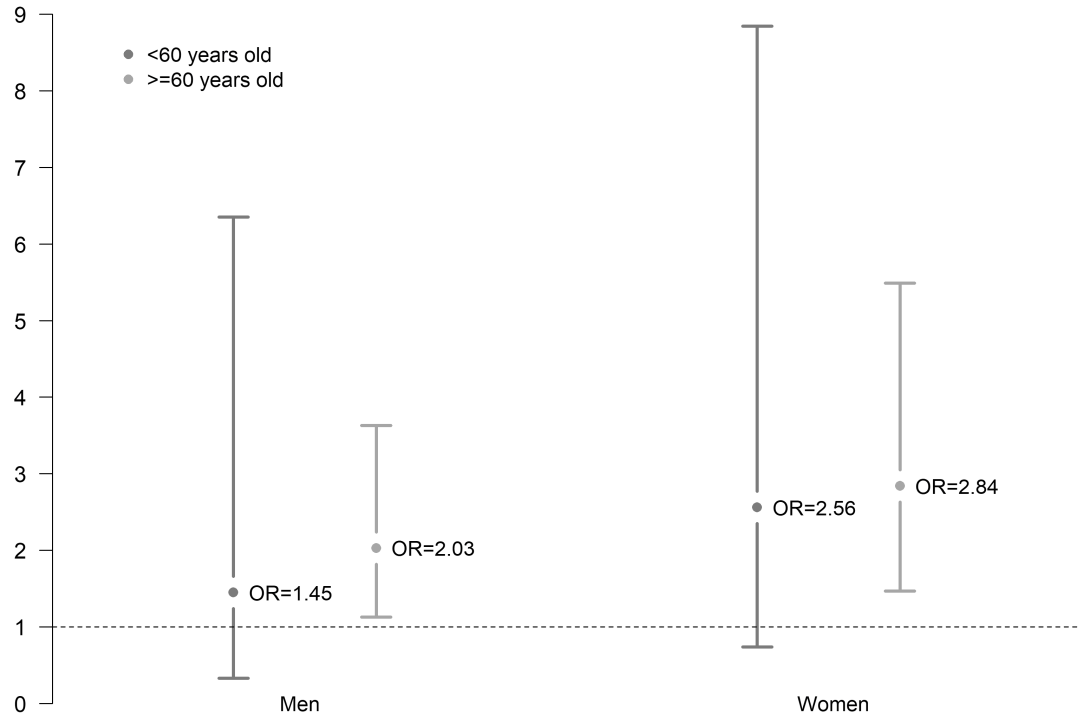

Figure 4.4: Probability of carotid plaque in individuals with peripheral artery disease by sex and age.

120, 121]. In general, the presence of subclinical atherosclerosis at different locations has been associated with higher risk of cardiovascular events in individuals with familial hypercholesterolemia [122] or in percutaneous coronary intervention patients[123].

Our analysis, consistent with previous studies, showed increased burden of subclinical disease in men, compared with women[124, 125]. On the one hand, men presented with a continuous dose-response association between ABI and IMT, particularly up to ABI values around 1.2, where a nonsignificant change in the trend was observed. A U-shaped pattern was previously described in a cross-sectional analysis not stratified by sex in a Chinese population of Inner Mongolia [126]. In addition, The Copenhagen City Heart Study showed that the magnitude of association between these biomarkers was higher in individuals with diabetes, compared with those without the disease [110]. The slope described in the latter group was similar to that observed in men in our results. In contrast, Zhang et al found that the association between IMT and ABI in patients with diabetes did not remain after adjusting for cardiovascular risk factors, but the IMT association with toebrachial index persisted. Finally, no association was found between ABI and IMT in the Spanish Registry of patients older than 60 years with a recent non-cardioembolic ischaemic stroke (ARTICO), performed in individuals with history of a

non-cardioembolic stroke in the preceding 3 months [111]. Less specific is the assessment of subclinical burden with magnetic resonance imaging (MRI) performed in the Cooperative Health Research in the Region of Augsburg (KORA-MRI) cohort. In this study, the carotid plaque in different arteries, together with other markers of subclinical disease, were measured in individuals without CVD. Thus, the comprehensive analysis of all markers showed that early signs of metabolic and cardio-cerebrovascular complications were more present in individuals with prediabetes, compared with controls [127].

On the other hand, women did not present with a doseresponse association, but a critical increase in the probability of carotid plaque was observed once peripheral artery disease (symptomatic or asymptomatic) was present. This finding, also highlighted by Colledanchise et al[128], may have particular value for cardiovascular risk assessment in women. Indeed, the Atherosclerosis Risk in Communities study showed that accounting for carotid plaque presence in addition to IMT leads to greater improvement of risk prediction in women than in men [129]. Thus, a combined assessment of subclinical atherosclerosis at the lower limb and CAs may improve disease detection over an assessment of either artery alone in both men and women, but particularly in women, in whom traditional risk assessments are less effective [8].

Our study has several limitations. The degree of atherosclerosis in the lower limb and CA was measured using different techniques. Although the final measurement can be comparable, future cohort studies could assess the extent of atherosclerosis using the same technique in both vascular beds (eg, US at femoral artery and CA). Selection bias may affect any crosssectional study, but is likely to be modest in magnitude in this study because it was population-based and participant selection was not based on the presence or absence of subclinical atherosclerosis. In addition, this design cannot establish temporality.

4.5 Conclusions

In this study we investigated the relationship between subclinical atherosclerosis biomarkers, focusing on lower limb atherosclerosis (ABI) and carotid atherosclerosis (measured by IMT and the presence of atherosclerotic plaque). We examined these associations within a general population and a sub-sample without a history of intermittent claudication.

Our analysis revealed a higher burden of subclinical disease in men, showing an association between ABI and IMT, similar to previous studies. The association between these biomarkers was stronger in individuals with diabetes. In contrast, among women,

while a dose-response relationship was not evident, a substantial increase in the likelihood of carotid plaque was observed in the presence of peripheral artery disease. This emphasizes the potential benefits of combining evaluations of subclinical atherosclerosis in both the CAs and lower limbs for improved disease detection, particularly in women, where conventional risk assessments may be less effective.

The study also highlights the systemic nature of polyvascular subclinical diseases and their coexistence with atherosclerosis in different vascular areas. This emphasizes the importance of recognizing atherosclerosis as a systemic disease to improve preventive measures and outcomes.

As a main limitation, the degree of atherosclerosis in the lower limb and CA was measured using different techniques. Although the final measurements may be comparable, future cohort studies could assess the extent of atherosclerosis using the same technique in both vascular beds, such as US in the femoral and CAs, for consistency.

In conclusion, this study showed two patterns of association between subclinical biomarkers of lower limb and CA atherosclerosis. Men showed a significant linear association between ABI levels and CCA IMT values, while women with symptomatic or asymptomatic peripheral artery disease presented with high risk of atherosclerotic plaque at the CA. Morover, our study points out the systemic nature of the atherosclerotic process. Individuals with biomarkers of atherosclerosis in a given territory are more likely to present with subclinical disease in another. The increased risk of ischemic events associated with this condition, and the differences found between men and women have important implications for cardiovascular risk management.

Chapter 5

Deep-stratification of the cardiovascular risk by ultrasound CA images

5.1 Introduction

In this section, we study the problem of characterizing the CIMT region and the atherosclerotic plaque to improve cardiovascular risk prediction. Thus, this section presents a state-of-the-art review of automatic methods that characterize the walls of the CA in longitudinal B-mode US images to enhance the assessment of cardiovascular health (part of this review is included in our chapter "Last Advances on Automatic Carotid Artery Analysis in Ultrasound Images: Towards Deep Learning" published in [24]). Moreover, this section introduces the details of our proposal, "Deep Stratification of Cardiovascular Risk by Ultrasound Carotid Artery Images" (see Section 1.5), which consists in a novel DL model that characterizes CA US images to enhance the survival model presented in [8]. In particular, this method extracts relevant features from images of the CA, specifically from the atherosclerotic plaque, using a DNN, and these features are added to the risk function [8] to improve cardiovascular risk prediction, specifically reclassification.

5.2 State of the art

Atherosclerosis is characterized by focal thickenings of the innermost layer of the artery, which is reflected in the artery walls. CA B-mode US is a well-established method that

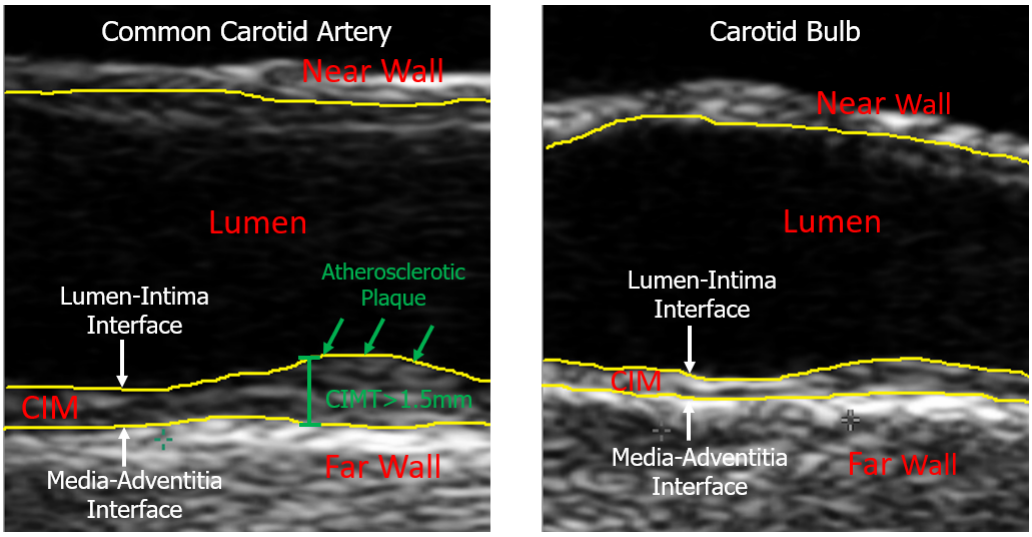

Figure 5.1: US CA images from two territories: CCA (left) and bulb (right). The different parts of the CA are delimited with lines: Near wall, Far wall, Lumen and CIM region. In both cases, the carotid IMT is estimated in the CIM region. Atherosclerotic plaque is a portion within the CIM with an IMT greater than 1.5mm [7].

helps to quantify and visualize atherosclerotic lesions since they provide the measurement of carotid IMT (see Figure 5.1) and the atherosclerotic plaque identification, following the criteria outlined in the Mannheim Consensus [7]. Therefore, the study of these images has been considered of clinical relevance. For example, tools that can monitor atherosclerosis can also improve diagnosis and subsequent treatment [4].

Furthermore, it is well known that the disruption of an atherosclerotic plaque plays a crucial role in the pathogenesis of CVD events [130, 131]. Plaque disruption is characterized by the content of lipid, muscle cells, and the thickness of the fibrous cap, among other factors [132]. Thus, there exists a medical interest related to the characterization of atherosclerotic plaques in CA. Non-invasive CA B-mode US is a well-established method that helps to visualize and quantify atherosclerotic lesions. Therefore, CA US characterization of plaque morphology is useful in assessing the vulnerability of the atherosclerotic lesions. Moreover, plaque and also CA walls characterization can be used as a powerful tool for assessing cardiovascular risk and predicting cardiovascular events [133].

The main purpose of image-techniques developed in this field is to create an image-based system that characterizes the atherosclerotic plaque and the CA walls. Given CA US images, the challenges of these methods can be mainly grouped in four distinct objectives (see Section 5.2.2 for more details):

- ***Objective 1:*** To classify atherosclerotic plaque between symptomatic and

asymptomatic.

- ***Objective 2:*** To stratify cardiovascular risk.
- ***Objective 3:*** To predict the risk of future cardiovascular events.
- ***Objective 4:*** To classify tissue components of the atherosclerotic plaque.

Several review articles can be found in the literature which include studies and techniques to deal with these objectives. Sharma et al. [134] provided the first state-of-the-art review to comprehend the field of ultrasonic vascular morphology tissue classification. In particular, they revised different ML techniques in tissue morphology and classification using US imaging. More recently, Saba et al. [135] provided guidelines about obtaining IMT and carotid plaque measurements and how these measurements are validated for risk stratification assessment and the prediction of events. This article concludes that advances in technology have helped to generate more accurate and consistent measurements of CA image-based features. In particular, AI methods such as ML and DL approaches have been widely adopted for CVD risk stratification assessment and the prediction of events using these CA image features. The very recent review article presented in [136] focuses on cardiovascular risk stratification through the use of DL techniques. In this study, it is observed that CNN algorithms are widely employed because they further enhance result accuracy compared to ML methods, as they automate the feature extraction process. Specifically, this review article provides an overview of DL methods for assessing cardiovascular risk by characterizing plaque through carotid US image techniques. These methods involve cardiovascular risk stratification systems that use DL methods for carotid wall segmentation in 2D US images, and subsequently acquire phenotypes based on images of the segmented region, such as carotid IMT and plaque area, among others.

5.2.1 Comparison of relevant works for CA characterization

Table 5.1 summarizes relevant works from the literature related to plaque and CA wall characterization in longitudinal B-mode US images and it compares the main characteristics of every method. The remainder of this subsection is devoted to discussing the information contained in Table 5.1: the properties of the data used in the different studies, the objectives of the different works, the considered image features, the used methods and the results.

Note that there is no fair way to do a general comparison of the results (see "Results" column from Table 5.1) because the validation methods, the GT, and the datasets are different in each proposal.

Author	Year	Cross-Sectional/ Follow-Up	Different Devices	Image Modality	Artery Territory	Work Objective	Image Features	Methods	N	Results	GT
Gronholdt et al.[16]	2001	FU (4.4 years)	No	UF	*NS*	Risk prediction of events (3)	GSM	Statistics Cox, Kaplan Meier	246 plaques 111 asym & 135 sym	Relative risk 3.1 between 2 plaque types	44 events in 4.4 years
Brajesh et al.[137]	2002	CS	No	UF	ICA	Mult. class.: 5 tissues (4)	PDA, GSM	Statistics Spearman	20 plaques (19 patients) 7sym & 13 asym	Spearman cc: 0.7	Endarterectomy
Nikolaos et al.[138]	2011	CS	No	2Frs	*NS*	Bin. class.: symp/asym (1)	GSM, WT FS: dv	SVM, PNN	20 plaques 11 Sym & 9 Asym	Acc: 90% (Diast.) 75% (Syst.)	Based on the clinical symptoms
Kyriacou et al.[139]	2012	FU (4 years)	No	UF	ICA	Risk prediction of events (3)	TPA, GSM, pdf and cdf	SVM, PNN	1121 stenosis	Acc 77%	Events with 157 death
Acharya et al.[140]	2012	CS	No	UF	ICA	Bin. class.: Sym/Asym (1)	WT FS: t-test	SVM	346 plaques 150 Asym & 196 Sym	Acc 83.7%	Based on the clinical symptoms
Irie et al.[17]	2013	FU (4.6 years)	No	4Frs	CCA, Bulb, ICA	Risk prediction of events (3)	TPA, plaque shape, GSM	Statistics AUC, Cox	287 plaques	AUC 0.82%	34 Events during 55 months
Acharya et al.[141]	2013	CS	Yes	UF	CCA	Bin. class.: sym/asym (1)	GLCM FS: t-test	SVM,kNN,PNN DT,GMM,NBC	146/346 plaques 44/196 Sym & 102/150 Asym	Acc 93.1% and 85.3%	Based on the clinical symptoms
Acharya et al.[142]	2013	CS	No	UF	Bulb	Bin. class.: sym/asym (1)	GLCM, RLM,WT, HOS FS: t-test	SVM	146 plaques (99 patients)	Acc 91.7%	Based on the clinical symptoms
Acharya et al.[143]	2013	CS	No	UF	CCA	Bin. class.: sym/asym (1)	LBP, GLCM, RLM,WT, HOS FS: t-test, kullback, dv	SVM	160 plaques 110 Asym & 50 Sym	Acc 90.7%	Based on the clinical symptoms
Gastounioti et al.[144]	2014	CS	Yes	Video	*NS*	Bin. class.: sym/asym (1)	kinematic features FS: Fisher, Wilcoxon, PCA	SVM,kNN,PNN DT, DA	56 plaques 28 Sym & 28 Asym	Acc 88%	Based on the clinical symptoms
Acharya et al.[145]	2015	CS	No	UF	CCA	Bin. class.: Sym/Asym (1)	IMT,IMTv . GL using HOS. FS: ANOVA	SVM,kNN,PNN	118 plaques (59 patients)	Acc 99.1%	Based on the clinical symptoms
Lekadir et al.[32]	2017	CS	No	UF	*NS*	Mult. class.: 3 tissues (4)	Patch based (end-to-end)	CNN	56 plaques	Acc 78.5% patch based Mean cc area 0.91%	Clinician expert
Araki et al.[146]	2017	CS	No	UF	CCA(far & near wall)	Risk stratification (2)	GLCM, RLM	SVM	407 plaques	Acc 99%	Lumen diameter for risk stratification
Saba et al.[133]	2017	CS	No	UF	CCA(far & near wall)	Risk stratification (2)	GLCM, RLM	PCA, SVM	407 plaques	Acc 98.83%	Lumen diameter for risk stratification
Mitchell [19]	2018	FU (13.3 years)	No	UF	CCA	Risk prediction of events (3)	TPA, GSM	Cox	2,205 individuals	AUC 76%	384 events in 13.3 years
Khanna et al.[18]	2019	FU (10 years)	No	UF	CCA	Risk prediction of events (3)	IMT and TPA phenotypes in two periods of time	Statistics AUC	202 individuals (2 images for period)	AUC 92.7%	risk stratification using risk functions
Saba et al.[147]	2021	CS	No	UF	ICA	Bin. class.: sym/asym (1)	Entire image	CNN	346 plaques 196 Sym & 150 Asym	Acc 86,17%	Based on the clinical symptoms
Our proposal	2023	FU (10 years)	No	UF	CCA & Bulb	Risk prediction of events (3)	Entire image	CNN & Cox	4,769 individuals	AUC 84%	151 events in 10 years

FU: Follow-Up, CS: Cross-Sectional, UF: Unique Frame, Frs: Frames, Symp: symptomatic, Asym: asymptomatic, IMTv: IMT variability, Acc: Accuracy, FS: Features selection, dv : divergence value, pdf: probability density function, Kullback: Kullback-Leiber, cdf: cumulative density function, *NS*: "Not Specified" in the referenced paper

Table 5.1: Most recent/relevant techniques for CA plaque characterization together with their main characteristics: author and reference, year of publication, if the method includes follow-Up measurements, if the dataset contains images acquired from different devices, the type of data as an unique frame or video, the artery territory, the objectives of the proposal method, the image features used, the main method used, the number of subjects or plaques and their characteristics (N), the results, and the GT used.

5.2.2 Key objectives in CA characterization for enhanced cardiovascular risk assessment and prediction

Characterization of CA images involves extracting image patterns that describe or classify atherosclerotic plaques and CA walls, aiming to achieve any of the four mentioned objectives. The most advanced works that utilize B-mode US images to characterize plaques and CA walls for assessing cardiovascular risk and predicting events can be primarily categorized into four distinct objectives found in the literature. These objectives all aim to improve the assessment and prediction of cardiovascular events and related risks. The details of these objectives are explained below.

- ***Objective 1:*** There are image-based techniques for binary classification of plaques: symptomatic and asymptomatic [138, 140, 141, 142, 143, 144, 145, 147] (see "Bin. class.: sym/asym" in column "Work Objective" from Table 5.1). Symptomatic plaques are from patients who have suffered any cerebrovascular event. In contrast, asymptomatic plaques are from patients who have not experienced any of these diseases.

- ***Objective 2:*** In the recent literature, some attempts have appeared to assess the CV risk of subjects using CA image features. This is carried out by solving a classification problem between two ranges: low and high risk [133, 146] (see "Risk stratification" in column "Work Objective" from Table 5.1).

- ***Objective 3:*** Despite the advances in imaging modalities and identifying plaque vulnerability characteristics, such as its composition, few of these plaques rupture and even fewer lead to clinical events [130, 131]. Therefore, it is important to perform studies to evaluate the individual risk that entails atherosclerosis evolution. This fact has motivated several studies to analyze the CA in a longitudinal study (i.e., repeated observations of the same subjects during a period of time) in order to predict the occurrence of CV events during a period [16, 17, 18, 19, 139] (see "Risk prediction of events" in column "Work Objective" from Table 5.1). Longitudinal studies involve repeated observations of the same subjects during a period of time (see column "Cross-Sectional/Follow-Up" from Table 5.1).

- ***Objective 4:*** It is established that the composition of atherosclerotic plaque is related to CVD [132, 131]. Some proposals in the literature deal with the classification of the plaque components (generally lipid, fibromuscular, and calcium). This classification is usually performed by an expert [148, 149] or using image-based techniques built on the gray intensity levels from the plaque region [32, 137] (see "Mult. class." in the column "Work Objective" from Table 5.1). These

image based-techniques address the classification problem with a multi-class classification method [137, 32]. The number of studies related to this objective are relatively small probably because the GT is difficult to obtain, either because it requires surgery [137] or it is manually obtained [32].

5.2.3 Different types of datasets

This subsection presents the characteristics of the data used for CA image characterization in various studies, including whether the data incorporates follow-up measurements (indicating a longitudinal study rather than a cross-sectional one), whether it is sourced from a single device, the inclusion of a single or multiple frames, the territory of the artery examined, the number of samples used, if the images contain plaque, characteristics of patients in terms of cardiovascular health (stenosis) and the GT employed.

Most of the studies focus on plaque characterization of a single frame of B-mode US longitudinal images from the CA [16, 18, 19, 32, 133, 137, 139, 140, 141, 142, 145, 143, 146, 147] (see "Unique Frame" in column "Image Modality" from Table 5.1). This is because US imaging is a non-expensive and non-invasive technique for CA visualization that has been extensively used to examine atherosclerosis of a patient (see Section 1.1.2). Different image modalities are also used in the literature using more than one frame, as in [17], where the scans of the CCA, the Bulb, and the ICA are performed bilaterally in three different longitudinal projections, as well as transversal projections to analyze the entire plaque. Other studies include the information of the CA appearance during the cardiac cycle. In these cases, the specific instants (systole and diastole) are analyzed separately in two frames [138], adding the information of the mechanical interactions from image sequences [144] (see "Video" in column "Image Modality" from Table 5.1).

Regarding the artery territory, in contrast to the research works reviewed in Section 2.2, the images used several studies belong to ICA and Bulb (see column "Artery Territory" Table 5.1). This is because plaques occur only occasionally in the other regions of the artery. Besides, not all studies focus on the CIM region. Near wall characterization also adds information of the entire artery [133, 146] (see "CCA (far & near wall)" in column "Artery territory" from Table 5.1).

The GT in the revised literature is closely related to the objective of the particular work (see column "GT" from Table 5.1). The GT in *Objective 1* is based on clinical symptoms, which means whether the individual whose image is analyzed suffered any symptom related to CVDs or not [141, 142, 138, 143, 144, 145, 147]. The GT for the *Objective 2* is a previous risk stratification using the lumen diameter, which is a factor related to atherosclerosis [133, 146]. For the *Objective 3*, the methods are validated using the events occurred in a period of time [16, 17, 19, 139, 147], except in [18]. In this

last paper, the validation is a comparison of the risk stratification (done using several cardiovascular risk factors) obtained from several risk prediction functions. Finally, the GT used for *Objective 4* is obtained from an endarterectomy (i.e., a surgical process that removes a sample of plaque) [137] or from a tissue component classification done by an expert [32].

The size of the datasets (see column "N" from Table 5.1) are similar to the studies presented in Section 2.2. The largest datasets presented in [139] and [19] with 1,121 and 2,205 subjects respectively and included in their follow-up study. Note that in the studies for the *Objective 4* the samples are small compared to the sample size of the other studies. This could be due because the endarterectomy used in the GT from [137] is aggressive for the patient, and the manual classification for the GT in [32] is tedious and very time-consuming.

The datasets can include images of CA from individuals with atherosclerotic plaque ("plaques"), from general population ("individuals") or from individuals with stenosis ("stenosis"), which is a clinical term to design a narrowing of the artery. If the number of plaque images does not correspond to the number of individuals, the number of patients is specified in parentheses.

Regarding the acquisition devices (see column "Different Devices" from Table 5.1), most of the works use datasets provided by a single device. In contrast, the images used in [141] and in [144] were obtained from two different types of equipment. Despite the challenge they present, their proposals result in most robust methods for risk prediction (*Objective 3*) [141] and for the classification of the presence or absence of past CV symptoms (*Objective 1*) [144].

5.2.4 Image features for CA characterization

The following section describes the key image features identified in the literature for characterizing the CA wall in US images.

Feature based on CA image phenotypes

Carotid IMT and plaque measurements are frequently utilized in the literature, as they are validated for use as calculators in risk stratification assessment and event prediction [135, 136]. Some studies use image features, called *image phenotypes*, which represent quantitative measures associated with intima-media thickness (IMT) or atherosclerotic plaque. These measures encompass parameters such as mean IMT, maximum IMT, minimum IMT, or IMT variability ([145, 18]). Most studies using image phenotypes employ phenotypes related to atherosclerotic plaque, which are metrics such as Total

Plaque Area (TPA) or Grayscale Median (GSM) ([139, 17, 16, 137, 138, 18]). Some studies use image phenotypes of atherosclerotic plaque to compare them with the occurrence of CVD or other pathologies during a follow-up period [17, 139]. To our knowledge, the most recent work utilizing these types of features is presented in [18]. This study introduces an image-based method to develop a 10-year risk calculator, based on the fusion of various cardiovascular risk factors and changes, during the follow up, in the CA phenotypes. The image phenotypes were extracted from the segmented region obtained through the $AtheroEdge^{TM}$ system [41] (mentioned in Section 2.2).

Features based on gray intensity values

The features used in the literature to characterize atherosclerotic tissue are, in general, based on gray intensity values (see column "Image Features" from Table 5.1). The most standard feature is the GSM method [17, 137, 133, 146, 138]. The technique proposed in [137] for the *Objective 2* is a combination of GSM and Pixel Distribution Analysis (PDA). However, it demonstrates an agreement between these image features and histologic measurements. The studies proposed in [133, 146] presented good accuracies for risk stratification using GSM features. The estimation of the spatial distribution of gray levels is a suitable technique for texture analysis. Gray Level Co-occurrence Matrix [150] and Run Length Matrix (RLM) [151] methods based on gray level values are used to examine the texture in CA US images [141]. For a more objective analysis, the group of Acharya et al. [141, 142, 143] developed novel integrated indices using a combination of significant features to deal with *Objective 1*. As a result, they concluded that grayscale features based on a combination of trace transform [152] and texture properties are suitable for the classification of symptomatic and asymptomatic plaques. Another different approach using the information of the pixel intensity values and their distribution is the tissue classification method (*Objective 4*) proposed in [32]. In contrast to the other proposals, the image feature used in this case is the entire patch around the pixel that is used as the input to the model.

Feature based on frequency approaches

Frequency-based approaches, such as the ones based on Wavelet Transforms (WT), can decompose the frequency content of the image and, consequently, reveal texture characteristics from different materials of the plaque [138, 140, 142, 143]. Several studies present a scale-frequency approach showing that WT features are a good alternative for the characterization of plaque tissue between the symptomatic and asymptomatic groups (*Objective 1*). In this sense, Tsiaparas et al. [138] demonstrated that WT features are more accurate than classical features as GSM, since they capture both the frequency and spatial content of the image. The methods presented in [140, 142,

143, 145] use a combination of some techniques mentioned above such as GLCM, RLM and WT resulting in good accuracies for the binary classification of the *Objective 1*. In particular, Acharya et al. [143] also used a gray-based feature texture known as Local Binary Pattern (LBP), whilst [142, 143, 145] added the features extracted by the Higher-Order Spectra (HOS) technique [153], which provides high noise immunity.

5.2.5 Characterizing the CA: Statistical and DL Approaches

Different methods have been proposed in the literature to address the various objectives mentioned before, using the respective types of image features (see the "Methods" column in Table 5.1).

Statistical methods for atherosclerotic plaque classification

Several statistical methods are used in order to characterize the atherosclerotic plaque or CA wall in US iamges. For the *Objective 1*, common statistical methods are used in the literature in order to select the relevant features for the binary discrimination. These methods are Student's t-test [140, 141, 142], ANOVA test [145], and Divergence value to rank the features [138, 143]. An interesting work that combines three different selection strategies is presented in [144]. These strategies are Fisher discriminant ratio, Wilcoxon rank-sum test, and Principal Component Analysis (PCA), and were used to select the features that are able to better discriminate the two groups. In particular, the features used in this study are kinematic features of the arterial wall estimated with the motion analysis from B-mode US image sequences, occurring during the cardiac cycle. Statistical methods are also used to evaluate the classification of atherosclertoic plaque composition (*Objective 4*), as seen in [137], which applied the Spearman coefficient of correlation for comparisons between PDA for different tissue components and the histologic analysis of plaques.

Statistical methods for cardiovascular risk prediction

Kaplan-Meier analysis and Cox regression are statistical methods commonly used in survival studies to analyze and predict events in longitudinal studies, such as those utilized in *Objective 3*. Specifically, both of these methods were employed in the study by Gronholdt et al.[16], while only Cox regression was utilized in the study conducted by Irie et al. [17]. Also, the Area Under the Curve (AUC) was used to validate the same objective in [17, 18]. In this case, AUC measures the ability of the binary classifier in risk stratification for the validation in [18] (see "GT" column from Table 5.1) and in risk prediction of events in [17]. In particular, using the AUC, Khanna et al. [18] concluded that the addition of the image-based phenypes to the classical cardiovascular risk factors outperforms the ten currently available conventional cardiovascular risk calculators.

ML approaches for CA characterization

On the other hand, the basic ML methods presented for the *Objective 1* are supervised classifiers based on the assumption that each of these features belong to two distinct classes: symptomatic and asymptomatic. In these cases the classification methods are: k-Nearest Neighbor (kNN) [141, 144, 145], Decision Trees (DT) [141, 144], Discriminant Analysis (DA), [144], Gaussian Mixture Model (GMM) [141], and Naïve Bayes classifier (NBC) [141]. The most common ML method used in the revised literature is Support Vector Machine (SVM), used for classification in *Objective 1* [138, 140, 141, 142, 143, 144, 145] and for risk stratification in *Objective 2* [133, 146].

DL approaches for CA characterization

DL strategies as Probabilistic Neural Networks (PNN) are also used for *Objective 1* [138, 141, 144, 145] and for risk prediction in *Objective 3* [139]. These DL strategies use hand-crafted feature vectors as input to the network and a traditional pipeline design, instead of using the raw image as input and allowing an end-to-end learning. In contrast, other studies use DL methods to automate the feature extraction process. For their part, Lekadir et al. [32] present, for the first time in the literature, a DL approach that performs end-to-end learning using a CNN with image patches as the input to the model to address *Objective 4*. This approach conducts multi-class classification of each pixel of the plaque into a tissue component. The entire patch incorporates all the information around the pixel that is analyzed by the model. Then, the CNN automatically selects the relevant information optimal for discriminating the different plaque constituents, resulting in good accuracy results and correlation. Another end-to-end DL approach using CNNs is presented in [147] to address the automated carotid plaque characterization based on a binary classification system (*Objective 3*).

5.3 Enhancing cardiovascular risk prediction through DL analysis of CA images

In the field of cardiovascular epidemiology, practitioners use risk prediction functions [8, 9, 10, 11, 12] to estimate the risk of suffering an event in a period of time. These functions are based on survival models and estimate the risk using a set of clinical variables of each individual. These functions accurately stratify individuals into low, moderate, and high-risk categories. However, they tend to classify a considerable number of individuals into the middle-risk category, and often, a subsequent reclassification into high-risk groups is required. An example of this is the risk prediction function

presented in the REGICOR study [8], which has been demonstrated to make accurate predictions of cardiovascular events [8, 10, 11, 154]. However, it concentrates the majority of its events (60%) in the medium-risk category (Table 1.1 of Section1.1.3)

5.3.1 Our approach

In this research, we present a novel approach to improve the survival model for risk stratification proposed by Marrugat et al. [8]. In particular, our approach uses *deep* CA US image features in the survival model aiming at reclassifying individuals from the *moderate*- to the *high*-risk category. In particular, we consider a DNN architecture to extract a set of deep features from the CA images, add them to the REGICOR function, and analyze the new survival model in terms of prediction and reclassification. We show that the DNNs are able to learn new feature embeddings useful to improve risk stratification by classifying events from *low* or *moderate* categories to higher categories. To do so, we compare the performance of our model using different sets of deep features and with another model that uses a set of phenotypes manually defined from the CIM region. Additionally, we assess the relevance of these features by comparing the risk function outlined in [8] to a model with the same variables, except for the invasive ones (i.e., those requiring blood extraction), which are substituted with the image features. In this sense, we assess a model that does not include invasive variables but incorporates additional information about atherosclerosis, including details of the atherosclerotic plaque location. Finally, the best sets of image features are compared in terms of reclassification. In particular, we investigate whether the inclusion of deep image features in the survival model results in the reclassification of individuals who have experienced an event from the *moderate*-risk group to the *high*-risk group.

This approach is presented in a paper entitled "Deep-stratification of the cardiovascular risk by ultrasound CA images", mentioned in Section 1.5, which was submitted in a Q2 journal.

5.3.2 Related work

The study of CA US plaque images has been considered clinically relevant. In particular, several attempts in the literature tried to assess the cardiovascular risk of subjects using CA image features, as discussed below.

The main purpose of studies in [133, 146] was to create an image-based system to characterize the plaque and the CA walls in US CA images. In these works, authors used the lumen diameter for risk stratification as GT to solve a classification problem between two ranges: low and high risk. Their proposal was to estimate the spatial distribution of gray levels to examine the texture for CCA far and near wall, reaching

high classification accuracies with two classification methods: SVM and PCA.

Other works ([16, 17, 18, 19]) focused on analyzing the CA in longitudinal studies.These works obtained CA image features, either manually or using semi-automatic methods, and used them to create risk prediction functions. Most of the image features considered are related to IMT (mean IMT, maximum IMT, minimum IMT, IMT variability) and atherosclerotic plaque (TPA, GSM of plaque). Since these features are used repeatedly in the literature, from now on, we will refer to this set of six features as *classical image phenotypes*. In particular, the model presented in [18] used the classical image phenotypes in two instants of time combined with conventional (non-imaging) risk variables achieving better results than classical survival models. Alternatively, Kyriacou et al. [139] used PNN and SVM classifiers to combine clinical features, image phenotypes, and other CA image features (based on texture and morphology) for plaque classification (event vs non-event). Despite the promising results for predicting events in individuals with plaque, this classification task is different from the risk stratification problem we address in this study.

Moreover, several works in the literature [155, 156, 157, 158] compare classical risk prediction functions with different ML approaches. The main difference between both approaches is that ML methods use the event/non-event information for prediction (binary classification task) and survival models use the time until the event to predict the risk of suffering an event. In these studies, they used classical clinical variables, also known as *risk factors* and some additional characteristics from a population initially free of CVD in a longitudinal study. The ML techniques outperform existing approaches in cardiovascular event prediction. In this context, Weng et al. [155] compared different ML algorithms: RF, logistic regression, gradient boosting, and NNs, which reached the best results in cardiovascular prediction. The most recent approaches [156, 157] proposed boosted ensemble algorithms followed by automated feature selection using information gain ratio. Both of them reached very high accuracies in cardiovascular death [156] and cardiovascular event [157] prediction. Although they did not use CA images, Ambale-Venkatesh et al. [158] included features from electrocardiography images and reached the highest accuracy using the RF algorithm to predict the events and to select relevant features from a large set of variables (more than 700).

In terms of subject reclassification (i.e., moving subjects who suffered an event to higher risk categories and subjects free of event to lower risk categories), recent research works [159, 160] used Net Reclassification Improvement (NRI) to evaluate if the addition of one or more variables to a survival model improves its predictive capacity. In particular, these improvements are based on the reclassification of subjects with event into higher categories. Moreover, Tamarappoo et al. [157] applied this measure to evaluate the

improvement in their proposed ML prediction model and reached an improvement of approximately 50% in reclassification.

5.4 Methodology

We propose to improve the survival model based on the REGICOR risk function [8] by combining its clinical variables with a novel set of deep features extracted from CA US images. Figure 5.2 depicts the different stages of the proposed method, which are subsequently described.

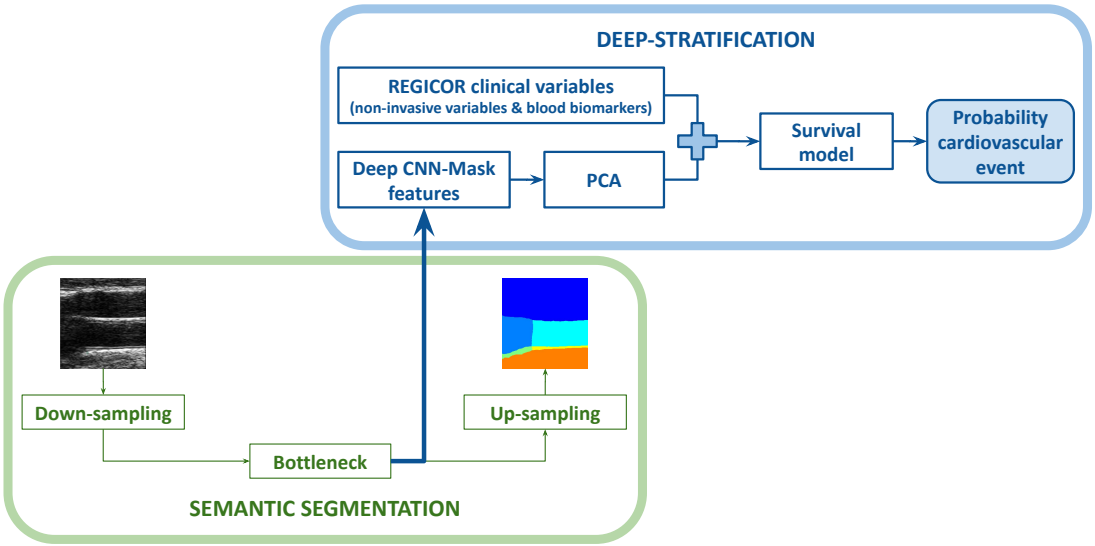

Figure 5.2: Proposed methodology for the deep-stratification of the cardiovascular risk. The survival model receives an input vector with 12 features, which include 8 clinical variables used in the REGICOR risk function and 4 deep CNN-Mask features extracted from a SS model of the carotid intima-media [33] and transformed by PCA.

5.4.1 REGICOR clinical variables

Most of the risk prediction functions in the field of cardiovascular epidemiology are based on survival models, which are CoxPh [8, 9, 10, 12]. The CoxPh analyzes the risk affecting the survival of a population of subjects [14]. In these models, the outcome is the time until an event occurs, and the predictor covariates are the risk factors. In particular, CoxPh survival models, such as the ones used in Framingham [9] or in REGICOR [8], allow us to estimate the probability of suffering a cardiovascular event in the next period of time [14], say ten years, by means of the following formula:

$$prob(event|x) = 1 - S^{exp(\sum_{n=1}^{N} \beta_n x_n - \sum_{n=1}^{N} \beta_n \overline{x}_n)}, \tag{5.1}$$

where N is the number of risk factor variables, x_n is the value of the n-th variable for the individual x, β_n is the Cox coefficient for the n-th variable, $\overline{x}_n$ is the average value of the n-th variable in the validation population, and S is the average ten-year survival in the validation population. One of the best-known survival models in the literature is Framingham [9]. REGICOR risk function [8] is a model with the same risk factors as Framingham [9] but validated in the Spanish population. In particular, in the REGICOR risk function: $N = 8$, the average values correspond to the Spanish population and S is the average ten-year survival in the Spanish population. The REGICOR risk function uses the following eight clinical variables:

- *Non-invasive variables*: age, sex, diastolic blood pressure, systolic blood pressure, and smoke.
- *Blood biomarkers*: diabetes, total cholesterol, and HDL cholesterol.

5.4.2 Deep CNN-mask features

The extraction of the deep features is based on the model defined by Gago et al. [33] for the segmentation of the carotid intima-media. Specifically, this work designed a SS model that uses the U-Net [161], a widely recognized architecture that incorporates a downsampling path for feature extraction and an upsampling path for region segmentation. The downsampling path of the proposed model employs an EfficientNet B0 [56] as its backbone while maintaining the bottleneck and the upsampling path of the original U-Net.

The deep features used in our proposal are obtained from this SS model. In particular, we use the deep features extracted from the bottleneck, which is located between the down-sampling and up-sampling paths (see Figure 5.2). As the segmentation model produces a mask of the CIM region, the 1,152 features derived in this manner are referred to as *deep CNN-Mask features*.

5.4.3 Dimensionality reduction using PCA

The *one in ten rule* [162] used in statistics determines that the number of variables for a survival model should be around 1 variable for every 10 events. Taking into account the number of events in our study (3.22%, see Table 1.1) and the number of deep features (1,152) obtained for each territory (CCA and bulb), the dimension of the feature vector must be reduced.

For this purpose, we use PCA [163], an algorithm that applies a linear transformation to compress a dataset onto a subspace of lower dimensionality while retaining the majority of the relevant information. The number of principal components to retain is typically

determined by looking at the proportion of variance explained by each component and selecting a threshold, such as retaining the top n components that explain a certain percentage of the total variance.

In the current study, there are four CA images available for each subject: left and right sides of CCA and bulb territories. The deep CNN-Mask features are computed from the four images and then PCA is applied. The final vector per territory is calculated as the average of the feature vectors obtained from both sides (left and right). According to the experimentation, a variance percentage of 85% is applied to the two CCA images and 70% in the case of the bulb, thus obtaining two features per territory. That is, four deep features are concatenated with the eight REGICOR variables (which results in a final feature vector with $N = 12$), to feed the survival model, as following described.

5.4.4 Survival model

At this point, we have obtained a 12-dimensional vector with the following features: eight clinical variables, which are the ones used in the REGICOR risk function; and four deep CNN-mask features, which are obtained after applying PCA to the deep features computed from a SS model trained on US CA images from two territories (CCA and bulb). These 12 features feed the survival model, as shown in Equation 5.1, to finally estimate the probability of suffering a cardiovascular event in the next ten years. We call this strategy *deep-stratification* approach.

In particular, for this work, we evaluate the respective CoxPh model (see Section 5.4.1, REGICOR Clinical Variables), which estimates the time until the event. This model is obtained with `coxph()` function from Epi package [164] (R software [80]).

5.5 Dataset

This research work analyzes the participants from REGICOR, the set of images collected for each subject was obtained from left and right CA in two different territories (CCA and bulb). During the CA acquisition, some images were discarded if the sonographers considered that the image quality was not sufficient. Due to the poor quality of the bulb images, they collected a total of 10,151 CCA images and 9,143 Bulb images. Among them, 8,484 images (4,751 CCA images, and 3,733 Bulb images) have carotid IMT reference values, given by the AVICA. Due to the poor quality of the images, some images were discarded, resulting in a total of 4,727 CCA images and 3,721 bulb images with IMT reference values.

The clinical data include eight classical risk factors used in the REGICOR risk function. We call them *REGICOR variables* and they are: gender, age, smoking, systolic and

diastolic blood pressure, total cholesterol, HDL cholesterol, and diabetes. Moreover, these data include the time until the event or the time to the date of the last contact. Given the nature of our study, we only considered subjects with no history of CVD (coronary artery disease, stroke, or intermittent claudication), therefore 314 subjects were discarded. Finally, a total of 4,769 subjects were included in the dataset.

Table 5.2 shows a summary of the clinical data considered in this research. Note that, from the analyzed cohort of 4,769 subjects who were free from CVD at baseline, there are 151 incident cases (3.17%) with cardiovascular events (acute myocardial infarction, other ischemic heart diseases, stroke, and the same causes of death) during the ten-year follow-up period.

Table 5.2: Summary of clinical data of the REGICOR subjects considered in this study, grouped by 'sex' and with the p-value for the differences between the two groups. Categorical variables are expressed as *n (%)* and continuous variables as *mean (standard deviation)*.

	All N=4,769	Men N=2,620	Women N=2,149	p.value
Age	59.5 (11.8)	59.7 (11.8)	59.4 (11.8)	0.483
Total cholesterol	205 (35.5)	209 (35.2)	201 (35.3)	<0.001
HDL cholesterol	52.7 (11.8)	56.6 (11.6)	48.0 (10.3)	<0.001
Systolic blood pressure	129 (19.7)	126 (20.1)	133 (18.2)	<0.001
Diastolic blood pressure	77.2 (10.1)	75.1 (9.77)	79.7 (9.91)	<0.001
Diabetes	608 (12.7%)	252 (9.62%)	356 (16.6%)	<0.001
Smoke	810 (17.1%)	347 (13.3%)	463 (21.7%)	<0.001
Event	151 (3.17%)	58 (2.21%)	93 (4.33%)	<0.001

5.6 Experimental setup

This section describes the setup used in the experimentation carried out to evaluate our deep-stratification approach. First, we explain the performance measures to evaluate the prediction capability of the survival model and the reclassification. Next, we describe the train-test split applied to the REGICOR dataset for validation purposes. Note that the code of our proposed framework will be publicly available after paper acceptance[1].

5.6.1 Evaluation metrics

In order to evaluate the performance of our deep-stratification approach we used two different metrics: the AUC and the Net Reclassification Improvement (NRI).

[1] https://github.com/mmarvila/CA_deep_stratification

The AUC metric is used to assess the performance of the survival model. In this context, this metric agrees with Harrell's C [165], which is a goodness of fit measure of risk scores models such as statistical survival models.

On the other hand, NRI [166] is used to evaluate the reclassification improvement in risk prediction. NRI is a widely used metric in the recent clinical literature [159, 160, 157], which intuitively summarizes the improvement in the classification of individuals in risk categories. Therefore, it is used to summarize the incremental improvement obtained with new variables. The total improvement is the sum of the improvements in the reclassification of individuals without event and with event separately as is shown in the following formula:

$$NRI = (N1 - N2) + (N3 - N4) \tag{5.2}$$

where $N1$ and $N2$ are the percentages of individuals who have suffered an event and those who have been reclassified into higher and lower categories, respectively; and $N3$ and $N4$ are the percentages of individuals free of event who have been reclassified into lower and higher categories, respectively.

Note that when the problem is the probability of suffering an event during a period of time, we use the event variable (*yes/no*) and the time until the event (or the time until the date of the last contact in case of non-event subjects). For this reason, the statistical techniques utilized for NRI, such as the `nricens` function from `nricens`[167] package (R software [80]), which is employed in this study, incorporate survival functions that consider the time to the event in addition to the values shown in the formula. That is, these functions generate an NRI output that cannot be derived directly from the aforementioned formula 5.2.

5.6.2 Train-test split

Table 5.3 shows the number of images used to evaluate our deep-stratification approach. As explained in Section 5.5, the REGICOR dataset contains a total of 10,151 CCA images and 9,143 bulb images. Among them, 4,727 CCA images and 3,721 bulb images have IMT reference values that can be used as the GT for carotid IMT estimation. Note that the first two rows of the table (IMT GT) correspond to the same train-validation-test split used in [33] (60% training set, 20% validation set, and 20% test set), which has been used here to evaluate image-based features.

Table 5.3: Number of images in the REGICOR dataset: train-validation-test split to evaluate the image-based features (IMT GT) and test split to evaluate the survival models (IMT GT + NO IMT GT).

		TRAIN	VALIDATION	TEST	TOTAL
IMT GT	CCA	2836	946	945	4727
	BULB	2232	744	745	3721
NO IMT GT	CCA	-	-	5424	5424
	BULB	-	-	5422	5422
TOTAL	CCA	2836	946	6369	10151
	BULB	2232	744	6167	9143

The images without IMT values can be used for the evaluation of the survival model. For this reason, we have also considered them and, therefore, the test set used in this case is composed of 6,369 CCA and 6,167 bulb images.

5.7 Results

This section details the four experiments conducted to evaluate our deep-stratification approach and analyzes the results obtained. The first two experiments are intended to select the best set of image-based features. In particular, we compare two sets of deep features in Experiment 1 and a set of hand-crafted features in Experiment 2. In both cases, we consider two territories (CCA and bulb) and several sizes of feature vectors. Next, in Experiment 3, we assess the relevance of the image-based features with respect to the blood biomarkers. For this purpose, we compare the survival model of the REGICOR function [8] but with the image-based features instead of the blood biomarkers. Finally, in Experiment 4, we analyze the most competitive configurations of the previous experiments in terms of the reclassification of the survival model.

The computational time and complexity of the proposed methodology mostly depends on the model used to extract deep features. As mentioned in [37], the time needed to process an input image is 0.026 seconds using a GeForce RTX 2080ti 11GB GPU also from NVIDIA. On the other hand, the computational time to obtain the proposed CoxPh survival model is less than one millisecond per individual.

5.7.1 Experiment 1: analysis of the deep features

In order to evaluate the adequacy of the proposed deep CNN-Mask features, we compare them with another set of deep features. For the extraction of the alternative deep features, we use a CNN model defined for carotid IMT estimation and plaque detection

in [33]. This model was tuned using Bayesian optimization, with a final architecture composed of four blocks of convolutional layers followed by a max-pooling operation and two blocks of fully connected layers followed by batch normalization and dropout. In this case, the deep features were extracted from the second block of fully connected layers. The 32 features derived in this manner are referred to as *deep CNN-IMT features*.

As we mentioned in Section 5.5 the CA images of the REGICOR dataset correspond to two territories, CCA and bulb. The quality of the images in CCA is better, whilst there is an increased burden of atherosclerotic plaque in the bulb images. For this reason, we compute the deep features from both territories, individually and jointly for comparison.

For each CA image, the size of the feature vector is 1,152 for the proposed deep CNN-Mask features and 32 for the alternative deep CNN-IMT features. Since the number of events in the dataset is small (151 from 4,769 subjects, see Table 5.2), the size of the feature vectors must be reduced. As previously explained in Section 5.4.3, the number of events in the dataset should be about 10 per risk factor variable in the survival model [162]. Thus, we set the maximum number of variables to be included in the survival model to 16. Taking into account that our proposed model already includes the 8 REGICOR risk function variables [8] (see Figure 5.2), the number of deep features should be less than or equal to 8. To reduce the size of the two feature vectors considered, we apply PCA to obtain a maximum of 8 variables and keep at least 70% of the variance. Table 5.4 shows the number of features obtained after applying PCA with different variance percentages. For CCA images, a variance of 99% in deep CNN-Mask features and 90% in CNN-IMT features result in feature vectors with more than 8 variables, so lower variances must be considered for the proposed survival model. Regarding the other territory, bulb, a variance lower than 95% must be considered in both feature sets.

As detailed in Section 5.4, each subject has two CA images (left and right) per territory (CCA and bulb). Thus, the final feature vector is calculated as the average of the feature vectors extracted from both sides. In case one of the two images is missing, the subject is discarded. For this reason, using the 6,369 CCA and 6,167 bulb images mentioned in Section 5.6.2, we obtain the deep features for the following number of subjects: 2,796 subjects for CCA, 2,760 subjects for bulb, and 2,501 for both territories.

Table 5.5 shows the performance of the survival model using the two sets of deep features (CNN-Mask and CNN-IMT), in the two territories (CCA and bulb) individually and jointly, and with different kept variances for PCA, based on the results reported in Table

Table 5.4: Kept variance and number of features obtained when applying PCA to the two sets of deep features.

	CNN-Mask		CNN-IMT	
Territory	Var.	No. feats.	Var.	No. feats.
CCA	99%	>8		
	95%	4	90%	>8
	85%	2	85%	8
	70%	1	70%	5
BULB	95%	>8	95%	>8
	90%	5	90%	6
	85%	4	85%	4
	70%	2	70%	2

5.4. In all cases, the deep features are concatenated with the 8 REGICOR variables [8] that are used as the baseline (AUC = 0.825). For each configuration, we report the total number of features (No. feats.), the predictive capacity of the survival model (AUC), the AUC increase with respect to the baseline, and the p-value of the AUC increase, which is considered statistically significant if $p < 0.06$. Note that equal values in the AUC metric have different increments due to rounding precision (three decimal digits), and vice versa.

Table 5.5: Experiment 1. AUC results of the survival model fed with the eight REGICOR variables and different sets of deep features (CNN-Mask and CNN-IMT), applied to the input images of two territories (CCA and bulb). The number of features obtained after applying PCA to the deep features is specified between parentheses (F), after the variance percentage. The statistically significant results ($p < 0.06$) are in bold.

Deep	Territory		No.		AUC	
features	CCA	Bulb	feats.	AUC	increase †	p
CNN-Mask	PCA 95% (4F)	-	12	0.831	0.007	0.118
CNN-Mask	PCA 85% (2F)	-	10	0.831	0.006	0.230
CNN-Mask	PCA 70% (1F)	-	9	0.827	0.002	0.628
CNN-Mask	-	**PCA 90% (5F)**	**13**	**0.842**	**0.018**	**0.050**
CNN-Mask	-	**PCA 85% (4F)**	**12**	**0.842**	**0.017**	**0.052**
CNN-Mask	-	PCA 70% (2F)	10	0.834	0.010	0.296
CNN-Mask	**PCA 95% (4F)**	**PCA 85% (4F)**	**16**	**0.847**	**0.023**	**0.008**
CNN-Mask	**PCA 85% (2F)**	**PCA 90% (5F)**	**15**	**0.846**	**0.022**	**0.016**
CNN-Mask ⋆	**PCA 85% (2F)**	**PCA 70% (2F)**	**12**	**0.842**	**0.017**	**0.054**
CNN-IMT	PCA 85% (8F)	-	16	0.833	0.008	0.076
CNN-IMT	**PCA 70% (5F)**	**-**	**13**	**0.832**	**0.008**	**0.046**
CNN-IMT	-	PCA 90% (6F)	14	0.835	0.011	0.198
CNN-IMT	-	PCA 85% (4F)	12	0.836	0.011	0.070
CNN-IMT	-	PCA 70% (2F)	10	0.834	0.010	0.296
CNN-IMT	PCA 70% (5F)	PCA 70% (2F)	15	0.836	0.011	0.066

⋆ Our proposed method.
† AUC increase with respect to the 8 REGICOR variables [8] (baseline).

As can be observed, the AUC increase reaches statistically significant values using either of the two sets of deep features. However, the best AUC results are obtained with the deep CNN-Mask features, with AUC greater than 0.840 in several configurations. With

respect to the two territories, their combination provides the highest values when the deep CNN-Mask features are applied. Regarding the number of features, the highest AUC values are obtained with larger feature vectors, mainly because these configurations correspond to the joint use of the two territories. Note that the configurations that achieve statistically significant results ($p < 0.06$) are selected for further analysis (Experiments 3 and 4).

5.7.2 Experiment 2: analysis of the hand-crafted features

The aim of this experiment is to analyze the use of a new set of *hand-crafted features*, which could replace the deep features in our proposed methodology (see Figure 5.2). Based on the classical image phenotypes mentioned in Section 5.3.2, we consider six phenotypes manually defined from the CIM region. Thus, for each CA image we obtain the following image features: mean IMT, maximum IMT, minimum IMT, IMT variability, TPA, and GSM of plaque. Notice that TPA is measured in mm^2 and it is estimated in the region where the IMT reaches more than 1.5 mm, following the Mannheim consensus [7]. GSM refers to the GSM value in the same area where TPA is evaluated.

These phenotypes are extracted from the four CA images available for each subject (left and right sides of CCA and bulb territories), thus obtaining a total of 24 phenotypes per subject. As previously explained in Section 5.7.1, a maximum of 8 image-based features should be added so a dimensionality reduction procedure must be applied. The definition of these 24 hand-crafted features is based on prior knowledge about specific characteristics of the carotid images. Therefore, we can reduce the number of features, from 24 to a maximum of 8, by selecting the most relevant phenotypes according to the results of a statistical analysis performed on the training data. The procedure carried out is summarized as follows:

- **Base-e logarithmic adjustments.** Some phenotypes are not normally distributed and hence they should be normalized using base-e logarithmic adjustment. These phenotypes are mean IMT, maximum IMT, and IMT variability (on both sides).

- **Categorization of variables.** Due to the low percentage of plaques (3.4% in CCA and 25.8% in bulb), TPA and GSM phenotypes are categorized into three classes. The categories for TPA are *non-plaque*, *small plaque*, and *high burden of plaque*, where the threshold between the last two categories is the median of all TPA values from the same side (five for CCA and six for bulb). GSM is categorized into *non-plaque*, *echolucent*, and *non-echolucent*, where the threshold for echolucency detection is the third quartile of all GSM values from the same side

(107 in CCA and 95 in bulb). Finally, in order to analyze the interaction between the TPA and the GSM phenotypes, we create a new variable as a combination of both. The categories of this new variable are *non-plaque* (the subject does not have any plaque), *small plaque and non-echoic* (the subject has at least plaque in one side of the arteries, but none is huge or echoic), *small plaque and echoic* (the subject has at least plaque in one side that is echoic, but there is not any huge plaque), *huge plaque and non-echoic* (the subject has at least a huge plaque that is not echoic), and *huge plaque and echoic* (the subject has at least a huge plaque that is echoic). This categorization is done for CCA phenotypes and bulb phenotypes separately. Finally, since there is no event in the *small plaque and non-echoic* category for CCA, we merge it with the *non-plaque* category.

- **Mean between left and right sides.** In order to reduce the number of phenotypes, the mean IMT, maximum IMT, minimum IMT, and IMT variability are defined as the average of right and left side values [63]. If a value is missing on one side, we use the available value for this subject. If the value is missing on both sides, then the phenotype is considered missing.

- **Co-linearity.** We eliminate co-linear variables using the Variance Inflation Factor (VIF)[168]. In particular, we analyze all the variables from the model and discard the ones with VIF$>$ 2. Maximum IMT phenotypes from CCA and bulb are also discarded for the model.

- **Discarding variables.** Ultimately, our approach involves systematically eliminating non-statistically significant phenotypes from the survival model. However, we make a deliberate choice to retain the phenotype variables that are deemed confounders. Note that a variable is considered a confounder if at least one of the coefficients of the variables that remained in the model changed more than 15%. After the analysis, all the selected phenotypes are considered confounders so we keep all of them.

As a result, Table 5.6, shows the coefficients for the CoxPh model (see Section 5.4.1) and their corresponding p-value. These coefficients correspond to a survival model including the eight REGICOR variables and the eight phenotypes selected. Note that the variable is statistically significant for the model if $p < 0.06$.

Table 5.7 shows the performance of the survival model using the hand-crafted features in the two territories (CCA and bulb), individually for the Statistical Analysis (SA) above described and jointly for PCA (maximum 8 variables and at least 70% of variance). In all cases, the hand-crafted features were concatenated with the eight REGICOR variables [8] that are used as the baseline (AUC = 0.825). As in Experiment 1, we

Table 5.6: Coefficients for the CoxPh model and p-values of the risk factors used in the survival model: eight factors from the REGICOR risk function and the six hand-crafted phenotypes selected based on the statistical analysis performed.

Risk factor	Territory	Coefficient	p
Age	-	0.06	<0.01
Sex	-	0.38	0.06
Total cholesterol	-	0.01	0.04
HDL cholesterol	-	-0.03	0.00
Systolic blood pressure	-	0.00	0.62
Diastolic blood pressure	-	0.01	0.23
Diabetes	-	0.49	0.02
Smoker	-	0.12	0.66
log(mean IMT)	CCA	2.55	<0.01
minimum IMT	CCA	-1.26	0.26
log(IMT Variability)	CCA	-0.43	0.17
Small plaque and echoic	CCA	-0.61	0.32
Huge plaque and non-echoic	CCA	0.36	0.59
Huge plaque and echoic	CCA	-0.70	0.25
log(mean IMT)	Bulb	-1.48	0.30
minimum IMT	Bulb	0.22	0.83
log(IMT Variability)	Bulb	0.71	0.14
Small plaque and echoic	Bulb	0.15	0.61
Huge plaque and non-echoic	Bulb	0.13	0.78
Huge plaque and echoic	Bulb	0.26	0.44

report the total number of features (No. feats.), the predictive capacity of the survival model (AUC), the AUC increase with respect to the baseline, and the p-value of the AUC increase, which is considered statistically significant if $p < 0.06$. Note that equal values in the AUC metric have different increments due to rounding precision (three decimal digits), and vice versa.

Table 5.7: Experiment 2. AUC results of the survival model fed with the 8 REGICOR variables and the hand-crafted features applied to the input images of two territories (CCA and bulb). SA stands for statistical analysis and PCA is followed by the variance percentage applied. In both cases, the number of features obtained is specified between parentheses (F). The statistically significant results ($p < 0.06$) are in bold.

Image features	Territory		No. feats.	AUC	AUC increase †	p
	CCA	Bulb				
Hand-crafted	**SA (4F)**	-	12	**0.843**	0.018	**0.010**
Hand-crafted	-	SA (4F)	12	0.839	0.015	0.116
Hand-crafted	**SA (4F)**	**SA (4F)**	16	**0.856**	0.031	**0.004**
Hand-crafted	PCA 99% (5F)		13	0.830	0.006	0.278
Hand-crafted	PCA 95% (4F)		12	0.826	0.001	0.734
Hand-crafted	PCA 90% (3F)		11	0.824	-0.001	1.314
Hand-crafted	PCA 80% (2F)		10	0.824	<0.000	1.280

† AUC increase with respect to the 8 REGICOR variables [8] (baseline).

As can be seen, the AUC increase is statistically significant when using the features selected by the statistical analysis on the CCA territory, both individually or combined with the bulb. In particular, the best performance is achieved when using the two territories jointly. On the contrary, the configurations that used the feature vectors obtained after applying PCA to the hand-crafted features do not have statistical significance. Note that the configurations that achieve statistically significant results ($p < 0.06$) are selected for further analysis (Experiments 3 and 4).

5.7.3 Experiment 3: analysis of the REGICOR variables

The aim of this experiment is to analyze the power of image-based features and see if it is possible for them to replace the 3 blood biomarkers used in the REGICOR risk function [8].

Table 5.8 shows the performance of the survival model using the five non-invasive REGICOR variables concatenated with the different configurations of image-based features selected in the previous experiments, according to their statistical significance. Note that the target of the experiment is to analyze if these features can replace the three blood biomarkers, so the survival model with the eight REGICOR variables and the survival model with the five non-invasive are used as the baselines (AUC = 0.825 and AUC=0.806 respectively). As in previous experiments, we report the total number of features (No. feats.), the predictive capacity of the survival model (AUC), the AUC

increase with respect to the baseline, and the p-value of the AUC increase, which is considered statistically significant if $p < 0.06$. Note that equal values in the AUC metric have different increments due to rounding precision (three decimal digits), and vice versa.

Table 5.8: Experiment 3. AUC results of the survival model fed with the 5 non-invasive REGICOR variables and different configurations of image-based features selected in Experiments 1 and 2, applied to the input images of two territories (CCA and bulb). SA stands for statistical analysis and PCA is followed by the variance percentage applied. In both cases, the number of features obtained is specified between parentheses (F). The statistically significant results ($p < 0.06$) are in bold.

	Territory		No.		AUC		AUC	
Image features	CCA	Bulb	feats.	AUC	increase †	p	increase † †	p
REGICOR risk function[8]	-	-	8	0.825	-	-	0.019	0.076
CNN-Mask	-	PCA 90% (5F)	10	0.826	0.002	0.894	0.021	**0.046**
CNN-Mask	-	PCA 85% (4F)	9	0.826	0.002	0.892	0.021	**0.046**
CNN-Mask	PCA 95% (4F)	PCA 85% (4F)	13	0.831	0.007	0.57	0.026	**0.01**
CNN-Mask	PCA 85% (2F)	PCA 90% (5F)	12	0.831	0.006	0.63	0.025	**0.014**
CNN-Mask ⋆	PCA 85% (2F)	PCA 70% (2F)	9	0.827	0.002	0.874	0.021	**0.048**
CNN-IMT	PCA 70% (5F)	-	10	0.813	-0.012	1.716	0.007	0.102
Hand-crafted	SA (4F)	-	9	0.825	0.000	0.978	0.019	**0.024**
Hand-crafted	SA (4F)	SA (4F)	13	0.839	0.014	0.352	0.033	**0.004**

⋆ Our proposed method
† AUC increase with respect to the 8 REGICOR variables [8].
† † AUC increase with respect to 5 non-invasive REGICOR variables

As can be observed in Table 5.8, there is a positive increment in most of the survival models fed with image-based features with respect to the survival model fed with the three blood biomarkers (REGICOR risk function [8]). Note that only in the case of the deep CNN-IMT features the AUC increment is negative. In addition, the AUC increment is not statistically significant when adding the blood biomarkers to the survival model fed with the five non-invasive features. However, it is statistically significant in most of the survival models that are fed with image-based features, except in the case of the deep CNN-IMT features.

5.7.4 Experiment 4: analysis of the reclassification results

This experiment aims at analyzing the models selected in Experiments 1 and 2 in terms of their reclassification results for cardiovascular events. For this purpose, we consider the NRI metric (see Section 5.6.1) and the following cut-off points, which correspond to the risk categories defined in [8] and discussed in Table 1.1:

- *low*: Subjects with a probability of suffering an event <0.05.
- *low-moderate*: Subjects with a probability of suffering an event in the range $[0.05, 0.1)$.
- *high-moderate*: Subjects with a probability of suffering an event in the range

$[0.1, 0.15)$.

- *high*: Subjects with a probability of suffering an event ≥ 0.15.

Table 5.9 shows the performance of the survival model using the eight REGICOR variables [8] concatenated with the different configurations of image-based features selected in Experiments 1 and 2, according to their statistical significance. For each configuration, we report the total NRI value (NRI) and its Confidence Interval (CI), the NRI value for the subjects who suffered an event (NRI events) and its CI, and the NRI value for the subjects free of event (NRI controls) and its CI. Note that the NRI values are statistically significant if their CI does not include 0 and they are shown in bold.

Table 5.9: Experiment 4. NRI results of the survival model fed with the 8 *REGICOR variables* and the different configurations of image-based features selected in Experiments 1 and 2, applied to the input images of two territories (CCA and bulb). SA stands for statistical analysis and PCA is followed by the variance percentage applied. In both cases, the number of features obtained is specified between parentheses (F). The statistically significant results (CI does not include 0) are in bold.

Image features	Territory		NRI [CI 95%]	NRI events [CI 95%]	NRI controls [CI 95%]
	CCA	Bulb			
CNN-Mask	-	PCA 90% (5F)	11.54 [-0.05;0.30]	9.99 [-0.07;0.28]	1.55 [0.00;0.03]
CNN-Mask	-	PCA 85% (4F)	11.56 [-0.05;0.30]	10.05 [-0.07;0.28]	1.52 [0.00;0.03]
CNN-Mask	PCA 95% (4F)	PCA 85% (4F)	**17.91 [0.01;0.34]**	16.1 [-0.01;0.32]	**1.81 [0.01;0.03]**
CNN-Mask	PCA 85% (2F)	PCA 90% (5F)	16 [-0.01;0.32]	14.76 [-0.02;0.31]	1.24 [<0.00;0.03]
CNN-Mask ⋆	PCA 85% (2F)	PCA 70% (2F)	**20.82 [0.04;0.38]**	**20.02 [0.03;0.37]**	0.81 [-0.01;0.02]
CNN-IMT	PCA 70% (5F)	-	**17.50 [0.03;0.33]**	**17.14 [0.03;0.32]**	0.36 [-0.01;0.01]
Hand-crafted	SA (4F)	-	9.79 [-0.03;0.21]	8.85 [-0.04;0.20]	0.95 [<0.00;0.02]
Hand-crafted	SA (4F)	SA (4F)	6.47 [-0.11;0.26]	5.58 [-0.12;0.25]	0.9 [-0.01;0.02]

⋆ Our proposed method

The results presented in Table 5.9 indicate statistically significant improvements in reclassification for three specific configurations. These improvements were achieved using deep features, resulting in an increase of more than 17%. Only these three configurations show statistically significant results in either the "NRI events" or in the "NRI controls" column. Particularly, with our proposal, we show a significant increment in subjects who suffered an even, with an NRI of 20.02%, while the increment using CNN-IMT features is lower, 17.14%. Instead, the other configuration using CNN-Mask shows a statistically significant increment in subjects free of event, although it is relatively small (1.8%). In contrast, the results obtained from the hand-crafted features do not demonstrate statistical significance in any case.

Table 5.10 shows the reclassification of the event group using the previously defined risk categories. The risk categories and the number of subjects are shown using the REGICOR risk function [8] (rows) and our proposal (columns). The values above the diagonal indicate subjects that have been assigned a higher category compared to REGICOR [8]. Conversely, values below the diagonal represent the number of subjects that have been downgraded. Similarly, the values on the diagonal indicate the number of subjects classified with the same category using both our proposal and REGICOR [10]. Although here we cannot show the calculation of the NRI values (as we mentioned in Section 5.6.1) Table 5.10 shows that, for the events, there are many more individuals who are reclassified into higher categories (17=2+5+6+4) than not than lower categories (4=1+1+1+1).

Table 5.10: Comparison between the REGICOR risk function [8] and our proposed method in terms of reclassification results for cardiovascular events.

REGICOR	Our proposed method				
risk function	<0.05	$[0.05, 0.1)$	[0.1,0.15)	≥ 0.15	TOTAL
<0.05	24	2	0	0	26
$[0.05; 0.1)$	1	4	5	6	16
$[0.1; 0.15)$	1	1	2	4	8
≥ 0.15	0	0	1	9	10
TOTAL	26	7	8	19	60

5.7.5 Comparison with the literature

The predictive capacity of our proposed method (AUC = 0.842, Table 5.5) is similar to or higher than the results proposed in the literature (see Section 5.3.2). Even without the 3 blood biomarkers used in the REGICOR risk function, we achieved a good cardiovascular risk prediction (AUC = 0.827, Table 5.8).

The best result found in the literature is reported in [18] (AUC = 0.93). This study uses risk factors and phenotypes at two different times, thus making data collection more complex. Regarding the ML approaches, we do not reach the results reported in [158] (AUC = 0.86), but their proposed survival model includes data from questionnaires (lifestyles, history, medication, etc.), more biomarkers, electrocardiography, and magnetic resonance imaging features. That is, they use a set of characteristics that make the study more expensive and that are not appropriate to be obtained in primary care centers. Regarding deep features, our best result is with "PCA 95%, CCA & 85%, BULB" features, which reach 0.847 in the AUC metric (Table 5.5. In the literature, we also found the study conducted by Rine Nakanishi [156] who demonstrates a slightly superior AUC result of 0.85. However, they do use computed tomography images, a more expensive technique than US imaging.

In terms of reclassification, the total NRI reported by Tamaroppoo et al. [157] (53%) is better than the one obtained with our method (20.82%, Table 5.9). However, our method outperforms it in the event group, which is the objective of the presented proposal due to its clinical relevance. More specifically, the NRI of the event group reported in [157] is 8% versus 20.02% achieved with our proposal.

It is important to note that conducting a comprehensive and fair comparison of results poses a challenge, given the variation in datasets across each proposal.

5.8 Conclusions

This work presents, for the first time in the literature, a survival model for cardiovascular risk prediction which integrates CA image features extracted from DNNs. The new survival model is capable of predicting the risk of suffering a cardiovascular event, which results in a deep-stratification of the cardiovascular risk. The proposal improves the original survival model presented in [8] by adding information from CA US images. For that, we concatenated deep features from a CNN previously defined for CA image SS. These features are able to improve the model in terms of prediction (AUC=0.84, with an increment of 0.017 with respect to REGICOR risk function [8]) and reclassification (NRI=20.8%, NRI events=20%). We successfully achieved a reduction in the number of individuals in the middle-risk category and moved them to the *high*-risk category, which is our main goal.

In order to validate our proposal, we performed a comparison of different sets of image features and different configurations of these features. First, we compared our proposal with another set of deep features that reached a statistically significant improvement in prediction and reclassification, but with a smaller increase than with our proposal (AUC=0.83, NRI= 17.5%, and NRI events= 17.1%). Second, we compared with a set of phenotypes manually defined from the CIM region and selected according to the statistical analysis results. In this case, the improvement reached in prediction is high (AUC=0.86) and statistically significant, but the findings in reclassification were not statistically conclusive. In addition, our findings demonstrate that CA image features are able to replace invasive variables, such as blood biomarkers, while simultaneously providing localized information concerning atherosclerotic plaque.

The main limitation of our work is the small number of events in the dataset (151 events over 4,769 subjects). With so few events, we are forced to greatly reduce the number of new image features and we are also exposed to overfitting. In this scenario, the survival models may not have enough statistical power to show all the differences between the different sets of image features. In addition, the proposed method has been

tested on a single dataset, so it has not been possible to analyze its generalizability to other domains.

For future research, it would be useful to validate our method with an independent cohort that has more events. This would allow us to overcome the aforementioned limitations, increasing the statistical significance of the study and testing the power of generalization of our approach. In addition, it would be interesting to use other deep features obtained with CNNs combined with other DNNs trained for another task, such as a binary classification task (to predict event/non-event) or a regression task (to estimate the time until the event). Another line of research could be the interpretability of the specific features extracted from CA images. Understanding the contribution of individual features to the survival model, for example generating saliency maps, can provide information about which regions in CA images are associated with cardiovascular risk. Finally, it would be interesting to perform a longitudinal analysis of the deep features, including changes over time in CA, as it is suggested in [18], which uses risk factors and image phenotypes at two different times.

Chapter 6

Conclusion

In this chapter, we present the thesis's final conclusions, with a focus on enhancing risk stratification, through DL image techniques. First, the most significant achievements are shown considering the objectives and conceptual stages outlined in Section 1 and the corresponding chapters where they have been addressed. Following this, a summary of the contributions is provided. Finally, the limitations of the thesis and future perspectives are discussed.

Initially, we have developed an automated semantic segmentation method for identifying anatomical components and atherosclerotic plaque in CA US images (**Chapter 2**), addressing the conceptual stage "IMT region segmentation". This method is a fully automatic single-step approach that allows us to estimate the IMT and segment atherosclerotic plaque in a fast and useful manner for large datasets of images (addressing stages "IMT estimation" and "Plaque detection"). Then, **Chapter 3** and **Chapter 4** presented two clinical applications derived from the "IMT estimation" and "Plaque detection". The first, evaluates the impact of chronic inflammation in autoimmune diseases on subclinical atherosclerosis and arterial stiffness. The second, shows the relation between lower limb atherosclerosis biomarkers assessed using ABI and carotid atherosclerosis evaluated through CCA IMT and the presence of plaque. Finally, the approach presented in **Chapter 5**, introduces a new method for extracting image features from CA, addressing the stage "IMT region and plaque characterization". Using these features, we have demonstrated an improvement of risk stratification, specifically in classifying events from moderate to high risk (it addresses "Cardiovascular risk prediction improvement" stage).

6.1 Summary of contributions

In this study, we have developed a method for integrating individual artery condition data into traditional survival models (Chapter 5). Our technique characterizes B-mode CA US images by extracting information without the need for manually defined features. Using NNs, we have uncovered feature embeddings that capture valuable data relationships and patterns while filtering out irrelevant details. This work introduces a innovative survival model in the literature, one that integrates CA US image features extracted using DNNs to effectively predict cardiovascular risk. Additionally, it reclassifies individuals from the middle-risk category to the high-risk category. Moreover, our findings emphasize the potential of CA US image features to replace invasive variables like blood biomarkers while providing localized atherosclerotic plaque information.

Furthermore, these features are extracted using a fully automated method that accurately localizes the carotid IMT region in longitudinal B-mode CA US longitudinal images CA images (Chapter 2). In particular, we introduced a novel single-step approach, using DenseNets, for semantic segmentation of longitudinal CA US images. This proposal applies CNNs for precise pixel-level labeling, resulting in enhanced subclinical atherosclerosis detection through efficient CIM region segmentation, IMT estimation and atherosclerotic plaque detection. In addition, compared to other methods in the literature, this approach offers several advantages: it can effectively manage extensive image datasets; it has demonstrated the method's ability to generalize, making it trainable and applicable to images from various equipment sources; and has demonstrated its ease of adaptability to diverse CA territories. The superior performance of the method presented is attributed to the effective use of deep learning (DenseNets), the results of which suggest that it is the best way to address segmentation.

Moreover, this thesis presents a review of the literature in B-mode CA US images segmentation and IMT estimation (Chapter 2), and characterization of atherosclerotic plaque classification and cardiovascular risk assessment in CA US images (Chapter 5). This thesis presents a summary of the main literature in tables that contain the key characteristics of these works. It aims to provide a comprehensive and synthetic comparison while emphasizing the shortcomings of the various proposals.

In this thesis two clinical applications of the CIM region segmentation method are also presented (Chapters 3 and 4). In the first study, we have assessed the risk of cardiovascular events in patients with autoimmune diseases, specifically examining the impact of chronic inflammation on subclinical atherosclerosis. To estimate subclinical atherosclerosis, we utilized the proposed segmentation method for IMT assessment mentioned above. Our findings revealed that the diagnosis of autoimmune diseases

poses a risk factor for subclinical atherosclerosis in men; this difference is statistically insignificant in women. While previous general population studies had established a link between inflammatory biomarkers and arterial stiffness, our cross-sectional analysis does not identify significant differences in these biomarkers between individuals with and without autoimmune diseases. In the second study, we have examined the coexistence of subclinical atherosclerosis in the lower limb, assessed using ABI, and in the CCA, measured via IMT or the presence of atherosclerotic plaque. In conclusion, our study revealed two distinct patterns of association between subclinical biomarkers of lower limb and CA atherosclerosis. Men exhibited a significant linear association between ABI levels and CCA IMT values, while women with symptomatic or asymptomatic peripheral artery disease had a higher risk of atherosclerotic plaque in the CA. Theses findings underscore the systemic nature of the atherosclerotic process, suggesting that individuals with atherosclerosis biomarkers in one area are more likely to have subclinical disease in another.

Furthermore, this thesis aims to contribute to Sustainable Development Goal (SDG) number 3 ("Ensure healthy lives and promote well-being for all at all ages"). In particular, since the thesis focuses on enhancing cardiovascular risk prediction functions, it contributes to SDG 3.4 ("reduce by one third premature mortality from non-communicable diseases through prevention and treatment and promote mental health and well-being").

6.2 Limitations and future perspective

The limitations in this thesis mostly arise from the number of images used in some experiments. In the carotid IMT region segmentation approach, a small number of GT images were utilized, and the generalization test employees a limited dataset (Chapter 2). On the other hand, in the deep stratification for cardiovascular risk assessment (Chapter 5), the number of individuals who experienced events in the dataset was significantly smaller compared to those who did not. This resulted in an increased risk of overfitting and an absence of generalization. Consequently, the segmentation model may have difficulty generalizing to images from different equipment, and survival models may lack the statistical power to reveal differences among the various sets of image features. This idea aligns with the review article [51] supporting the use of large training datasets in DL models for measuring CA parameters in US images, emphasizing the capture of broader complexities and intricacies of the dataset for enhanced cardiovascular risk monitoring. Therefore, expanding the size of some datasets stands as the initial point of improvement in our study.

It is important to mention that the main drawback of the CIM region segmentation

method (Chapter 2) is the application of an ad-hoc post-processing procedure immediately after segmentation. This limitation has been addressed in the derivative publication ([33], Section 1.5), whose proposal involves the CNN taking the original image and its mask and generating a prediction of the IMT value employing a regression model using Bayesian optimization.

Despite the aforementioned aspects related to the size of the dice set, the main future lines lie in two aspects. The first aspect is to further improve the segmentation results in terms of an adequate generalization to other datasets, by exploring new domain transfer techniques. Another plan is to add information indicating the presence of plaque into the NN in a way that it can learn the differences in shape between images of healthy subjects (thin CIM region shape) and images of subjects with atherosclerosis (irregular CIM region shape). The second aspect is related to the improvement of CV risk prediction (Chapter 5). It would be useful to validate our method with an independent cohort. In addition, it would be interesting to use other deep features obtained with CNNs combined with other DNNs trained for another task, such as a binary classification task (to predict event/non-event) or a regression task (to estimate the time until the event). Furthermore, since NNs allow integrating several types of data, the NNs used could mix images with other data, relevant for risk prediction such electrocardiogram, Cardiac Computed Tomography (Cardiac CT), Cardiac Magnetic Resonance Imaging (Cardiac MRI), etc... This could also be another potential line of research.

This paragraph discusses the main limitations regarding clinical articles (Chapters 3 and 4). Firstly, while our matched cohorts have offered valuable insights into CCA IMT and its relationship with to cardiovascular risk factors, the utility of CCA IMT for predicting cardiovascular risk beyond conventional factors is still debated [93, 94]. Secondly, although the results remained consistent, adjusted for cardiovascular risk and other variables, and aligned with previous research findings, we have included a low prevalence of autoimmune diseases (Chapter 3). And third, another limitation is that we have employed different techniques to assess the degree of atherosclerosis in the lower limb and CA (Chapter 4). Although the ultimate measurements can be compared, future cohort studies may enhance comparability by employing a uniform technique for assessing atherosclerosis in both vascular beds, such as US images for both the femoral artery and CA.

6.3 Challenges in deep learning

DL techniques have revolutionized the field of medical imaging, as it was prognosticated in recent publications [169, 170]. Although there are still several open issues to

be addressed, DL has already demonstrated significant potential to overcome human performance in selected tasks, such as medical image segmentation [171]. Moreover, DL provides key information in the clinical decision-making process [172, 173]. Currently, the main challenges of DL in medical imaging are mainly related to data quality and quantity for building reliable and generalizable DL models, as well as the design of new models for maximum transparency and dependability. The success of DL systems in medical imaging relies on the availability of high-quality, sufficiently large datasets. Many medical fields still lack of proper big datasets necessary data for training and validating these models effectively. Creating rich, multi-center datasets and addressing challenges in DL like data augmentation and synthesis is crucial for advancing DL in medical imaging [174]. Moreover, the lack of understanding in how DL models make predictions is a significant concern for their reilable application in medicine. To address this, strategies for explainability, interpretability [175], and uncertainty quantification [176] are gaining popularity to improve transparency, trust, and believability. Medical diagnosis DL models should prioritize not only accuracy but also explainability and certainty, ensuring that practitioners are informed when uncertainty is high for better decision-making.

Appendix A

Acronyms

List of acronyms used in this thesis:

AI Artificial Intelligence
ABI Ankle Brachial Index
AVICA Academic Vascular Image Center in Amsterdam
AUC Area Under the Curve
CV Cardiovascular
CA Carotid Artery
cc correlation coefficient
CCA Common Carotid Artery
CIM Carotid Intima-Media
CNN Convolutional Neural Networks
CoxPh Cox Proportional Hazards model
CVD Cardiovascular Disease
DA Discriminant Analysis
DL Deep Learning
DNN Deep Neural Networks
DT Decision Trees
FCN Fully Convolutional Neural Networks
GLCM Gray Level Co-occurrence Matrix
GMM Gaussian Mixture Model
GPU Graphics Processing Unit
GSM Grayscale Median
GT Ground Truth
HDL High-Density Lipoprotein
HOS Higher Order Spectra

ICA Internal Carotid Artery
IMT Intima Media Thickness
IOV Inter-Observer Variability
kNN k-Nearest Neighbor
LBP Local Binary Pattern
LDL Low-Density Lipoprotein
LI Lumen-Intima
MA Media-Adventitia
ML Machine Learning
NN Neural Network
NBC Naive Bayes Classifier
NRI Net Reclassification Improvement
PCA Pixel Component Analysis
PDA Pixel Distribution Analysis
PNN Probabilistic Neural Networks
RLM Run Length Matrix
ROI Region of Interest
RF Random Forest
SDG Sustainable Development Goal
SS Semantic Segmentation
SVM Support Vector Machine
TPA Total Plaque Area
US Ultrasound
WT Wavelet Transform

Bibliography

[1] WHO. *World Health Statistics. Monograph on the Internet. Geneva: World Health Organization*. 2023. URL: https://www.who.int/health-topics/cardiovascular-diseases#tab=tab_1.

[2] João L. Cavalcante et al. "Aortic Stiffness". In: *Journal of the American College of Cardiology* 57.14 (2011), pp. 1511–1522.

[3] Göran K. Hansson. "Inflammation, atherosclerosis, and coronary artery disease". In: *The New England journal of medicine* 352.16 (2005), pp. 1685–95.

[4] Carlos Lahoz and José M Mostaza. "Atherosclerosis As a Systemic Disease". In: *Revista Española de Cardiología (English Edition)* 60.2 (2007), pp. 184–195.

[5] From Wikimedia Commons Blausen.com staff (2014). "Medical gallery of Blausen Medical 2014". WikiJournal of Medicine 1 (2). DOI:10.15347/wjm/2014.010. ISSN 2002-4436. [CC BY 3.0 (https://creativecommons.org/licenses/by/3.0)]. *Carotid Arteries*. 2014. URL: https://commons.wikimedia.org/wiki/File:Blausen_0170_CarotidArteries.png.

[6] Thomas L. Szabo. *Diagnostic ultrasound imaging: inside out*. Academic press, 2004.

[7] P.-J. Touboul et al. "Mannheim carotid intima-media thickness and plaque consensus (2004-2006-2011)." In: *Cardiovascular Diseases* 34.4 (2012), pp. 290–296.

[8] Jaume Marrugat et al. "Validez relativa de la estimación del riesgo cardiovascular a 10 años en una cohorte poblacional del estudio REGICOR". In: *Revista Española de Cardiología* 64.15 (2011), pp. 385–394.

[9] Ralph B. D'Agostino et al. "Validation of the Framingham Coronary Heart Disease Prediction Scores: Results of a Multiple Ethnic Groups Investigation". In: *JAMA* 286.2 (2001), pp. 180–187.

[10] Jaume Marrugat et al. "Derivation and validation of a set of 10-year cardiovascular risk predictive functions in Spain: The FRESCO Study". In: *Preventive Medicine* 61 (2014), pp. 66–74.

[11] R.M. Conroy et al. “Estimation of ten-year risk of fatal cardiovascular disease in Europe: the SCORE project”. In: *European Heart Journal* 24.11 (2003), pp. 987–1003.

[12] Julia Hippisley-Cox et al. “Predicting cardiovascular risk in England and Wales: prospective derivation and validation of QRISK2”. In: *BMJ* 336.1475 (2006).

[13] Maria Grau and Jaume Marrugat. “Funciones de riesgo en la prevención primaria de las enfermedades cardiovasculares”. In: *Revista Española de Cardiología* 61.4 (2008), pp. 404–416.

[14] N E Breslow. “Analysis of Survival Data under the Proportional Hazards Model”. In: *International Statistical Review / Revue Internationale de Statistique* 43.1 (1975), pp. 45–57.

[15] Maria Garcia-Gil et al. “Effectiveness of Statins as Primary Prevention in People With Different Cardiovascular Risk: A Population-Based Cohort Study.” In: *Clin Pharmacol Ther* 104.4 (2018), pp. 719–732.

[16] Marie-Louise M. Gronholdt et al. “Ultrasonic Echolucent Carotid Plaques Predict Future Strokes”. In: *Circulation* 104.1 (2001), pp. 68–73.

[17] Yoko Irie et al. “The utility of ultrasonic tissue characterization of carotid plaque in the prediction of cardiovascular events in diabetic patients”. In: *Atherosclerosis* 230.2 (2013), pp. 399–405.

[18] Narendra N. Khanna et al. “Performance evaluation of 10-year ultrasound image-based stroke/cardiovascular (CV) risk calculator by comparing against ten conventional CV risk calculators: a diabetic study”. In: *Computers in Biology and Medicine* 105 (2019), pp. 125–143.

[19] C. Mitchell et al. “Ultrasound carotid plaque features, cardiovascular disease risk factors and events: The Multi-Ethnic Study of Atherosclerosis”. In: *Atherosclerosis* 276 (2018), pp. 195–202.

[20] Wikipedia contributors. *Artificial intelligence — Wikipedia, The Free Encyclopedia*. [Online; accessed 29-October-2023]. 2023. URL: https://en.wikipedia.org/w/index.php?title=Artificial_intelligence&oldid=1181810241.

[21] Richard Szeliski. *Computer Vision*. Springer Cham, 2022.

[22] Thomas Trappenberg. *Fundamentals of machine learning*. Oxford University Press, 2019.

[23] Zewen Li et al. “A survey of convolutional neural networks: analysis, applications, and prospects”. In: *IEEE transactions on neural networks and learning systems* (2021).

[24] Chee-Peng Lim et al. *Handbook of Artificial Intelligence in Healthcare*. Springer Cham, 2022.

[25] Maria Grau et al. “Trends in cardiovascular risk factor prevalence (1995-2000-2005) in northeastern Spain”. In: *European journal of cardiovascular prevention and rehabilitation* 14.5 (2007), pp. 653–659.

[26] Eric de Groot et al. “Measurement of arterial wall thickness as a surrogate marker for atherosclerosis”. In: *Circulation* 109.23 suppl 1 (2004), pp. III–33.

[27] Eric de Groot et al. “Measurement of carotid intima-media thickness to assess progression and regression of atherosclerosis”. In: *Nat Clin Pract Cardiovasc Med* 5.5 (2008), pp. 280–288.

[28] Maria del Mar Vila et al. “Semantic segmentation with DenseNets for carotid artery ultrasound plaque segmentation and CIMT estimation”. In: *Artificial Intelligence in Medicine* 103 (2020), p. 101784. ISSN: 0933-3657.

[29] Maria del Mar Vila et al. “Graphics for the Masses: A Hardware Rasterization Architecture for Mobile Phones”. In: *ACM Trans. Graph.* 22.3 (2003), pp. 801–808.

[30] Maria del Mar Vila et al. “Polyvascular Subclinical Atherosclerosis: Correlation Between Ankle Brachial Index and Carotid Atherosclerosis in a Population-Based Sample”. In: *Angiology* 74.5 (2023), pp. 443–451.

[31] C. Zhang et al. “Carotid Artery Segmentation in Ultrasound Images”. In: *MICCAI Workshop on Computing and Visualization for Intravascular Imaging and Computer Assisted Stenting*. 2015.

[32] Karim Lekadir et al. “A Convolutional Neural Network for Automatic Characterization of Plaque Composition in Carotid Ultrasound”. In: *IEEE Journal of Biomedical and Health Informatics* 21.1 (2017), pp. 48–55.

[33] Lucas Gago et al. “An end-to-end framework for intima media measurement and atherosclerotic plaque detection in the carotid artery”. In: *Computer Methods and Programs in Biomedicine* 223 (2022), p. 106954.

[34] Xiangyang Xu et al. “Ultrasound intima–media segmentation using Hough transform and dual snake model”. In: *Computerized Medical Imaging and Graphics* 36.3 (2012), pp. 248–258.

[35] Filippo Molinari et al. “Completely automated multiresolution edge snapper—a new technique for an accurate carotid ultrasound IMT measurement: clinical validation and benchmarking on a multi-institutional database”. In: *IEEE Transactions on Image Processing* 21.3 (2012), pp. 1211–1222.

[36] Francesco Faita et al. “Real-time Measurement System for Evaluation of the Carotid Intima-Media Thickness With a Robust Edge Operator”. In: *Journal of Ultrasound in Medicine* 27.9 (2008), pp. 1353–1361.

[37] M.C. Bastida-Jumilla et al. "Frequency-domain active contours solution to evaluate intima–media thickness of the common carotid artery". In: *Biomedical Signal Processing and Control* 16 (2015), pp. 68–79.

[38] C. Rajasekaran et al. "Automated Diagnosis of Cardiovascular Disease Through Measurement of Intima Media Thickness Using Deep Neural Networks". In: *2019 41st Annual International Conference of the IEEE Engineering in Medicine and Biology Society (EMBC)*. 2019, pp. 6636–6639.

[39] Christos P. Loizou et al. *Integrated System for the Complete Segmentation of the Common Carotid Artery Bifurcation in Ultrasound Images*. Springer Berlin Heidelberg, 2013, pp. 292–301.

[40] Shen Zhao et al. "Robust segmentation of intima–media borders with different morphologies and dynamics during the cardiac cycle". In: *IEEE Journal of Biomedical and Health Informatics* 22.5 (2017), pp. 1571–1582.

[41] Filippo Molinari et al. "Automated carotid IMT measurement and its validation in low contrast ultrasound database of 885 patient Indian population epidemiological study: results of AtheroEdge® software". In: *International Angiology* (2014), pp. 209–219.

[42] Chunjun Qian and Xiaoping Yang. "An integrated method for atherosclerotic carotid plaque segmentation in ultrasound image". In: *Computer Methods and Programs in Biomedicine* 153 (2018), pp. 19–32.

[43] Rosa-María Menchón-Lara and José-Luis Sancho-Gómez. "Fully automatic segmentation of ultrasound common carotid artery images based on machine learning". In: *Neurocomputing* 151 (2015), pp. 161–167.

[44] Mainak Biswas et al. "Two-stage artificial intelligence model for jointly measurement of atherosclerotic wall thickness and plaque burden in carotid ultrasound: A screening tool for cardiovascular/stroke risk assessment". In: *Computers in Biology and Medicine* 123 (2020), p. 103847.

[45] Jae Shin et al. "Automating Carotid Intima-Media Thickness Video Interpretation With Convolutional Neural Networks". In: *Proceedings of the IEEE Conference on Computer Vision and Pattern Recognition (CVPR)*. 2016.

[46] Mainak Biswas et al. "Deep learning strategy for accurate carotid intima-media thickness measurement: an ultrasound study on Japanese diabetic cohort". In: *Computers in Biology and Medicine* 98 (2018), pp. 100–117.

[47] Pankaj K. Jain et al. "Far wall plaque segmentation and area measurement in common and internal carotid artery ultrasound using U-series architectures: An unseen Artificial Intelligence paradigm for stroke risk assessment". In: *Computers in Biology and Medicine* 149 (2022), p. 106017. ISSN: 0010-4825.

[48] Filippo Molinari, Guang Zeng, and Jasjit S. Suri. “A state of the art review on intima–media thickness (IMT) measurement and wall segmentation techniques for carotid ultrasound”. In: *Computer Methods and Programs in Biomedicine* 100.3 (2010), pp. 201–221.

[49] Christos P. Loizou. “A review of ultrasound common carotid artery image and video segmentation techniques”. In: *Medical & Biological Engineering & Computing* 52.12 (2014), pp. 1073–1093.

[50] Saba Luca et al. “Global perspective on carotid intima-media thickness and plaque: should the current measurement guidelines be revisited?” In: *International Angiology* 38.6 (2019), pp. 451–465.

[51] Mainak Biswas et al. “A Review on Joint Carotid Intima-Media Thickness and Plaque Area Measurement in Ultrasound for Cardiovascular/Stroke Risk Monitoring: Artificial Intelligence Framework”. In: *J Digit Imaging* 3.34 (2021), pp. 581–604.

[52] Rosa-María Menchón-Lara et al. “Measurement of Carotid Intima-Media Thickness in ultrasound images by means of an automatic segmentation process based on machine learning”. In: *Eurocon 2013*. 2013, pp. 2086–2093.

[53] Rosa-María Menchón-Lara and José-Luis Sancho-Gómez. “Ultrasound image processing based on machine learning for the fully automatic evaluation of the Carotid Intima-Media Thickness”. In: *2014 12th International Workshop on Content-Based Multimedia Indexing (CBMI)*. 2014, pp. 1–4.

[54] Rosa-María Menchón-Lara et al. “Automatic detection of the intima-media thickness in ultrasound images of the common carotid artery using neural networks”. In: *Medical & Biological Engineering & Computing* 52 (2014), pp. 169–181.

[55] Gao Huang et al. “Densely Connected Convolutional Networks”. In: *Proceedings of the IEEE Conference on Computer Vision and Pattern Recognition (CVPR)*. 2017.

[56] Mingxing Tan and Quoc Le. “EfficientNet: Rethinking Model Scaling for Convolutional Neural Networks”. In: *Proceedings of the 36th International Conference on Machine Learning*. Ed. by Kamalika Chaudhuri and Ruslan Salakhutdinov. Vol. 97. Proceedings of Machine Learning Research. 2019, pp. 6105–6114.

[57] Jonathan Long, Evan Shelhamer, and Trevor Darrell. “Fully Convolutional Networks for Semantic Segmentation”. In: *Proceedings of the IEEE Conference on Computer Vision and Pattern Recognition (CVPR)*. 2015.

[58] Kaiming He et al. “Deep Residual Learning for Image Recognition”. In: *2016 IEEE Conference on Computer Vision and Pattern Recognition (CVPR)*. 2016, pp. 770–778.

[59] Simon Jégou et al. “The One Hundred Layers Tiramisu: Fully Convolutional DenseNets for Semantic Segmentation”. In: *2017 IEEE Conference on Computer Vision and Pattern Recognition Workshops (CVPRW)*. 2017, pp. 1175–1183.

[60] Sergey Ioffe and Christian Szegedy. “Batch Normalization: Accelerating Deep Network Training by Reducing Internal Covariate Shift”. In: *Proceedings of the 32nd International Conference on Machine Learning*. Vol. 37. 2015, pp. 448–456.

[61] Vinod Nair and Geoffrey E. Hinton. “Rectified linear units improve restricted boltzmann machines”. In: *27th International Conference on Machine Learning*. 2010, pp. 807–814.

[62] Nitish Srivastava et al. “Dropout: A Simple Way to Prevent Neural Networks from Overfitting”. In: *Journal of Machine Learning Research* 15.56 (2014), pp. 1929–1958.

[63] Maria Grau et al. “Carotid intima-media thickness in the Spanish population: reference ranges and association with cardiovascular risk factors.” In: *Revista Española de Cardiología* 65.12 (2012), pp. 1086–1093.

[64] Olaf Ronneberger, Philipp Fischer, and Thomas Brox. “U-net: Convolutional networks for biomedical image segmentation”. In: *Medical Image Computing and Computer-Assisted Intervention – MICCAI 2015*. Springer International Publishing, 2015, pp. 234–241.

[65] Kaiming He et al. “Delving deep into rectifiers: Surpassing human-level performance on imagenet classification”. In: *Proceedings of the IEEE International Conference on Computer Vision (ICCV)*. 2015.

[66] T. Tieleman and G. Hinton. “RMSProp adaptive learning”. In: *COURSERA: Neural Networks for Machine Learning* (2012).

[67] Bianchini Elisabetta et al. “Functional and Structural Alterations of Large arteries: Methodological Issues”. In: *Current Pharmaceutical Design* 19.13 (2013), pp. 2390–2400.

[68] J.M. Baena-Díez et al. “Association between chronic immune-mediated inflammatory diseases and cardiovascular risk”. In: *Heart* 104.2 (2018), pp. 119–126.

[69] A. Dalbeni et al. “Traditional cardiovascular risk factors and residual disease activity are associated with atherosclerosis progression in rheumatoid arthritis patients”. In: *Hypertens Res* 43.9 (2020), pp. 922–928.

[70] S. Jain et al. “Inflammation and arterial stiffness in humans”. In: *Atherosclerosis* 237.2 (2014), pp. 381–90.

[71] L. Zanoli et al. “Vascular consequences of inflammation: a position statement from the ESH Working Group on Vascular Structure and Function and the ARTERY Society”. In: *J Hypertens* (9).9 (2020), pp. 1682–1698.

[72] F. Agüero et al. “Prevalence of lower extremity peripheral arterial disease in individuals with chronic immune mediated inflammatory disorders”. In: *Atherosclerosis* 242.1 (2015), pp. 1–7.

[73] R. Martí-Lluch et al. “Differences in cardio-ankle vascular index in a general Mediterranean population depending on the presence or absence of metabolic cardiovascular risk factors”. In: *Atherosclerosis* 264 (2017), pp. 29–35.

[74] P. Karakasis et al. “Accelerated Atherosclerosis and Management of Cardiovascular Risk in Autoimmune Rheumatic Diseases: An Updated Review”. In: *Curr Probl Cardiol* 12.48 (2023), p. 101999.

[75] B. Bolíbar et al. “Grupo SIDIAP. Base de datos SIDIAP: la historia clínica informatizada de Atención Primaria como fuente de información para la investigación epidemiológica”. In: *Med Clin (Barc)* 138.14 (2012), pp. 617–621.

[76] Jaume Marrugat et al. “Validity of an adaptation of the Framingham cardiovascular risk function: the VERIFICA study”. In: *Journal of Epidemiology & Community Health* 61.1 (2007), pp. 40–47.

[77] Luc M. Van Bortel et al. “Clinical applications of arterial stiffness, Task Force III: recommendations for user procedures”. In: *American Journal of Hypertension* 15.5 (2002), pp. 445–452.

[78] M. Loboz-Rudnicka et al. “Impact of cardiovascular risk factors on carotid intima-media thickness: sex differences”. In: *Clin Interv Aging* 23.11 (2016), pp. 721–731.

[79] J.J. DuPont et al. “Sex Differences In Mechanisms Of Arterial Stiffness”. In: *British Journal of Pharmacology* 176.21 (2019), pp. 4208–4225.

[80] R Core Team. *R: A Language and Environment for Statistical Computing*. R Foundation for Statistical Computing. Vienna, Austria, 2021. URL: https://www.R-project.org/.

[81] Peng Wang et al. “Increased carotid intima-media thickness in rheumatoid arthritis: an update meta-analysis”. In: *Clinical Rheumatology* 35.2 (2016).

[82] Pauline Henrot et al. “Assessment of subclinical atherosclerosis in systemic lupus erythematosus: A systematic review and meta-analysis”. In: *Joint Bone Spine* 85.2 (2018), pp. 155–163.

[83] Tzu-Wei Wu et al. “Associations of Cardiovascular Risk Factors with Carotid Intima-Media Thickness in Middle-Age Adults and Elders”. In: *Journal of Atherosclerosis and Thrombosis* 24.7 (2017), pp. 677–686.

[84] Ruocen Bai et al. “The Relationship of Ankylosing Spondylitis and Subclinical Atherosclerosis: A Systemic Review and Meta-Analysis”. In: *Angiology* 70.6 (2019), pp. 492–500.

[85] Emese Balogh et al. “Autoimmune and angiogenic biomarkers in autoimmune atherosclerosis”. In: *Clinical Immunology* 199 (2019), pp. 47–51.

[86] Z. Szekanecz et al. “Autoimmune atherosclerosis in 3D: How it develops, how to diagnose and what to do”. In: *Autoimmun* 15.7 (2016), pp. 756–769.

[87] R. Agca et al. “EULAR recommendations for cardiovascular disease risk management in patients with rheumatoid arthritis and other forms of inflammatory joint disorders: 2015/2016 update”. In: *Ann Rheum Dis* 76.1 (2017), pp. 17–28.

[88] M. Mosca et al. “European League Against Rheumatism recommendations for monitoring patients with systemic lupus erythematosus in clinical practice and in observational studies”. In: *Ann Rheum Dis* 69.7 (2010), pp. 1269–1274.

[89] Claudia Mendoza-Pinto et al. “Endothelial dysfunction and arterial stiffness in patients with systemic lupus erythematosus: A systematic review and meta-analysis”. In: *Atherosclerosis* 297 (2020), pp. 55–63.

[90] P. Ambrosino et al. “Non-invasive assessment of arterial stiffness in patients with rheumatoid arthritis: a systematic review and meta-analysis of literature studies”. In: *Ann Med* 47.6 (2015), pp. 457–467.

[91] P. Wang et al. “ Assessment of Aortic Stiffness in Patients with Rheumatoid Arthritis Using Pulse Wave Velocity: An Update Meta-analysis”. In: *Arch Med Res* 50.7 (2019), pp. 401–412.

[92] Rogério Teixeira et al. “Ultrasonographic vascular mechanics to assess arterial stiffness: a review”. In: *European Heart Journal - Cardiovascular Imaging* 17.3 (2015), pp. 233–246.

[93] N. Katakami et al. “Clinical Utility of Carotid Ultrasonography in the Prediction of Cardiovascular Events in Patients with Diabetes: A Combined Analysis of Data Obtained in Five Longitudinal Studies”. In: *J Atheroscler Thromb* 25.10 (2018), pp. 1053–1066.

[94] Y. Kokubo et al. “Impact of Intima-Media Thickness Progression in the Common Carotid Arteries on the Risk of Incident Cardiovascular Disease in the Suita Study”. In: *J Am Heart Assoc* 7.11 (2018).

[95] J.F. Polak and DH O’Leary. “ Carotid Intima-Media Thickness as Surrogate for and Predictor of CVD”. In: *Glob Heart* 11.3 (2016), pp. 295–312.

[96] G. Nagy, N Németh, and EI Buzás. “Mechanisms of vascular comorbidity in autoimmune diseases”. In: *Curr Opin Rheumatol* 30.2 (2018), pp. 197–206.

[97] Rafael Ramos et al. “Validity for use in research on vascular diseases of the SIDIAP (Information System for the Development of Research in Primary Care): the EMMA study”. In: *Rev Esp Cardiol (Engl Ed)* 65.1 (2012), pp. 29–37.

[98] F. Fina-Aviles et al. “The descriptive epidemiology of rheumatoid arthritis in Catalonia: a retrospective study using routinely collected data”. In: *Clin Rheumatol* 35.3 (2016), pp. 751–757.

[99] L. Carmona et al. “The prevalence of rheumatoid arthritis in the general population of Spain”. In: *Rheumatology (Oxford)* 41.1 (2002), pp. 88–95.

[100] P. López et al. “Epidemiology of systemic lupus erythematosus in a northern Spanish population: gender and age influence on immunological features”. In: *Lupus* 12.11 (2003), pp. 860–865.

[101] C. Saro Gismera et al. “Epidemiology in inflammatory bowel disease in five areas of Asturias. Spain.” In: *An Med Interna* 20.5 (2003), pp. 232–238.

[102] M. Sarabi and L. Lind. “Short-term effects of smoking and nicotine chewing gum on endothelium-dependent vasodilation in young healthy habitual smokers.” In: *J Cardiovasc Pharmacol* 35.3 (2000), pp. 451–456.

[103] Steven Yakubov. “Polyvascular atherosclerotic disease: recognizing the risks and managing the syndrome”. In: *Current Medical Research and Opinion* 25.11 (2009), pp. 2631–2641.

[104] V. Aboyans et al. “ESC Scientific Document Group. 2017 ESC Guidelines on the Diagnosis and Treatment of Peripheral Arterial Diseases, in collaboration with the European Society for Vascular Surgery (ESVS): Document covering atherosclerotic disease of extracranial carotid and vertebral, mesenteric, renal, upper and lower extremity arteriesEndorsed by: the European Stroke Organization (ESO)The Task Force for the Diagnosis and Treatment of Peripheral Arterial Diseases of the European Society of Cardiology (ESC) and of the European Society for Vascular Surgery (ESVS)”. In: *Eur Heart J* 39.9 (2018), pp. 763–816.

[105] M.D. Danese et al. “Estimation of the increased risk associated with recurrent events or polyvascular atherosclerotic cardiovascular disease in the United Kingdom.” In: *Eur J Prev Cardiol* 28.3 (2021), pp. 335–343.

[106] V. Aboyans et al. “Measurement and interpretation of the ankle-brachial index: a scientific statement from the American Heart Association”. In: *Circulation* 126.24 (2012), pp. 2890–2909.

[107] F. Sartipy et al. “Ten Year Mortality in Different Peripheral Arterial Disease Stages: A Population Based Observational Study on Outcome”. In: *Eur J Vasc Endovasc Surg* 55.4 (2018), pp. 529–536.

[108] J.H. Stein et al. “American Society of Echocardiography Carotid Intima-Media Thickness Task Force. Use of carotid ultrasound to identify subclinical vascular disease and evaluate cardiovascular disease risk: a consensus statement from the American Society of Echocardiography Carotid Intima-Media Thickness Task

Force. Endorsed by the Society for Vascular Medicine". In: *J Am Soc Echocardiogr* 21.4 (2008), pp. 93–111.

[109] Y. Zhang et al. "Carotid Artery Plaques, Carotid Intima-Media Thickness, and Risk of Cardiovascular Events and All-Cause Death in Older Adults: A 5-Year Prospective, Community-Based Study". In: *Angiology* 69.2 (2018), pp. 120–129.

[110] K. Winckler et al. "Carotid intima media thickness and ankle brachial index are inversely associated in subjects with and without diabetes". In: *Scand J Clin Lab Invest* 78.6 (2018), pp. 464–469.

[111] Y. Zhang et al. "Carotid intima-media thickness and plagues are associated with indicators of peripheral artery diseases in patients with diabetes". In: *Diabetes Res Clin Pract* 144 (2018), pp. 245–251.

[112] Jorge García García et al. "Carotid Intima-Media Thickness is Not Associated with Markers of Atherosclerosis in Stroke Patients". In: *Journal of Stroke and Cerebrovascular Diseases* 25.5 (2016), pp. 1070–1075.

[113] F.F. Pan et al. "Carotid plague formation is associated with ankle-brachial index in elderly people". In: *C. Aging Clin Exp Res* 32.11 (2020), pp. 2217–2223.

[114] Vito M. R. Muggeo. "Testing with a nuisance parameter present only under the alternative: a score-based approach with application to segmented modelling". In: *Journal of Statistical Computation and Simulation* 86.15 (2016), pp. 3059–3067.

[115] Rafael Ramos et al. "Prevalence of symptomatic and asymptomatic peripheral arterial disease and the value of the ankle-brachial index to stratify cardiovascular risk". In: *Eur J Vasc Endovasc Surg* 38.3 (2009), pp. 305–311.

[116] A. Velescu et al. "Peripheral Arterial Disease Incidence and Associated Risk Factors in a Mediterranean Population-based Cohort. The REGICOR Study". In: *European Journal of Vascular and Endovascular Surgery* 51.5 (2016), pp. 696–705.

[117] Maria Grau et al. "Why should population attributable fractions be periodically recalculated? An example from cardiovascular risk estimation in southern Europe". In: *Prev Med* 51.1 (2010), pp. 78–84.

[118] P. Morillas et al. "Prevalence of Peripheral Arterial Disease in Patients With Acute Coronary Syndrome (PAMISCA) Investigators. Impact of clinical and subclinical peripheral arterial disease in mid-term prognosis of patients with acute coronary syndrome". In: *Am J Cardiol* 104.11 (2009), pp. 1494–1498.

[119] J.F. Polak, M Szklo, and DH O'Leary. "Carotid Intima-Media Thickness Score, Positive Coronary Artery Calcium Score, and Incident Coronary Heart Disease: The Multi-Ethnic Study of Atherosclerosis". In: *J Am Heart Assoc* 6.1 (2017).

[120] MH Geisel et al. “Comparison of coronary artery calcification, carotid intima-media thickness and ankle-brachial index for predicting 10-year incident cardiovascular events in the general population.” In: *Eur Heart J* 38.23 (2017), pp. 1815–1822.

[121] Nicholas Grubic et al. “The Role of Carotid and Femoral Plaque Burden in the Diagnosis of Coronary Artery Disease”. In: *Curr Cardiol Rep* 22.10 (2020).

[122] Alessandro Mattina et al. “Polyvascular subclinical atherosclerosis in familial hypercholesterolemia: The role of cholesterol burden and gender”. In: *Nutrition, Metabolism and Cardiovascular Diseases* 29.10 (2019), pp. 1068–1076. ISSN: 0939-4753.

[123] Manon G. van der Meer et al. “The impact of polyvascular disease on long-term outcome in percutaneous coronary intervention patients”. In: *European Journal of Clinical Investigation* 44.3 (2013).

[124] M. Bermúdez-López et al. “Subclinical atheromatosis localization and burden in a low-to-moderate cardiovascular risk population: the ILERVAS study”. In: *Rev Esp Cardiol (Engl Ed)* 74.12 (2021), pp. 1042–1053.

[125] B López-Melgar et al. “Subclinical Atherosclerosis Burden by 3D Ultrasound in Mid-Life: The PESA Study”. In: *J Am Coll Cardiol* 70.3 (2017), pp. 01–313.

[126] Y. Wang et al. “A U-shaped relationship between ankle-brachial index and carotid intima-media thickness in a Chinese population of Inner Mongolia”. In: *Int Angiol* 30.5 (2011), pp. 451–457.

[127] Fabian Bamberg et al. “Subclinical Disease Burden as Assessed by Whole-Body MRI in Subjects With Prediabetes, Subjects With Diabetes, and Normal Control Subjects From the General Population: The KORA-MRI Study”. In: *Diabetes* 66.1 (2016), pp. 158–169.

[128] Kayla N. Colledanchise et al. “Combined Femoral and Carotid Plaque Burden Identifies Obstructive Coronary Artery Disease in Women”. In: *Journal of the American Society of Echocardiography* 33.1 (2020), pp. 90–100.

[129] V. Nambi et al. “Carotid intima-media thickness and presence or absence of plaque improves prediction of coronary heart disease risk: the ARIC (Atherosclerosis Risk In Communities) study”. In: *J Am Coll Cardiol* 55.15 (2010).

[130] Konstantinos Toutouzas et al. “Vulnerable plaque imaging: updates on new pathobiological mechanisms”. In: *European Heart Journal* 36.45 (2015), pp. 3147–3154.

[131] J.S. Suri, C. Kathuria, and F. Molinari. *Fundamentals of machine learning.* Springer Science & Business Media, 2010.

[132] Erling Falk. “Pathogenesis of Atherosclerosis”. In: *Journal of the American College of Cardiology* 47.8, Supplement (2006), pp. C7–C12.

[133] Luca Saba et al. “Plaque tissue morphology-based stroke risk stratification using carotid ultrasound: a polling-based PCA learning paradigm”. In: *Journal of Medical Systems* 41.6 (2017), p. 98.

[134] Aditya M. Sharma et al. “A Review on Carotid Ultrasound Atherosclerotic Tissue Characterization and Stroke Risk Stratification in Machine Learning Framework”. In: *Current atherosclerosis reports* 17.9 (2015), pp. 1–13.

[135] Saba Luca et al. “Global perspective on carotid intima-media thickness and plaque: should the current measurement guidelines be revisited?” In: *Int Angiol* 38.6 (2019), pp. 451–465.

[136] M. Bhagawati et al. “Cardiovascular disease/stroke risk stratification in deep learning framework: a review”. In: *Cardiovasc Diagn Ther* 3.13 (2023), pp. 557–598.

[137] Brajesh K. Lal et al. “Pixel distribution analysis of B-mode ultrasound scan images predicts histologic features of atherosclerotic carotid plaques”. In: *Journal of Vascular Surgery* 35.6 (2002), pp. 1210–1217.

[138] Nikolaos N. Tsiaparas et al. “Comparison of multiresolution features for texture classification of carotid atherosclerosis from B-mode ultrasound”. In: *IEEE Transactions on Information Technology in Biomedicine* 15 (2011), pp. 130–137.

[139] E.C. Kyriacou et al. “Prediction of high-risk asymptomatic carotid plaques based on ultrasonic image features”. In: *IEEE Trans Inf Technol Biomed* 16.5 (2012), pp. 966–73.

[140] U. Rajendra Acharya et al. “An Accurate and Generalized Approach to Plaque Characterization in 346 Carotid Ultrasound Scans”. In: *IEEE Transactions on Instrumentation and Measurement* 61.4 (2012), pp. 1045–1053.

[141] U. Rajendra Acharya et al. “Atherosclerotic plaque tissue characterization in 2D ultrasound longitudinal carotid scans for automated classification: a paradigm for stroke risk assessment”. In: *Medical Biological Engineering Computing* 51.5 (2013), pp. 513–523.

[142] U. Rajendra Acharya et al. “Understanding symptomatology of atherosclerotic plaque by image-based tissue characterization”. In: *Computer Methods and Programs in Biomedicine* 110.1 (2013), pp. 66–75.

[143] U. Rajendra Acharya et al. “Plaque Tissue Characterization and Classification in Ultrasound Carotid Scans: A Paradigm for Vascular Feature Amalgamation”. In: *IEEE Transactions on Instrumentation and Measurement* 62.2 (2013), pp. 392–400.

[144] Aimilia Gastounioti et al. “A novel computerized tool to stratify risk in carotid atherosclerosis using kinematic features of the arterial wall”. In: *IEEE Journal of Biomedical and Health Informatics* 19.3 (2014), pp. 1137–1145.

[145] U. Rajendra Acharya et al. “An automated technique for carotid far wall classification using grayscale features and wall thickness variability”. In: *Journal of Clinical Ultrasound* 43.5 (2015), pp. 302–311.

[146] Tadashi Araki et al. “Stroke risk stratification and its validation using ultrasonic echolucent carotid wall plaque morphology: a machine learning paradigm”. In: *Computers in biology and medicine* 80 (2017), pp. 77–96.

[147] Luca Saba et al. “Ultrasound-based internal carotid artery plaque characterization using deep learning paradigm on a supercomputer: a cardiovascular disease/stroke risk assessment system”. In: *Int J Cardiovasc Imaging* 5.37 (2021), pp. 1511–1528.

[148] Rolf Kern et al. “Characterization of carotid artery plaques using real-time compound B-mode ultrasound”. In: *Stroke* 35.4 (2004), pp. 870–875.

[149] G. Schulte-Altedorneburg et al. “Preoperative B-mode ultrasound plaque appearance compared with carotid endarterectomy specimen histology”. In: *Acta Neurologica Scandinavica* 101.3 (2000), pp. 188–194.

[150] Jens Michael Carstensen. “Description and simulation of visual texture”. PhD thesis. Technical University of DenmarkDanmarks Tekniske Universitet, Department of Informatics and Mathematical Modeling, Institut for Informatik og Matematisk Modellering, 1992.

[151] Mary M. Galloway. “Texture analysis using gray level run lengths”. In: *Computer Graphics and Image Processing* 4.2 (1975), pp. 172–179.

[152] A. Kadyrov and M. Petrou. “The Trace transform and its applications”. In: *Pattern Analysis and Machine Intelligence, IEEE Transactions on* 23.8 (2001), pp. 811–828.

[153] C. L. Nikias and J. M. Mendel. “Signal processing with higher-order spectra”. In: *IEEE Signal Processing Magazine* 10.3 (1993), pp. 10–37.

[154] Jaume Marrugat et al. “Comparing the Predictive Powers of Survival Models Using Harrell’s C or Somers’ D”. In: *J Epidemiol Community Health* 57.8 (2003), pp. 634–8.

[155] Stephen F. Weng et al. “Can machine-learning improve cardiovascular risk prediction using routine clinical data?” In: *PLOS ONE* 12.4 (2017), pp. 1–14.

[156] R. Nakanishi et al. “Machine Learning Adds to Clinical and CAC Assessments in Predicting 10-Year CHD and CVD Deaths”. In: *JACC Cardiovasc Imaging* 14.3 (2021), pp. 615–625.

[157] B.K. Tamarappoo et al. “Machine learning integration of circulating and imaging biomarkers for explainable patient-specific prediction of cardiac events: A prospective study”. In: *Atherosclerosis* (2021), pp. 76–82.

[158] Bharath Ambale-Venkatesh et al. “Cardiovascular event prediction by machine learning: the multi-ethnic study of atherosclerosis”. In: *Circulation Research* 121.9 (2017), pp. 1092–1101.

[159] D. Gonzalo-Calvo et al. “Soluble low-density lipoprotein receptor-related protein 1 as a biomarker of coronary risk: Predictive capacity and association with clinical events”. In: *Atherosclerosis* 287 (2019), pp. 93–99.

[160] S. Winther et al. “Coronary Calcium Scoring Improves Risk Prediction in Patients With Suspected Obstructive Coronary Artery Disease”. In: *Journal of the American College of Cardiology* 80.21 (2022), pp. 1965–1977.

[161] Olaf Ronneberger, Philipp Fischer, and Thomas Brox. “U-net: Convolutional networks for biomedical image segmentation”. In: *International Conference on Medical Image Computing and Computer-assisted Intervention*. 2015, pp. 234–241.

[162] Frank E. Harrell, K L Lee, and Daniel B. Mark. “Multivariable prognostic models: issues in developing models, evaluating assumptions and adequacy, and measuring and reducing errors.” In: *Statistics in medicine* 15 4 (1996), pp. 361–87.

[163] Hervé Abdi and Lynne J Williams. “Principal component analysis”. In: *Wiley Interdisciplinary Reviews: Computational Statistics* 2.4 (2010), pp. 433–459.

[164] Bendix Carstensen et al. *Epi: A Package for Statistical Analysis in Epidemiology*. R package version 2.44. 2021. URL: https://CRAN.R-project.org/package=Epi.

[165] Frank E. Harrell et al. “Evaluating the Yield of Medical Tests”. In: *JAMA* 247.18 (May 1982), pp. 2543–2546. ISSN: 0098-7484.

[166] Michael J. Pencina, Ralph B. D’Agostino, and Ramachandran S. Vasan. “Statistical methods for assessment of added usefulness of new biomarkers”. In: *Clinical Chemistry and Laboratory Medicine* 48.12 (2010), pp. 1703–1711.

[167] Eisuke Inoue. *nricens: NRI for Risk Prediction Models with Time to Event and Binary Response Data*. R package version 1.6. 2018. URL: https://CRAN.R-project.org/package=nricens.

[168] Gareth James et al. *An Introduction to Statistical Learning with Applications in R*. Springer, 2017.

[169] Koichiro Yasaka and Osamu Abe. “Deep learning and artificial intelligence in radiology: Current applications and future directions”. In: *PLOS Medicine* 15.11 (Nov. 2018), pp. 1–4.

[170] Filippo Pesapane, Marina Codari, and Francesco Sardanelli. “Artificial intelligence in medical imaging: threat or opportunity? Radiologists again at the forefront of innovation in medicine”. In: *European radiology experimental* 2.1 (2018), p. 35.

[171] Tao Lei et al. “Medical Image Segmentation Using Deep Learning: A Survey”. In: *arXiv preprint arXiv:2009.13120* (2020).

[172] Andre Esteva et al. “Dermatologist-level classification of skin cancer with deep neural networks”. In: *Nature* 542.7639 (2017), pp. 115–118.

[173] Awni Y. Hannun et al. “Cardiologist-level arrhythmia detection and classification in ambulatory electrocardiograms using a deep neural network”. In: *Nature Medicine* 25.1 (2019), pp. 65–69.

[174] Connor Shorten and Taghi M. Khoshgoftaar. “A survey on Image Data Augmentation for Deep Learning”. In: *Journal of Big Data* 6.1 (2019), p. 60. ISSN: 2196-1115.

[175] Alejandro Barredo Arrieta et al. “Explainable Artificial Intelligence (XAI): Concepts, taxonomies, opportunities and challenges toward responsible AI”. In: *Information Fusion* 58 (2020), pp. 82–115.

[176] Moloud Abdar et al. “A review of uncertainty quantification in deep learning: Techniques, applications and challenges”. In: *arXiv preprint arXiv:2011.06225* (2020).